Title
Mathematical Models and Control Algorithms for Traffic Automation

Author
You, Yiling

Publication Date
2022

Peer reviewed|Thesis/dissertation

Mathematical Models and Control Algorithms for Traffic Automation

by

Yiling You

A dissertation submitted in partial satisfaction of the

requirements for the degree of

Doctor of Philosophy

in

Applied Mathematics

in the

Graduate Division

of the

University of California, Berkeley

Committee in charge:

Professor Jon Wilkening, Co-chair
Professor Alexandre M. Bayen, Co-chair
Professor Ming Gu

Spring 2022

Mathematical Models and Control Algorithms for Traffic Automation

Abstract

Mathematical Models and Control Algorithms for Traffic Automation

by

Yiling You

Doctor of Philosophy in Applied Mathematics

University of California, Berkeley

Professor Jon Wilkening, Co-chair

Professor Alexandre M. Bayen, Co-chair

Transportation accounts for 28% of energy consumption in the US, with 75% of that occurring on highways. Workers spent on aggregate over three million driver-years commuting to their jobs, contributing significantly to the nation-wide congestion. Based on 2012 estimates, US commuters experienced an average of 52 hours of delay in 2011, which amounts to $121 billion of fuel costs and opportunity costs due to delay annually. Estimates project that 4.2% of fuel will be wasted in congestion in 2050 with the adoption of autonomous vehicles. Mixed autonomy, the intermediate regime between a system with no adoption of autonomy and a system where autonomy is fully employed, is proposed as a potential solution to fuel consumption reduction and flow capacity improvement.

The mixed autonomy is complicated to characterize and hard to tackle due to the degree of uncertainty in the system dynamics. The understanding of mixed autonomy is however crucial to designing automated and intelligent transportation systems, and to overhauling public policy with autonomous vehicles in the loop.

Approaches to mobile traffic control include machine learning methods, mathematical modeling and optimal control. The machine learning approaches achieve strong empirical results but in general lack optimality guarantees, theoretical studies of the convergence rate, out-of-sample performance guanrantees and interpretability. The mathematical approaches, on the other hand, are supported by highly developed mathematical theory, but suffer from a lack of attention to the theoretical characterization to the model solutions and the actuations function space. This is inevitable as mathematical methods trade model complexity for the tractability of analysis in the optimal control design.

This thesis investigates mathematical models and control algorithms for traffic automation at multiple levels.

At the vehicle level, this thesis demonstrates the lack of guarantee of well-posedness for the solution of the intelligent driver model (IDM) and closes the theoretical gap by proposing several modifications and rigorously showing the existence and uniqueness of their solutions.

At the mixed autonomy vehicle control level, a systematic way to design the basis-based feedback controller is introduced, which is defined by the solution of a finite-dimensional constrained optimization problem. This thesis discusses theoretical characterization of the actuation function space. An optimal Legendre polynomial basis controller is trained with field data and has been evaluated with simulation data and compared with a range of other mobile traffic controllers.

At the full origin-destination demand routing level, this thesis studies the repeated routing game problem on a parallel network with affine latency functions on each edge, transforming the dynamic traffic assignment problem into a control-theoretic problem. The impact of model parameters on the traffic performance is theoretically studied, and an algorithmic solution based on explicit model predictive control (MPC) is proposed.

To Mom and Dad.

Contents

List of Figures

List of Tables

Acknowledgments

I would like to express my deepest gratitude to my advisor, professor Alexandre Bayen, for giving me the opportunity to join his lab during my second year of PhD. He always impresses and enlightens me with his professionalism, leadership, insightfulness and incredible time management skills. Professor Alexendre introduces me to the topic of transportation and is consistently willing to provide guidance.

I would also like to thank professor Jon Wilkening, who encouraged me to join UC Berkeley Mathematics department and later kindly agreed to serve on my qualifying exam and dissertation committee.

I am indebted to professor Ming Gu for serving on my qualifying exam and dissertation committee. I am grateful to professor Venkatacha Anantharam for offering the inspiring class *Stochastic Systems: Estimation and Control* and kindly serving on my qualifying exam committee. Professor Shankar Sastry is gratefully acknowledged for sharing his vision on traffic routing and autonomy control with me.

I am thankful to professor Benedetto Piccoli from Rutgers University for the mathematical guidance on PDE traffic model, nonlocal conservation laws and hybrid control theory, and most importantly, for always keeping his Italian humor at the expert level. I would like to thank professor Benjamin Seibold from Temple University for sharing his insights about car-following models and traffic energy modeling.

I am grateful for the opportunity to work with and learn from my fantastic Bayen Lab mates, Alexander Keimer, Alben Bagabaldo, Theophiles Cabannes, Marsalis Gibson, Jessica Lazarus, Eugene Vinitsky, Aboudy Kreidieh, Joy Carpio, Fangyu Wu, Kathy Jang, Zhe Fu, Nathan Lichtle, Arwa AlAnqary, Yashar Farid, Shuxia Tang, Fang-Chieh Chou, Ashkan Yousefpour, Saleh Albeaik and Jiayi Li. I would also like to express my gratitude to the amazing scholars in the CIRCLES ODE/PDE team from Rutgers University, Amaury Hayat, Sean McQuade, Xiaoqian Gong and Maria Teresa Chiri.

My 4 years of PhD journey would have been joyless without the company from friends and colleagues. I am lucky and grateful to have Haotian Gu, Dun Tang, Ziwen Zhao, Jiahao Yao, Yue Zhang, Yixuan Li, Xiaohan Yan, Jiasu Wang, Mitchell Taylor, Yanhe Huang, and Eduardo Reyes as central companions to the whole experience at UC Berkeley Mathematics community. I wouldn't have resumed playing the keyboard in a band without the best vocal and guitarist, Rebekah Zhao, and the most passionate drummist, Can Huang. I shared countless weekend nights and holiday times with Anlu Zhou, Tianyu Han, Yunbo Liu, Fan Zhang, Lin Yang, Wenjun Wang, Haitian Liu, Yuhao Ding, Danlin Xiao, Sizhu Lu, Mogeng Yin, thanks for creating fun memories with me! And friends available for me around the clock, Yilin Jin and Yichen Lu at Chicago, Liuyi Song, Yue Xiao, Zhifan Ye, Fuyi Wang, Yimin Qu and Jieyi Zhu at Shanghai, Sirui Wang at Philadelphia, Yixian Wu at Austin, Louise Lu at Baltimore, and friends at the bay area, you all made my existence and connection to the world real.

Special thanks to Nintendo for supplying games that never disappoint, to Lego for landing the wildest imagination to the table, and to my skateboard for chasing the wind and hitting

the ground with me.

This thesis is partially written during an unprecedented time when my hometown, Shanghai, China, is under another wave of lockdown due to the COVID-19 pandemic. It is heartbreaking to witness sorrow and suffering as an outsider but barely capable of changing the situation. I am however grateful to have family members supporting and standing with each other. Home sweet home, "you will burn and you will burn out; you will be healed and come back again". May the Force be with you.

Chapter 1

Introduction

1.1 Mixed Autonomy Traffic

History of the Automated Highway System (AHS)

An Automated Highway System (AHS) is a specially equipped roadway on which vehicles can be operated automatically. The idea of automated driving dates way back at the 1939 World's Fairs in New York, when General Motors (GM) presented a vision of automated controlled vehicle with no driver involved. In the U.S. as well as in many other places, heavy usage of the larger roads slows most peak-hour travel on freeways to less than 56 kilometers (35 miles) per hour. Excess traffic not only causes more than five billion hours of delay every year, but also wastes countless gallons of fuel and multiplies exhaust emissions. The AHS is proposed as a solution to boost highway capacity instead of constructing new highways, which is enormously more expensive [115].

Multiple types of the AHS are proposed. Two distinct types are a dedicated lane system and a mixed traffic system. The former system reserved certain lane for automated vehicles, and the former system allows the fully automated vehicles and the human driven vehicles to share the road [115].

Among the early development of control algorithms of road vehicles, [30] reviews the state of development of Advanced Vehicle Control Systems (AVCS), the subclass of Intelligent Transportation Systems (ITS) that provides the driver with assistance in controlling their vehicle, including the extension to full control of vehicle motions. The types of control in AVCS includes lateral, longitudinal and integrated, along with crash warning and collision avoidance. The authors of [61] developed an adaptive, vision- and machine learning-based robust driving system to execute tactical driving maneuvers such as lane changing and intersection navigation. [57, 56] describe the design of AHS developed at the California Partners for Advanced Transit and Highways (PATH) programs, detailing the design and safety verification of the on-board vehicle control system and the link-layer traffic-flow controller.

To demonstrate the technical feasibility of automating highways, the National Automated Highway System Consortium (NAHSC) initiated a four-day field demonstrations on August

7, 1997. The demonstrations showed the increase of highway capacity with greater levels of vehicle cooperation, and the automated vehicles demonstrated adaptive cruise control (ACC) [115].

Mixed Autonomy

There are two commonly studied regimes in traffic, either where autonomous vehicles (AV) are few enough as having no affect on the surrounding traffic dynamics [139, 129, 130], or so ubiquitous as becoming a coordination problem [33, 54, 99]. We refer to these as the isolated autonomy and full autonomy cases respectively. The intermediate regime is termed mixed autonomy, which is complicated to characterize and hard to tackle due to the degree of uncertainty in the system dynamics. The understanding of mixed autonomy is however crucial to design automated and intelligent transportation systems, and to the corresponding public policy with AVs in the loop.

Human-robot and multi-robot systems. Recent development in control theory and computing power made automated and industrial robots possible. Nowadays more digitally operated and commercial robots are used to perform jobs more cheaply, more accurately and more reliably. As the application scenarios of robotics problems broaden, robots no longer act in isolation. Researchers have been formalizing and algorithmically solve the problem of robot action in coordination with people, i.e., the problem as a human-robot system.

The topics in human-robot and multi-robot system are vast. In [78, 18, 38], the authors model irrational/suboptimal human behavior and develop algorithms which are robust to misspecification. The problem of learning the human preference with active interaction to query for the most informative piece of data are studied in [120, 119]. With the development of learning algorithms, multiple authors study the intersection of learning and robotics and develop methods to learn the robots' act from demonstrations [159, 90, 35]. Designs of game-theoretic approach for human-robot interaction opens the possibility to characterize negotiation strategies, as proposed in [41, 79].

Human-vehicle systems. Many of the general human-robot system approaches can be applied to the specific systems where human interact with automated vehicles. The authors of [132] propose a vehicle-level controller design framework for autonomous truck platoons to ensure safe interaction with a human-driven car, where the interaction is modelled as a hierarchical dynamic game, played between the human driver and the nearest truck in the platoon. [121, 39] focus on trajectory planning algorithms for autonomous driving when human-driven vehicles are also present on the road. Finally at the routing policies level, the authors of [15, 16] develop algorithms to learn the preferences of the users and formulate a planning optimization that chooses prices to maximize a social objective. On the topic of gathering accurate traffic information, [51] presents a field experiment nicknamed *Mobile Century*, which is a traffic monitoring system based on GPS-enabled smartphones.

The Machine Learning Approaches to Mobile Traffic Control

Machine learning gained recent popularity in mobile traffic control for fitting control strategies and traffic models. The development in machine learning combined with better optimization algorithms and growing computing power make deep learning methods popular to fit large and complex models to data. For example, Artificial neural network (ANN) model is one of the common parametric universal nonlinear function approximators [55], theoretically expressive enough to approximate any finite dimensional function. Besides their strong modelling capacity, deep learning methods are capable of integrating real massive data and automating feature engineering procedure. Specifically, deep learning models are developed to predict traffic flow [111, 92]. For the general discussion of the uses of deep learning in transportation, see [63] for a study of differences and similarities between the neural networks and statistical approaches. For a comprehensive survey of the traffic state estimation on highway, we refer to [125].

Reinforcement Learning Approaches

Deep reinforcement learning (deep-RL) provides a formalism for deep learning of sequential decision making problems with feedback, including continues feedback control. The formulation of deep-RL renders itself as a potentially suitable solution to mobile traffic control. [155, 154, 156] formulate and approach the mixed-autonomy traffic control problem (where both automated and human-driven vehicles are present) using the framework of deep-RL, with the benchmarks for multiple traffic scenarios provided in [145]. The authors of [147] derive novel deep-RL based control policies for autonomous vehicles to improve the throughput of a bottleneck modeled after the San Francisco-Oakland Bay Bridge. [66] demonstrates the ability for model-free deep-RL techniques to generate traffic control strategies for connected and automated vehicles (CAVs) in various network geometries. Deep-RL are also leveraged to design traffic signal timing [83] and to control ramp metering [12].

Limitations of Machine Learning Approaches

The machine learning approaches to mobile traffic control are limited in several ways.

Lack of optimality guarantees: due to the complexity of the Neural Network (NN) structures, numerical methods are oftentimes used to approximate the optimal coefficient given the objective. These empirical studies however lack guarantee of the convergence to an optimal, especially when the underlying task is difficult due to either sparse feedback signal or partial observation. And even when an optimal is obtained, it would be hard to analyze the properties of the reached optimal.

Lack of theoretical studies of the convergence rate: it is not uncommon that online machine learning is necessary for the traffic control problems, when data becomes available in a sequential order and is used to update the best model parameters. Hence a theoretical rate of the convergence to the optimal solution is crucial to guarantee the feasibility of updating the optimal online. However getting such analytical convergence guarantee results

are difficult, both due to the fact that the NN are nebulous black boxes, and the complexity of algorithm design.

Lack of out-of-sample performance guarantees: the benefit of deep learning methods is to leverage a "use-it-for-all" model structure (i.e., the NN) and to automate feature engineering by fitting the model with massive data. However the down side of this approach is that without physics-based modeling or tailoring the model structure to be problem-specific, the NN has no guarantee of extrapolation performance to the out-of-sample data.

Lack of interpretability: due to the black-boxness of the NN models, model interpretation is difficult for deep learning approaches. However, the capability of interpreting the modeling results is essential for improving the model architecture and public policy correspondingly.

Mathematical Approaches to Mobile Traffic Control

Mathematical approaches have historically been essential for the modelling of traffic and optimal control. This class of approaches are usually physics-based, supported by highly developed mathematical theory, and tailored to the specific application in an attempt to balance model accuracy and model complexity.

Mathematical Models

For a comprehensive overview of the modeling of driving behavior, empirical traffic flow phenomena and its stability analysis, we refer to [142].

The traffic dynamics are described by various mathematical models. A classical theory of traffic flow is developed by replacing individual vehicles with continuous fluid density and applying an empirical relation between speed and density. This is termed as a macroscopic traffic flow model, where individual drivers are negligible with respect to the total number of drivers present. The partial differential equations (PDE) are commonly used for the modeling of highway traffic. [87, 114] leverages the kinematic waves or shock waves in PDE to characterize traffic waves. [110] further describes PDE models in mathematical detail for basic flow simulation, ramp metering and diversion, surveillance, and representation of freeway incidents. [5] riches the traffic flow PDE model to a "second order" models, i.e., models with two equations (mass and "momentum"), replacing the space derivative with a convective derivative, and proves the new model nicely predicts instabilities near the vacuum, i.e., for very light traffic. [152] presents a new scalar hyperbolic PDE model for traffic velocity evolution on highways, based on the seminal Lighthill-Whitham-Richards (LWR) PDE for density.

Another class of traffic models is termed microscopic models, which represent individual vehicle movements. The ordinary differential equations (ODE) are applied for the modelling of longitudinal dynamics. The authors of [20] assess the range of options available in the choice of microscopic simulation models with car following models. [44] proposes a car-following model to predict the response of a vehicle in a stream of traffic to the behaviour of

its predecessor. The authors of [9, 8] establish ODE to present a dynamical model of traffic congestion based on the equation of motion of each vehicle. Experimental simulations with a continuous microscopic single-lane ODE model are conducted in [140], with results compared to real data, showing consistency with a recently proposed theoretical phase diagram for traffic near on-ramps.

Queueing systems are leveraged to model the intersections. Queueing models for road traffic flow are developed and discussed in [101, 49, 151].

Finally, stochastic jump systems are used for the modeling of lateral dynamics. The authors of [157] propose a stochastic lane changing model based on multi-lane microscopic traffic model and Markov chain macroscopic model.

Mathematical Methods for Traffic Optimization and Optimal Control

Mathematical methods for traffic optimization and optimal control are ubiquitous in the classical literature. For an all-inclusive overview of traffic control strategies for three areas – urban road networks, freeway networks, and route guidance – is provided in [108]. In response to the ill pattern in traffic, multiple optimal control designs are proposed where the automated vehicle adjust its motion reactive to the preceding traffic. The authors of [133] studies two model-based control laws for the mixed autonomy setting, where the models incorporate the knowledge of the traffic environment. The effect of the two automated vehicle control laws, the Followerstopper controller and the proportional–integral (PI) feedback controller with saturation, on the dissipation of stop-and-go waves is demonstrated experimentally. [153] studies the ability of small numbers of automated vehicles to stabilize a single-lane system of human-driven vehicles, by formalizing the problem in terms of linear string stability and deriving optimality conditions. The adaptive cruise control (ACC) [135, 59, 144] and cooperative ACC (CACC) [128, 112, 91, 127] automatically adapts the cruise control velocity of a vehicle if there is preceding traffic to a safe following distance, where CACC further uses control theory and wireless inter-vehicle communication link to simultaneously optimize the performance of several adjacent vehicles. [62] presents a vehicle driving system in a control-theoretic model predictive control (MPC) framework that effectively improves traffic flow.

Mathematical methods trade model complexity with for the tractability of analysis in the optimal control design. Under certain circumstances, analytical results can be derived for the control-theoretic performance bounds. In [3] the authors conduct a comprehensive analysis on the vehicle string stability by considering a realistic wireless channel under a mobile reactive jamming attack in the CACC system. [149] analyzes stability using bilateral control (BCM) by investigating the underlying systems of differential equations. Finally, [105, 43] theoretically studies the impact of signal delay through wireless vehicle-to-vehicle connection on the traffic control performance.

Limitations of the Previous Approaches

The previous mathematical approaches to mobile traffic control are limited in several ways.

Lack of attention to the theoretical characterization to the model solutions: as the complexity of the mathematical models increases, analytical characterization of the solutions becomes challenging. For instance, this is the case when researchers attempt to generalize linear system theory to highly nonlinear systems, or to extend the theoretical optimality guarantee in isolated/fully-controlled systems to the mixed systems. One example is with the deterministic time-continuous car-following model, the intelligent driver model (IDM), where there is a lack of the analysis of the well-posedness and physical feasibility of the solution.

Lack of characterization of the actuations function space: the design of mathematical models for traffic control is usually based on heuristic. There is a lack of the characterization of a "proper" controller function space as a general guideline to the systematic development of optimal controllers. One example of such characterization can be based on the basis functions, where the acceleration controller can be represented as a linear combination of a set of basis functions.

1.2 Contributions of the Thesis

We breakdown the technical contributions of this thesis as follows.

- **At the vehicle level,** this thesis focuses on a classical car-following model, the IDM. The thesis demonstrates the ill-posedness of the model and presents some improvements to avoid these problems, with solid theoretical foundation built for the well-posedness and safety guanratee.
- **At the mixed autonomy vehicle control level,** this thesis develops and studies performance for basis-based optimal controllers. A rigorous definition of the basis-based controller is given as the solution of a finite-dimensional constrained optimization problem.
- **At the full origin-destination demand routing level,** this thesis designs a control-theoretic scheme for repeated routing games. The parallel network flow allocation problem is cast and solved through Linear Quadratic Regulator (LQR) and model predictive control (MPC) techniques, with the model performance demonstrated with simulation results.

1.3 Outline of the Thesis

The rest of the thesis is organized as follows:

Chapter 2: Limitations and Improvements of the Intelligent Driver Model (IDM)

This chapter introduces a widely used car following model, the IDM, which characterizes the motion of the vehicle by a second order ordinary differential equation. The modeling of the autonomy discussed in this chapter is at the vehicle level, i.e., one focuses on the dynamics of the position and velocities of every vehicle. This chapter points out two mathematical and modelling drawbacks of the classical IDM, i.e., there is no guarantee of a non-negative velocity trajectory and the solution of the system of ODEs might cease to exist in finite time. This chapter theoretically analyzes the existence and uniqueness of a solution for small time horizons, with lower bound on the distance which can be interpreted as a safety distance. Analysis and comparison of adjustments to the classical IDM in this chapter shows the possibility to avoid the problems of the original model. With the modified IDM introduced in this chapter, the global well-posedness of the solutions is proved.

Chapter 3: Design of a Basis-based Feedback Controller with Optimal Control

This chapter introduces a systematic design of optimal basis-based feedback controllers. The modeling of the autonomy discussed in this chapter is at the mixed autonomy level, i.e., one concerns the problem of driving on highways or negotiating effectively with another agent. This chapter discusses the typical choices of basis functions of objective functionals. Numerical results are presented, key metrics and auxiliary visualization are proposed to explore the performance of the optimal controller, to detect potential flaw in the design, and to study the robustness of the optimal basis controller regarding the input tuple. With the approach of this chapter, the feedback controller is trained offline. Trained basis-based feedback controllers are applied online both to the simulator and the field experiments.

Chapter 4: Parallel Network Flow Allocation in Repeated Routing Games via LQR Optimal Control

This chapter studies the repeated routing game problem on a parallel network with affine latency functions on each edge. The modeling of the autonomy discussed in this chapter is at the full origin-destination demand level, i.e., one considers the traffic assignment problem. This chapter provides a control theoretic game design scheme for repeated routing games through the Linear Quadratic Regulator (LQR). The chapter also describes a algorithmic approach to solve the control routing problem using explicit MPC technique. Numerical solutions along with a geometric framework for visualizing optimal routing solutions for every feasible state in the routing game are presented.

Chapter 2

Limitations and Improvements of the Intelligent Driver Model (IDM)

2.1 Introduction

The field of car following modeling historically goes back to the early 1950s' (and probably before) [24, 42]. Most of the early work in this field focused on establishing the model equations, without paying much attention to the mathematical framework required to characterize solutions to the resulting ordinary differential equations (ODEs) describing the motion of the vehicles. The models are mainly classified into *acceleration models* for longitudinal movement, *lane-changing models* for lateral movement and *decisional models* for discrete-choice situations. Among all the car-following models introduced so far ([7, 14, 20, 104, 106] to just name a few) it is worth mentioning the Gazis-Herman-Rothery (GHR) model [24] which determines the relative velocity between two-lane based vehicles, the Safe Distance Model [44], the Optimal Velocity Model [8] in which the acceleration of the single vehicle is controlled according to the velocity of the leading vehicle, and the Intelligent Driver Model (IDM) which is subject of analysis in the present work. For a comprehensive overview of the main car-following models we refer to [142, 96, 53].

The IDM has been introduced in [140] and is a deterministic time-continuous model describing the dynamics of the positions and velocities of every vehicle. Similarly to any car-following model, the idea behind it is that drivers control their vehicles to react to the stimulus from preceding vehicles. It aims to balance two different aspects, the necessity to keep safe separation with the vehicle in front and the desire to achieve "free flow" speed. This model presents some peculiarities which made it subject of intense research in the last two decades. Indeed, it is constructed to be *collision-free*, all the parameters can be interpreted and empirically measured, the stability of the model can be calibrated to empirical data, and there exists an equivalent macroscopic counterpart [50]. In literature we find many extensions of the original IDM, each of which seeks to incorporate new realistic features. The Enhanced IDM [64] presents an improved heuristic of the IDM useful for multi-lane

simulations, which prevents the model from "over-reactions" even when the driver of the leading vehicle suddenly brakes with the maximum possible deceleration.

The Foresighted Driver Model (FDM) starts from the IDM and assumes that a driver acts in a way that balances predictive risk (due to possible collisions along his route) with utility (time required to travel, smoothness of the ride) [36].

Other extensions of the IDM aim to improve the driver safety and to respect the vehicle capability [29], to strengthen the power of each vehicle in proportion to the immediately preceding vehicle [84], and to incorporate the spatially varying velocity profile to account the variation in different types of maneuvers through intersection [86]. Another natural extension is given by Multi-anticipative IDM [143] which models the reaction of a driver to several vehicles ahead just by summing up the corresponding vehicle-vehicle pair interactions with the same weight coefficients.

More recently, stochastic versions of the IDM have been introduced: to describe a probabilistic motion prediction applicable for long term trajectory planning [52], to study mechanisms behind traffic flow instabilities, indifference regions of finite human perception thresholds and external noise [141], and to incorporate context-dependent upper and lower bounds on acceleration [124, 123].

Throughout the decades, most of the engineering community worked on improving the ability of the models to capture specific behavioral phenomena, at the expense of the characterization of the solutions. Thus, to this day, only a few articles use models, and corresponding solutions, that are well characterized in terms of existence, uniqueness, and regularity. An example of this practice is provided by the double integrator $\ddot{x}(t) = u \in U$, where U is the input set, used abundantly as a canonical example in numerous control articles. On the other hand, when models have inherent flaws leading to unbounded or undefined solutions, as in the case of unbounded acceleration, ad hoc methods have been traditionally applied *post facto* by engineering the numerical implementations. For instance, in commonly used microsimulation tools, such as SUMO [89], Aimsun [1] and others, unbounded quantities are clipped, leading to "acceptable" numerical solutions. However, in the process, the fidelity to the original model is compromised, and the numerical simulations may not represent any instantiation of the model. Consequently, the properties of the considered continuous model might be lost as well. Finally, the process of clipping can introduce additional issues, not necessarily present in the original model, and prevent the definition of any theoretical models corresponding to the obtained numerical simulations. The present article thus attempts to provide a full pipeline in which the model is first mathematically well defined (including existence, uniqueness and regularity characterization of the solutions), and then numerically implemented using appropriate numerical differentiation schemes. The final achievement is a thorough correspondence between theory and implementation. The well-posedness of car-following models is also fundamental to model the traffic flow from the mean-field perspective, see [40, 46].

The aim of this contribution

The introduced IDM has two mathematical and modelling drawbacks:

- The velocities of specific vehicles might become negative at specific times, which might not be desirable from a modelling point of view.
- The velocities of specific vehicles might diverge to $-\infty$ in finite time, so that the solution of the system of ODE's ceases to exist.

We will discuss these drawbacks and determine under which conditions on the initial datum and parameters they can happen. We will present several improvements so that the solutions exist on every finite time horizon.

Structure of this chapter

The chapter is organized in the following way. In Section 2.2 we review the classical Intelligent Driver Model (IDM) and describe briefly the physical meaning of the parameters involved. Well-posedness of the IDM for small time horizon is stated in theorem 2.2.1. In Section 2.3 we analyze peculiar and possibly pathological behaviors of the model. Specifically, we provide explicit settings in which it produces negative velocities (example 2.3.1), negative velocities and blow-up of the solution in finite time (example 2.3.2, example 2.3.3). Section 2.4 collects some of the main results of this work. Existence and uniqueness of a solution for small times with lower bound on the distance which can be interpreted as "collision free." Section 2.5 is devoted to the exploration, analysis and comparison of adjustments to the classic IDM in order to avoid the problems mentioned in Section 2.3 for general initial data. To this end, we introduce modified versions of the IDM for which well-posedness is proved: the *projected IDM*, the *acceleration projected IDM*, and the *velocity regularized acceleration IDM* defined respectively in definition 2.5.1, definition 2.5.2, definition 2.5.4. A further and more drastic adjustment to the classic model is proposed in definition 2.5.5 which involves a discontinuous acceleration, and therefore is denoted as *discontinuous improvement*. In Section 2.6 we present some well-posedness results for the many vehicle case (based on the previous analysis in Section 2.5, and finally, in Section 2.7 we draw conclusions from our work and mention possible research directions opened by this contribution.

2.2 The intelligent driver model (IDM): Definitions and basic results

In this section we introduce the intelligent driver model (IDM) as the following system of ordinary differential equations. To this end, we require to define the acceleration function as follows:

Definition 2.2.1 (The IDM acceleration)**.** *Let $T \in \mathbb{R}_{>0}$ be fixed. For a parameter set $(a, b, v_{free}, \tau, s_0, l, \delta) \in \mathbb{R}^3_{>0} \times (0, T) \times \mathbb{R}^2_{>0} \times \mathbb{R}_{>1}$ we define the following IDM car-following acceleration on the set*

$$\mathcal{A} \coloneqq \{(x, v, x_\ell, v_\ell) \in \mathbb{R}^4 : \ x_\ell - x - l > 0\},$$
$$\mathrm{Acc} : \begin{cases} \mathcal{A} & \to \mathbb{R} \\ (x, v, x_\ell, v_\ell) & \mapsto a\Big(1 - \big(\frac{|v|}{v_{free}}\big)^\delta - \Big(\frac{2\sqrt{ab}(s_0 + v\tau) + v(v - v_\ell)}{2\sqrt{ab}(x_\ell - x - l)}\Big)^2\Big). \end{cases}$$

Remark 2.2.1 (Absolute values in the IDM Acceleration)**.** *It is worth mentioning that in most literature the parameter δ is not precisely specified except that it is assumed to be positive. However, as we will show, velocities can become negative, and this is why we assumed that the acceleration term in definition 2.2.1 involves the absolute value of the velocity so that*

$$\big(\tfrac{|v|}{v_{free}}\big)^\delta \tag{2.2.1}$$

is well defined for all $v \in \mathbb{R}$ and $\delta \in \mathbb{R}_{>0}$. Obviously, this is only one choice, and it might be more reasonable to replace it by

$$\mathrm{sgn}(v)\big(\tfrac{|v|}{v_{free}}\big)^\delta \tag{2.2.2}$$

so that this term contributes positive to the acceleration for negative velocities and indeed counteracts a negative velocity. For $\delta \in 2\mathbb{N}_{\geq 1} + 1$ eq. (2.2.2) can actually be replaced by the version without the absolute value and the same is true for $\delta \in 2\mathbb{N}_{\geq 1}$ with the drawback that this part of the acceleration will always remain negative as we also assume for now in definition 2.2.1.

An analysis similar to the one in this paper can then be carried out with mentioning that although in this case the solution's velocity can diverge to $-\infty$.

As we will require for the leader a specific acceleration, the "free-flow acceleration," we define as follows

Definition 2.2.2 (Free flow acceleration)**.** *For $(a, v_{free}, \delta) \in \mathbb{R}^2_{>0} \times \mathbb{R}_{>1}$ the **free flow** acceleration is defined by*

$$\mathrm{Acc}_{\mathrm{front}} : \begin{cases} \mathbb{R}^2 & \to \mathbb{R} \\ (x, v) & \mapsto a\Big(1 - \big(\frac{|v|}{v_{free}}\big)^\delta\Big). \end{cases}$$

Having defined the acceleration function, we are ready to present definition 2.2.3:

Definition 2.2.3 (The IDM)**.** *Given definition 2.2.1, we call the following system of ordinary differential equations in position $\boldsymbol{x} = (x_\ell, x) : [0, T] \to \mathbb{R}^2$ and velocity $\boldsymbol{v} = (v_\ell, v) : [0, T] \to$*

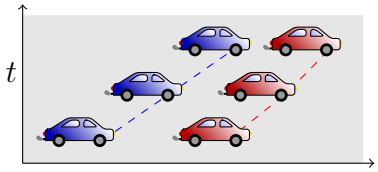

Figure 2.1: For $t \in [0,T]$ the leader $x_\ell(t)$ with its dynamics determined by the acceleration $u_{\text{lead}}(t)$ and the follower $x(t)$ with its dynamics governed by the classical IDM (acceleration Acc as in definition 2.2.1). The overall dynamics is stated in definition 2.2.3. The follower approaches the leader. Will they collide?

$\mathbb{R}^2$

$$\begin{aligned} \dot{x_\ell}(t) &= v_\ell(t), & t &\in [0,T], \\ \dot{v_\ell}(t) &= u_{lead}(t), & t &\in [0,T], \\ \dot{x}(t) &= v(t), & t &\in [0,T], \\ \dot{v}(t) &= \mathrm{Acc}(x(t), v(t), x_\ell(t), v_\ell(t)), & t &\in [0,T], \\ (x_\ell(0), x(0)) &= (x_{\ell,0}, x_0), \\ (v_\ell(0), v(0)) &= (v_{\ell,0}, v_0), \end{aligned} \tag{2.2.3}$$

with leading dynamics $u_{lead} : [0,T] \to \mathbb{R}$ *the car-following* ***IDM****.* $(x_0, x_{\ell,0}, v_0, v_{\ell,0}) \in \mathbb{R}^2 \times \mathbb{R}^2_{\geq 0}$ *are initial positions and velocities.*

This is schematically illustrated in fig. 2.1. We give a short overview of some of the meanings of the parameters in the IDM.

Remark 2.2.2 (Meaning of the previously introduced parameters)**.** *The parameters* a*,* b*,* v_{free}*,* τ*,* s_0*,* l *and* δ*, introduced in definition 2.2.1, are model parameters which have – according to [140] – the following meaning:*

acceleration a*: the maximum vehicle acceleration;*

comfortable braking deceleration b*: a positive number;*

desired velocity v_{free}*: the velocity the vehicle would drive at in free traffic;*

desired time headway τ*: the minimum possible time to the vehicle in front;*

minimum spacing s_0*: a minimum desired net distance;*

the length of the vehicle l*;*

the acceleration exponent δ*: Specifying how the acceleration decreases when approaching the desired velocity* v_{free}*.*

table 2.1 shows some suggested values for the parameters already identified in [140].

Table 2.1: According to [140] typical and physical meaningful variables for the IDM

Parameters	**Variable**	**Suggested value**
Maximum acceleration	a	$0.73\ m/s^2$
Desired deceleration	b	$1.67\ m/s^2$
Desired velocity	v_{free}	$120\ km/h$
Desired time headway	τ	$1.6\ s$
Minimum spacing	s_0	$2\ m$
Length of the vehicle	l	$5\ m$
Acceleration exponent	δ	4

For the system to be physically reasonable we require some additional assumptions on the order of the initial position and other parameters for the acceleration functions. This is made precise in the following assumption (1).

Assumption 1 (Assumptions on input datum and more)**.** *We assume that*

Leading velocity: $u_{lead} \in \mathcal{U}_{lead} \coloneqq \left\{ u \in L^\infty((0,T)) : v_{\ell,0} + \int_0^t u(s)\,\mathrm{d}s \geq 0 \ \forall t \in [0,T] \right\}$.

Input parameters for Acc**:** $(a, b, v_{free}, \tau, s_0, l, \delta) \in \mathbb{R}^3_{>0} \times (0,T) \times \mathbb{R}^2_{>0} \times \mathbb{R}_{>1}$.

Physical relevant initial datum: $(x_0, x_{\ell,0}, v_0, v_{\ell,0}) \in \mathbb{R}^2 \times \mathbb{R}^2_{\geq 0} :\ x_0 < x_{\ell,0} - l$.

The previous assumption on the involved datum enables it to prove the well-posedness on a significantly small time horizon, i.e., that there exists a solution on the time horizon and that this solution is unique:

Theorem 2.2.1 (Well-posedness of sufficiently small time horizon)**.** *Given $N \in \mathbb{N}_{\geq 0}$ and assumption (1), there exists a small enough time $T^* \in \mathbb{R}_{>0}$ so that the IDM in definition 2.2.3 admits a unique solution $(x, x_\ell) \in W^{2,\infty}([0,T^*])^2$.*

Proof. The right hand side of definition 2.2.3 is around the initial datum in assumption (1) locally Lipschitz-continuous. The existence and uniqueness on a small time horizon then follows by the Picard-Lindelöf Theorem ([28, Chapter 4] or [27, Thm 1.3]). □

2.3 Counterexamples

Given theorem 2.2.1, the next natural questions consist of whether the solution on the small time horizon can be extended to any finite time horizon and whether the model remains reasonable. As it turns out, neither points hold if we do not restrict our initial datum beyond assumption (1). Of course, such unreasonable behavior appears with specific initial datum, however this may in fact happen frequently when different traffic scenarios are analyzed.

Especially, such initial datum could happen in the presence of lane-changing, on ramps and other network components as it is the case for most commonly used micro-simulators. We present the shortcomings in the following.

Negative velocity

In this subsection, we show that the IDM can develop negative velocities for the following vehicle, although the leading vehicle might drive with positive speed. The reason for this is that if the following vehicle is too close to the leading vehicle, it needs to slow down. Assume now that it actually has already zero velocity, it will need to move backwards to make it to the "safety" distance s_0 it aims for.

Example 2.3.1 (Negative velocity). Assume that $x_0 = x_{\ell,0} - l - \varepsilon$ for $\varepsilon \in \mathbb{R}_{>0}$ yet to be determined and $v_0 = 0$. Then, we compute the change of velocity for the following vehicle and have for $t \in [0, T]$ according to definition 2.2.3

$$\dot{v}(t) = a\left(1 - \left(\tfrac{|v(t)|}{v_{\text{free}}}\right)^{\delta} - \left(\tfrac{2\sqrt{ab}(s_0 + v(t)\tau) + v(t)(v(t) - v_\ell(t))}{2\sqrt{ab}(x_\ell(t) - x(t) - l)}\right)^2\right).$$

Plugging in $t = 0$ leads to

$$\dot{v}(0) = a\left(1 - \left(\tfrac{2\sqrt{ab}s_0}{2\sqrt{ab}\varepsilon}\right)^2\right) = a\left(1 - \left(\tfrac{s_0}{\varepsilon}\right)^2\right).$$

Thus, whenever $\varepsilon < s_0$, the following vehicle has – at least for small time horizon – a negative speed, although the leading vehicle drives with arbitrary speed $v_\ell \in \mathbb{R}$. This is also detailed in the following fig. 2.2 and in fig. 2.3 it is demonstrated that for larger spacing this does not occur.

A more reasonable approach for avoiding this type of behavior is that the following car just waits until the leading car has moved farther away. This can be achieved by adjusting the model accordingly as done in Section 2.5.

Velocity exploding in finite time

In this subsection, we show that the solution can cease to exist in finite time. We first present an example, with fixed parameters, to explain the reasons behind this phenomenon. Then, we generalize the example and illustrate how this phenomenon may occur for parameters in a whole region of the space.

Example 2.3.2 (Negative velocity and a blow-up of the solution in finite time). Assume the constants and initial data are as in example 2.3.1, with $0 < \varepsilon < 1$ and non-negative initial velocity of the leading vehicle $v_{\ell,0} \geq 0$. The leading vehicle's position is given by

$$x_\ell(t) = x_{\ell,0} + v_{\ell,0}t + \tfrac{u}{2}t^2,$$

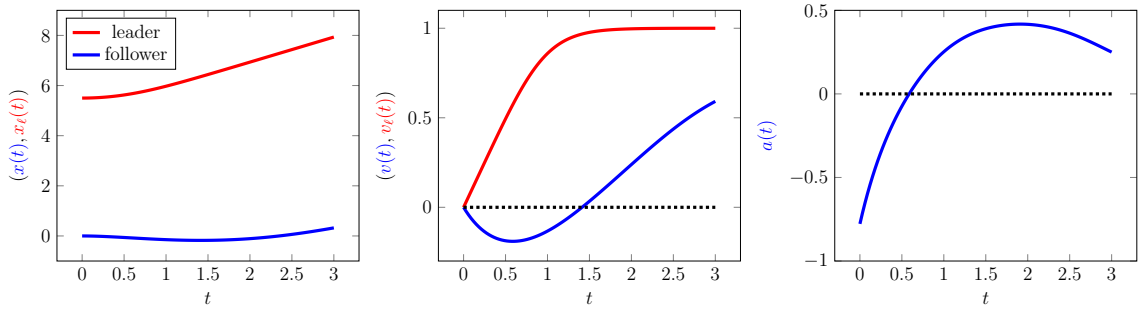

Figure 2.2: The IDM with parameters $a = 1,\ b = 2,\ v_{\text{free}} = 1,\ \tau = 1.6,\ l = 4,\ s_0 = 2,\ d = 4$ and datum $x_0 = 0,\ x_{\ell,0} = l + 1.5 < l + s_0,\ v_0 = 0,\ v_{\ell,0} = 0$. **Left:** vehicles' positions, **middle:** vehicles' velocities and **right:** followers acceleration. The leader follows the free flow acceleration profile as in definition 2.2.2. As the initial distance between the two vehicles is smaller than s_0, the following vehicle moves backwards to increase the space.

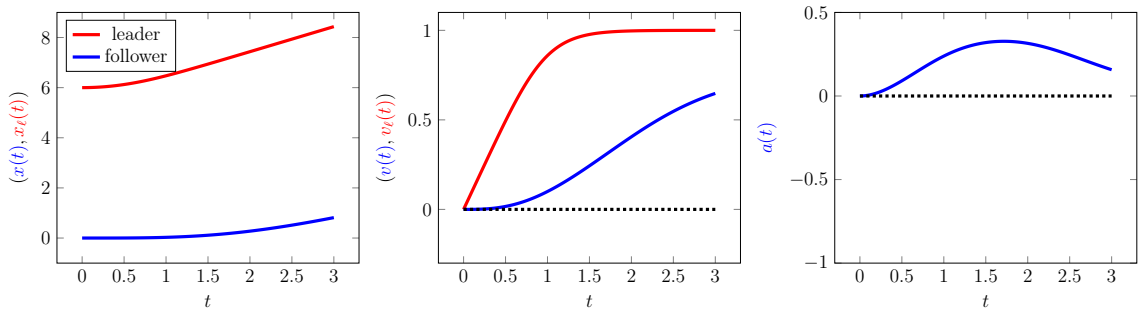

Figure 2.3: Continuation of fig. 2.2: The IDM with parameters $a = 1,\ b = 2,\ v_{\text{free}} = 1,\ \tau = 1.6,\ l = 4,\ s_0 = 2,\ d = 4$ and datum $x_0 = 0,\ x_{\ell,0} = l + 2 = l + s_0,\ v_0 = 0,\ v_{\ell,0} = 0$. The leader follows the free flow acceleration as in definition 2.2.2. The initial distance between the two vehicles is large enough so that the following vehicle does not attain negative velocity.

and the leading vehicle's velocity by

$$v_\ell(t) = v_{\ell,0} + ut.$$

Plugging this into the equations for the follower, we obtain the following system of ODEs

$$\begin{aligned}
\dot{x}(t) &= v(t) \\
\dot{v}(t) &= a\left(1 - \left(\frac{|v(t)|}{v_{\text{free}}}\right)^\delta - \left(\frac{2\sqrt{ab}(s_0 + v(t)\tau) + v(t)(v(t) - v_\ell(t))}{2\sqrt{ab}\cdot(x_\ell(t) - x_{\ell,0} + \varepsilon - \int_0^t v(s)\,\mathrm{d}s)}\right)^2\right) \\
x(0) &= x_{\ell,0} - l - \varepsilon \\
v(0) &= 0.
\end{aligned}$$

Now we fix $v_{\text{free}} = 1 = a$, $s_0 = 16$, $b = \frac{1}{4a}$, $\tau = 8$, $v_{\ell,0} = 0$, $u = 0$, $\delta = 4$ and $x_{\ell,0} = 0$, which gives

$$\begin{aligned}\dot{x}(t) &= v(t)\\ \dot{v}(t) &= 1 - \big(v(t)\big)^4 - \left(\tfrac{(4+v(t))^2}{\varepsilon - \int_0^t v(s)\,\mathrm{d}s}\right)^2.\end{aligned}$$

We now show that there exists $\bar{t}$ such that $v(\bar{t}) < -1$. Assume, by contradiction, that $v(t) \geq -1$ on $t \in [0,1]$, then since $\varepsilon < 1$ for $t \in [0,1]$ we get

$$\dot{v}(t) \leq 1 - \left(\tfrac{(4+v(t))^2}{\varepsilon - \int_0^t v(s)\,\mathrm{d}s}\right)^2 \leq 1 - \big(\tfrac{4}{\varepsilon+1}\big)^2 \leq 1 - \big(2\big)^2 = -3, \tag{2.3.1}$$

and by integration and by the previous assumption we have

$$-1 \leq v_0 + \int_0^t \dot{v}(s)\,\mathrm{d}s \leq v_0 - 3t$$

and therefore – plugging in for instance $t = 1$

$$-1 \leq \int_0^1 \dot{v}(s)\,\mathrm{d}s \leq -3,$$

a contradiction.

Blow-up of the solution in finite time Let $t^* \in (0,T]$ denote the first time such that $v(t^*) < -1$. Then, recalling the semi-group property of ODEs, we can consider the initial value problem in $\tilde{v} : [t^*, T] \to \mathbb{R}$

$$\begin{aligned}\tilde{v}(t^*) &= v(t^*) < -1\\ \dot{\tilde{v}}(t) &= 1 - \big(\tilde{v}(t)\big)^4 - \left(\tfrac{(4+\tilde{v}(t))^2}{\varepsilon - \int_0^t \tilde{v}(s)\,\mathrm{d}s}\right)^2 \qquad t \in [t^*, T].\end{aligned}$$

Estimating $\dot{\tilde{v}}$, we have

$$\dot{\tilde{v}}(t) \leq 1 - \big(\tilde{v}(t)\big)^4 \quad \forall t \in [t^*, T].$$

As the initial value $\tilde{v}(t^*) < -1$ we obtain that $\tilde{v}$ is monotonically decreasing and we can thus estimate

$$\dot{\tilde{v}}(t) \leq 1 - \big(\tilde{v}(t)\big)^2 \quad \forall t \in [t^*, T]$$

which can be solved explicitly to obtain

$$\tilde{v}(t) \leq \tfrac{v(t^*)\exp(2t) + v(t^*) + \exp(2t) - 1}{\exp(2t) + 1 + v(t^*)(\exp(2t) - 1)}.$$

However, the right hand side goes to $-\infty$ when $t \to \frac{1}{2}\ln\left(\frac{-1+v(t^*)}{1+v(t^*)}\right)$ and thus, also the solution for v ceases to exist for $t \geq t^* + \frac{1}{2}\ln\left(\frac{-1-v(t^*)}{1+v(t^*)}\right)$. This is illustrated in fig. 2.4.

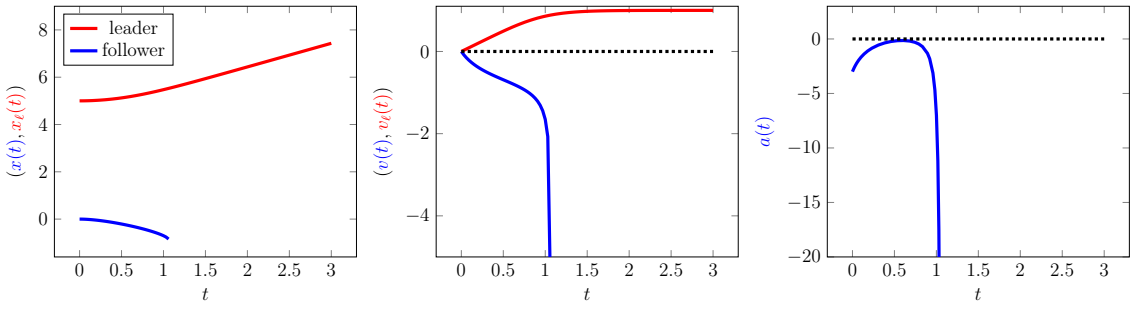

Figure 2.4: Same parameters as in fig. 2.2, but $x_{\ell,0} = l + 1 < l + s_0$. **Left:** Positions of the vehicles; **Middle:** Velocities of the vehicles, **Right:** Acceleration of the follower. Velocity of the follower diverging to $-\infty$ around $t \approx 1.06$. The solution ceases to exist for larger t.

In this example, we chose very specific parameters for convenience. However, the same behavior and divergence of the speed to $-\infty$ in finite time can be shown for a rather general range of parameters. This is presented in example 2.3.3. To prove this, we start by showing the following Lemma.

Lemma 2.3.1 (Sufficiently negative velocity in small time)**.** *Assume that the initial velocity of the following vehicle $v_0 = 0$, the initial velocity of the leading vehicle $v_{\ell,0} > 0$, and the initial positions of the two vehicles are separated by $l + \varepsilon$ for some $\varepsilon \in (0, s_0)$, i.e., $x_{\ell,0} - x_0 - l = \varepsilon < s_0$. Choose parameters s_0, τ and v_{free} such that $-\frac{s_0}{1.01\tau} < -v_{free}$, let $\delta > 1$ and let $v_{\max} > 0$ be an upper bound for the vehicles' velocities. Then there exists $t^{**} \in [0, T]$, such that $v(t^{**}) < -v_{free}$.*

Proof. We consider two different cases:

- If there exists $t^* \in [0, T]$, such that $v(t^*) < -v_{\text{free}}$, then we chose $t^{**} = t^*$.
- Otherwise, we assume that for every $t \in [0, T]$, $v(t) \geq -v_{\text{free}}$ which implies that $v(t) > -\frac{s_0}{1.01\tau}$, i.e.,
$$s_0 + v(t)\tau > \tfrac{s_0}{101} > 0. \tag{2.3.2}$$

By the definition of $v_{\max}$ and v_{free}, we have for every $t \in [0, T]$, $v_\ell(t) - v(t) \leq v_{\max} + v_{\text{free}}$. Furthermore, since $v_\ell(t) > 0$ and $v(t) < 0$, we have $v(t)(v(t) - v_\ell(t)) > 0$. Then one can find an upper bound for the distance between the two vehicles. That is, for every $t \in [0, T]$,

$$x_\ell(t) - x(t) - l \leq \varepsilon + (v_{\max} + v_{\text{free}})t. \tag{2.3.3}$$

Therefore, for every $t \in [0, T]$,

$$\dot{v}(t) = a\left(1 - \left(\tfrac{|v(t)|}{v_{\text{free}}}\right)^\delta - \left(\tfrac{2\sqrt{ab}(s_0 + v(t)\tau) + v(t)(v(t) - v_\ell(t))}{2\sqrt{ab}(x_\ell(t) - x(t) - l)}\right)^2\right) \tag{2.3.4}$$

$$\leq a\left(1-\left(\frac{2\sqrt{ab}(s_0+v(t)\tau)+v(t)(v(t)-v_\ell(t))}{2\sqrt{ab}(x_\ell(t)-x(t)-l)}\right)^2\right) \tag{2.3.5}$$

$$\leq a\left(1-\left(\frac{s_0+v(t)\tau}{x_\ell(t)-x(t)-l}\right)^2\right) \tag{2.3.6}$$

$$\leq a\left(1-\left(\frac{s_0+v(t)\tau}{\varepsilon+(v_{\max}+v_{\text{free}})t}\right)^2\right) \tag{2.3.7}$$

$$\leq a\left(1-\left(\frac{\frac{s_0}{101}}{\varepsilon+(v_{\max}+v_{\text{free}})t}\right)^2\right). \tag{2.3.8}$$

Note that inequality (2.3.5) is true since $\frac{|v(t)|}{v_{\text{free}}}$ is non-negative, inequality (2.3.6) is due to the fact that for every $t \in [0,T]$, $v(t)(v(t)-v_\ell(t)) > 0$, inequality (2.3.7) is because of the upper bounded for the distance between the two vehicles given by inequality (2.3.3), and inequality (2.3.8) is due to inequality (2.3.2).

Hence, for every $t \in [0,T]$,

$$\begin{aligned} v(t) &\leq a\int_0^t \left(1-\left(\frac{\frac{s_0}{101}}{\varepsilon+(v_{\max}+v_{\text{free}})s}\right)^2\right)\mathrm{d}s \\ &= a\left(t+\frac{s_0^2}{101^2(v_{\max}+v_{\text{free}})}\left(\frac{1}{\varepsilon+(v_{\max}+v_{\text{free}})t}-\frac{1}{\varepsilon}\right)\right) = at\left(1-\frac{s_0^2}{101^2}\frac{1}{\varepsilon(\varepsilon+(v_{\max}+v_{\text{free}})t)}\right). \end{aligned}$$

Setting $t=\varepsilon$, we have,

$$v(\varepsilon) \leq a\varepsilon\left(1-\frac{s_0^2}{101^2}\frac{1}{\varepsilon(\varepsilon+(v_{\max}+v_{\text{free}})\varepsilon)}\right) = a\frac{101^2\varepsilon(\varepsilon+(v_{\max}+v_{\text{free}})\varepsilon)-s_0^2}{101^2(\varepsilon+(v_{\max}+v_{\text{free}})\varepsilon)} \to -\infty \text{ as } \varepsilon \to 0.$$

Note that the upper bound for the velocity at time $t=\varepsilon$ goes to negative infinity as ε goes to zero. Therefore, for $\varepsilon > 0$ small enough, we have,

$$v(\varepsilon) \leq -v_{\text{free}}.$$

Hence, there exists $t^{**} = \varepsilon \in [0,T]$, such that $v(t^{**}) < -v_{\text{free}}$. □

The previous Lemma guarantees that for properly chosen initial datum and velocity the follower's velocity can become more negative than $-v_0$, the negative free-flow velocity. This enables us to prove that the solution ceases to exist in finite time. This result is related to the famous example of a blow-up of solutions to the Riccati ODEs for specific initial datum in finite time:

Example 2.3.3 (Negative velocity and a blow-"down" of the velocity in finite time). Again, we assume the parameters and initial data as in lemma 2.3.1. Then by lemma 2.3.1, there exists $t^{**} \in [0,T]$, such that $v(t^{**}) < -v_{\text{free}}$. Recall that $\delta > 1$. For any time t such that $v(t) < -v_{\text{free}}$,

$$\dot{v}(t) \leq a\left(1-\left(\frac{|v(t)|}{v_{\text{free}}}\right)^\delta\right) < 0$$

Thus v is strictly decreasing on the time interval $[t^{**}, T]$. In addition, we are going to show that v ceases to exist in finite time and that there exists $t_1 > 0$ such that $\lim_{t \to t_1} v(t) = -\infty$. Assume by contradiction that this is not the case. Then as $v(T) < -v_0$ the solution remains strictly decreasing as long as it exists and as it does not reach $-\infty$ in finite time it can be extended on $[0, +\infty)$ and is strictly decreasing on $[T, +\infty)$. Therefore we have the following

$$\int_T^t \frac{\dot{v}(s)}{1-\left(\frac{|v(s)|}{v_{\text{free}}}\right)^\delta} \, \mathrm{d}s \geq a(t-T), \ \forall t \in [T, +\infty). \tag{2.3.9}$$

As v is strictly decreasing we can perform a change of variable in the integral by setting $y = -v(s)$ to get

$$\int_{-v(T)}^{-v(t)} \frac{1}{\left(\frac{y}{v_{\text{free}}}\right)^\delta - 1} \, \mathrm{d}y \geq a(t-T), \ \forall t \in [T, \infty). \tag{2.3.10}$$

Note that $-v(T) > v_0$. We denote $\eta \coloneqq -v(T) - v_{\text{free}} > 0$, eq. (2.3.10) implies

$$\int_{v_{\text{free}}+\eta}^{+\infty} \frac{1}{\left(\frac{y}{v_{\text{free}}}\right)^\delta - 1} \, \mathrm{d}y \geq a(t-T), \ \forall t \in [T, \infty). \tag{2.3.11}$$

Letting $t \to +\infty$ this implies that

$$\int_{v_{\text{free}}+\eta}^{+\infty} \frac{1}{\left(\frac{y}{v_{\text{free}}}\right)^\delta - 1} \, \mathrm{d}y = \infty, \tag{2.3.12}$$

but because $\delta > 1$ we have $\int_{v_{\text{free}}+\eta}^{+\infty} \frac{1}{\left(\frac{y}{v_{\text{free}}}\right)^\delta - 1} \, \mathrm{d}y \in \mathbb{R}$, which gives a contradiction. Therefore, v ceases to exist and diverges to $-\infty$ in finite time.

As we have seen from the previous example 2.3.3 the velocity can blow-up in finite time. However, what is not clear is whether the position of the car can consequently also explode. Thanks to the relation between position and velocity, i.e., $x'(t) = v(t), \ t \in [0, T]$ this is a matter of whether $v \in L^1((0, t^*))$ if t^* is the time where the velocity goes to $-\infty$. And indeed, it can be shown that this holds true and the position remains bounded:

Corollary 2.3.1 (Boundedness of the position in the case of a blow-up of velocity)**.** *Let assumption (1), $\delta \in \mathbb{R}_{>2}$) and assume that – as investigated in example 2.3.3 – there exists a time horizon $t^* \in \mathbb{R}_{>0}$ so that*

$$\lim_{t \nearrow t^*} v(t) = \lim_{t \nearrow t^*} \dot{x}(t) = -\infty.$$

Then, the position at the time of the blow-up remains finite, i.e.

$$\exists c \in \mathbb{R} : \lim_{t \nearrow t^*} x(t) = c$$

or equivalently stated

$$v \in L^1((0, t^*)).$$

Proof. The proof consists of showing that the L^1 mass of the velocity remains bounded. To this end, we estimate the acceleration from above. Choose $t_1 \in [0, t^*]$ so that

$$\Big(v(s)^2 - v(s)v_\ell(s) + 2\sqrt{ab}\big(s_0 + v(s)\tau\big)\Big)^2 > 0 \wedge v(s) \leq -\max\big\{2v_{\text{free}}, 1\big\} \qquad \forall s \in [t_1, t^*).$$

Such a t_1 always exists as v diverges to $-\infty$ so that for s close enough to t^* the quadratic term in the previous estimate will always outnumber the affine linear term and v_ℓ is essentially bounded. Then, recalling definition 2.2.1 of the IDM we have for $s \in [t_1, t^*)$

$$\dot{v}(t) \leq -\tfrac{a}{2}\left(\tfrac{|v(t)|}{v_{\text{free}}}\right)^\delta.$$

Assuming $\delta \in \mathbb{R}_{>2}$ divide by $|v(t)|^{\delta-1}$ (this is possible because v is strictly decreasing and $v(t_1) < -1$), and integrating between t_1 and $t \in [t_1, t^*)$, one has

$$\begin{aligned} \int_{t_1}^{t} \tfrac{\dot{v}(\tau)}{|v(\tau)|^{\delta-1}} d\tau &\leq -\tfrac{a}{2v_{\text{free}}^\delta} \int_{t_1}^{t} |v(\tau)| \,\mathrm{d}\tau, \\ \tfrac{(-v)^{2-\delta}(t)}{\delta-2} - \tfrac{(-v)^{2-\delta}(t_1)}{\delta-2} &\leq -\tfrac{a}{2v_{\text{free}}^\delta} \int_{t_1}^{t} |v(\tau)| \,\mathrm{d}\tau. \end{aligned} \tag{2.3.13}$$

Dividing by $-a/2v_{\text{free}}^\delta < 0$ and letting $t \to t^*$, this gives

$$\left(\tfrac{a}{2v_{\text{free}}^\delta}\right)^{-1} \tfrac{(-v)^{2-\delta}(t_1)}{\delta-2} \geq \|v\|_{L^1((t_1,t^*))}. \tag{2.3.14}$$

Hence, $\|v\|_{L^1((t_1,t^*))} < +\infty$.

□

The previous estimate is particularly interesting as it illustrates that the model behaves still "somehwat" reasonable (even in the case of a diverge of the velocity to $-\infty$) and underlines the fact that a change in the acceleration to prevent the velocity to diverge might be enough to "improve" the model (compare Section 2.5).

2.4 Lower bounds on the distance in specific cases

In this section we state results guaranteeing the minimal distance between leader and follower for the IDM.

Theorem 2.4.1 (Minimal "safety distance" for the IDM)**.** *Let assumption (1) hold and particularly $v_\ell \geqq 0$. Assume that for an arbitrary time $T \in \mathbb{R}_{>0}$ the solution to the IDM exists. Then, the IDM as in definition 2.2.3 satisfies the following lower bound on the distance*

- *if the initial relative velocity is positive, i.e., $v_{\ell,0} - v_0 \geq 0$*

$$x_\ell(t) - x(t) - l \geq \min\left\{x_{\ell,0} - x_0 - l, \sqrt{\tfrac{as_0^2}{-B}}\right\} > 0 \quad \forall t \in [0, T] \tag{2.4.1}$$

- *if the initial relative velocity is negative, i.e.,* $v_{\ell,0} - v_0 < 0$

$$x_\ell(t) - x(t) - l \geq \min\left\{ \frac{-A+\sqrt{A^2+4aBs_0^2}}{2B}, \sqrt{\frac{as_0^2}{-B}} \right\} > 0 \quad \forall t \in [0,T] \tag{2.4.2}$$

with the constants A, B *given as*

$$\begin{aligned} A &\coloneqq -B \cdot (x_{\ell,0} - x_0 - l) + a\tfrac{s_0^2}{x_{\ell,0}-x_0-l} + \tfrac{1}{2}\big(v_{\ell,0} - v_0\big)^2 > 0 \\ B &\coloneqq \operatorname*{ess\text{-}inf}_{s\in[0,T]} u_{lead}(s) - a. \end{aligned} \tag{2.4.3}$$

Proof. We start with considering the difference of the change between leader's acceleration and follower's acceleration to obtain for $t \in [0,T]$

$$\begin{aligned} \ddot{x}_\ell(t) - \ddot{x}(t) &\geq u_{\text{lead}}(t) - a + a\Big(\tfrac{|v(t)|}{v_{\text{free}}}\Big)^\delta + a\Big(\tfrac{2\sqrt{ab}(s_0+v(t)\tau)+v(t)(v(t)-v_\ell(t))}{2\sqrt{ab}\big(x_\ell(t)-x(t)-l\big)}\Big)^2 \\ &\geq u_{\text{lead}}(t) - a + a\Big(\tfrac{2\sqrt{ab}(s_0+v(t)\tau)+v(t)(v(t)-v_\ell(t))}{2\sqrt{ab}\big(x_\ell(t)-x(t)-l\big)}\Big)^2. \end{aligned}$$

Let us first assume that $v_{\ell,0} - v_0 < 0$. Then, we know that on a time horizon $[0,t_1)$, $v_\ell(t) - v(t) < 0$ and the distance of follower and leader decreases but there is still no overtaking, i.e., $x_\ell(t) - x(t) - l > 0$. Thus, we can continue the previous estimate to arrive at (recall that $v_\ell(t) \geqq 0$ so that $v(t) > 0$ as $v(t) > v_\ell(t)$ for $t \in [0,t_1)$)

$$\ddot{x}_\ell(t) - \ddot{x}(t) \geq \operatorname*{ess\text{-}inf}_{s\in[0,T]} u_{\text{lead}}(s) - a + as_0^2 \tfrac{1}{(x_\ell(t)-x(t)-l)^2}.$$

Multiplying with $\dot{x}_\ell(t) - \dot{x}(t) < 0$ leads to

$$\big(\ddot{x}_\ell(t) - \ddot{x}(t)\big)\big(\dot{x}_\ell(t) - \dot{x}(t)\big) \leq \Big(\operatorname*{ess\text{-}inf}_{s\in[0,T]} u_{\text{lead}}(s) - a\Big)\big(\dot{x}_\ell(t) - \dot{x}(t)\big) + as_0^2 \tfrac{\dot{x}_\ell(t)-\dot{x}(t)}{(x_\ell(t)-x(t)-l)^2}$$

and integrating over $t \in [0,t_1]$ gives

$$\begin{aligned} \tfrac{1}{2}(v_\ell(t) - v(t))^2 \leq \tfrac{1}{2}(v_{\ell,0} - v_0)^2 &+ \Big(\operatorname*{ess\text{-}inf}_{s\in[0,T]} u_{\text{lead}}(s) - a\Big)\Big(x_\ell(t) - x(t) - x_{\ell,0} + x_0\Big) \\ &- as_0^2\Big(\tfrac{1}{x_\ell(t)-x(t)-l} - \tfrac{1}{x_{\ell,0}-x_0-l}\Big) \end{aligned}$$

Defining $A \coloneqq -B \cdot (x_{\ell,0} - x_0 - l) + a\frac{s_0^2}{x_{\ell,0}-x_0-l} + \frac{1}{2}\big(v_{\ell,0} - v_0\big)^2 > 0$ and $g(t) \coloneqq x_\ell(t) - x(t) - l$ with $B \coloneqq \operatorname*{ess\text{-}inf}_{s\in[0,T]} u_{\text{lead}}(s) - a.$ we have

$$\tfrac{1}{2}\big(g'(t)\big)^2 \leq A + Bg(t) - \tfrac{as_0^2}{g(t)}.$$

However, as the left hand side is quadratic, the following inequality needs to hold (recall that $g(t) > 0$ on $[0, t_1)$)

$$0 \leq Ag(t) + Bg(t)^2 - as_0^2.$$

Recalling that $B < 0$, we thus obtain as lower bound

$$g^* \coloneqq \tfrac{-A+\sqrt{A^2+4aBs_0^2}}{2B} > 0$$

which is greater zero as $A > 0$ and $aBs_0^2 < 0$ by assumption.

However, this is only a lower bound for the first time the relative velocity is negative as we needed to address the case where the initial relative velocity is negative. In the case where $v_{\ell,0} > v_0$ we will derive in the following a uniform lower bound. In both cases, assume that there is another time $t_2, t_3 \in (t_1, T)$ so that $v_\ell(t) - v(t) < 0 \forall t \in (t_2, t_3)$, we can assume that $v_\ell(t_2) = v(t_2)$. Applying then the previous estimates once more, we obtain this time as lower bound

$$x_\ell(t) - x(t) - l \geq \tfrac{-A_2+\sqrt{A_2^2+4aBs_0^2}}{2B} \ \forall t \in (t_2, t_3)$$

with $A_2 \coloneqq -B \cdot (x_\ell(t_2) - x(t_2) - l) + a\frac{s_0^2}{x_\ell(t_2)-x(t_2)-l} > 0$. Looking into the discriminant we find that

$$A_2^2 + 4aBs_0^2 = \left(\tfrac{as_0^2}{x_\ell(t_2)-x(t_2)-l} + B(x_\ell(t_2) - x(t_2) - l)\right)^2$$

so that we obtain for $t \in (t_2, t_3)$

$$x_\ell(t) - x(t) - l \geq \begin{cases} x_\ell(t_2) - x(t_2) - l & \text{if } x_\ell(t_2) - x(t_2) - l \leq \sqrt{\frac{as_0^2}{-B}} \\ \frac{-a\frac{s_0^2}{x_\ell(t_2)-x(t_2)-l}}{B} & \text{if } x_\ell(t_2) - x(t_2) - l \geq \sqrt{\frac{as_0^2}{-B}} \end{cases}.$$

Recalling that we can estimate from the previous (first) step and the fact that $x_\ell(t) - x(t) - l$ is non-decreasing between t_1 and t_2

$$x_\ell(t_2) - x(t_2) - l \geq \min\left\{g^*, x_{\ell,0} - x_0 - l\right\}$$

we obtain with the previous estimate that for any $t \in [0, t_3]$

$$x_\ell(t) - x(t) - l \geq \min\left\{g^*, x_{\ell,0} - x_0 - l, \sqrt{\tfrac{as_0^2}{-B}}\right\}.$$

However, this lower bound is independent of $x_\ell(t_2) - x(t_2) - l$ and we can thus iterated the procedure by going to the next time where $v_\ell(t) - v(t) < 0$ for some $t \in (t_3, T]$. However, in these cases the previously derived bound remains as is.

Looking into the derived lower bound in more details, one can actually distinguish the two cases $v_{\ell,0} - v_0 \leq (\geq 0)$ and obtain the same bounds. This concludes the proof. □

Remark 2.4.1 (Comments on the derived "safety distance" and the "extreme" case $B = 0$)**.** *We have not commented about the sign of A and B in eq.* (2.4.3)*. Clearly, assuming that $B \leq 0$ is reasonable as otherwise it holds*

$$\operatorname*{ess\text{-}inf}_{t\in[0,T]} u_{lead}(s) \geq a,$$

meaning that the leader speeds up all the time at least with the maximal acceleration of the follower, implying that the distance will always increase. Thus, assuming $B \leq 0$ the term $\frac{-A}{2B}$ is positive and $\frac{\sqrt{A^2+4aBs_0^2}}{2B}$ negative but its absolute values is smaller than $\frac{-A}{2B}$ so that the obtained lower bound in eq. (2.4.2) *is still positive.*

The lower bound together with the corresponding simulations is illustrated for a specific experimental setup in fig. 2.7. As the lower bound is not well-defined for $B = 0$, we compute the limes of the lower bound. Recalling that A is also a function of B namely, $A(B) = -B \cdot (x_{\ell,0} - x_0 - l) + a\frac{s_0^2}{x_{\ell,0}-x_0-l} + \frac{1}{2}(v_{\ell,0} - v_0)^2$ we have

$$\begin{aligned}\lim_{B\to 0} \frac{-A(B)+\sqrt{A(B)^2+4aBs_0^2}}{2B} &= \lim_{B\to 0} \frac{-A'(B)}{2} + \frac{A(B)A'(B)+2as_0^2}{2\sqrt{A(B)^2+4aBs_0^2}} \\ &= \frac{as_0^2}{\frac{as_0^2}{x_{\ell,0}-x_0-l}+\frac{1}{2}(v_{\ell,0}-v_0)^2}.\end{aligned}$$

Note that the obtained lower bound is always less or equal to the initial space headway, $x_{\ell,0} - x_0 - l$. Furthermore, negative relative initial velocity leads to smaller lower bound. But in the case of positive initial relative velocity, the given lower bound is very conservative and could be replaced by a stricter one. Altogether, even for $B = 0$ the obtained lower bound is reasonable.

2.5 Improvements for the IDM

In this section, we present several improvements of the IDM to fix the problems illustrated in Section 2.3 for general initial data. Before doing this, however, we present some other numerics on how the classical IDM behaves for specific data. This will serve as a comparison to the proposed improvements later:

Example 2.5.1 (Some additional numerical results for the classical IDM). All examples – except those which are physically unreasonable (compare Section 2.5) – will be tested on three different scenarios:

1. As the set of parameters where one can observe a negative velocity of the follower in the original IDM – see example 2.3.1 and fig. 2.2.

2. As the set of parameters where one can observe that the velocity of the follower diverges to $-\infty$ in finite time in the original IDM – see example 2.3.2 and fig. 2.4.

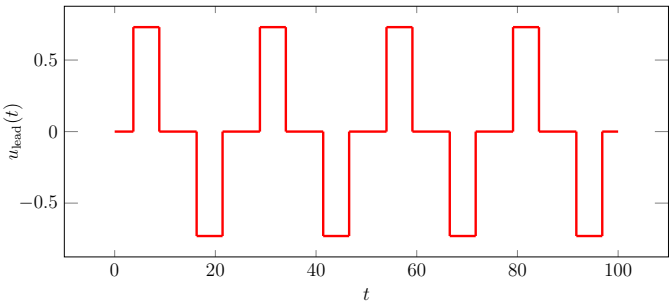

Figure 2.5: The acceleration profile u_{lead} of the leader. This is intended to specify a leader that repeats the pattern "accelerate, constant velocity, decelerate, constant velocity".

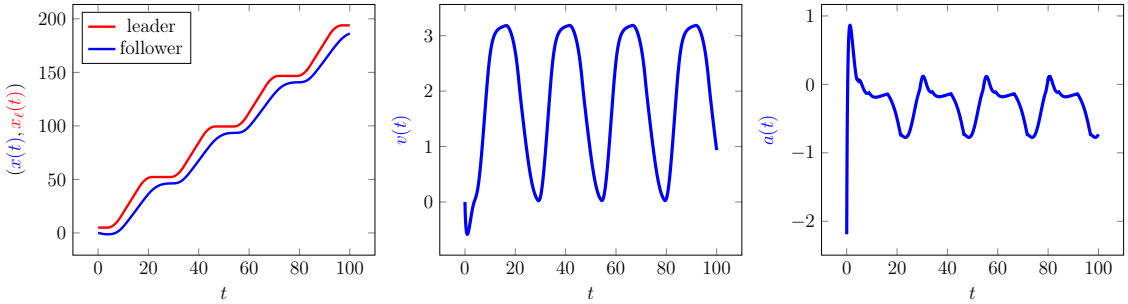

Figure 2.6: The original IDM, with parameters $x_0 = 0,\ x_{\ell,0} = l + 1 < l + s_0,\ v_0 = 0 = v_{\ell,0} = 0$. Both vehicles start with 0 velocity, and the leader follows the acceleration profile in fig. 2.5. **Left:** the position of both leader and follower, **middle:** the velocity of the follower and **right:** the acceleration of the follower. We leave the velocity and acceleration profile of the leader out as it is fully determined by the given u_{lead}.

3. A heavy stop and go wave traffic situation with the leader's acceleration satisfying $u_{\text{lead}} \equiv a \cdot \mathbb{1}_{\{t \in [0,T]:\ \sin(t/4) \geq 0.8\}} - a \cdot \mathbb{1}_{\{t \in [0,T]:\ \sin(t/4) \leq -0.8\}}$, $a = 0.73,\ b = 1.67,\ v_{\text{free}} = \frac{120}{36},\ \tau = 1.6,\ l = 4,\ s_0 = 2,\ d = 4$ illustrated in fig. 2.5. The results for the original IDM are then illustrated in fig. 2.6 and can serve as comparison.

Projection on nonnegative velocities and restricting the maximal deceleration

A straightforward improvement consists of projecting the velocity to nonnegative values. This is detailed in the following definition 2.5.1:

Definition 2.5.1 (IDM with projection to nonnegative velocities)**.** *Given assumption (1), we replace the acceleration in definition 2.2.1 and velocity for the IDM model in definition 2.2.3*

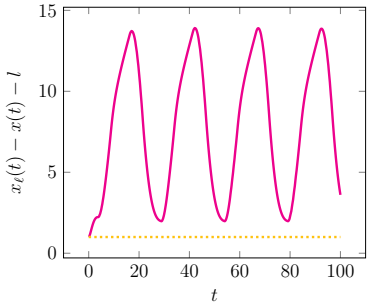

Figure 2.7: The original IDM with the same parameters as in fig. 2.6. Headway (in magenta) $x_\ell(t) - x(t) - l$ is illustrated together with the lower "a priori" bound as derived in eq. (2.4.1) in theorem 2.4.1. Computing this headway, we have for the numbers A, B as in eq. (2.4.3) $B = -0.73 - 0.73 = -1.46$, $A = 1.46 \cdot 1 + 0.73\frac{4}{1} = 4.38$ and $s_0 = 2$, and thus as lower bound on the headway is – following eq. (2.4.1) (recall that $v_{\ell,0} - v_0 = 0$ so that this case applied) $\min\left\{x_{\ell,0} - x_0 - l, \sqrt{\frac{as_0^2}{-B}}\right\} = 1$ which is pictured in dotted yellow. As can be seen the lower bound is always valid and for $t = 0$ even sharp.

by

$$\dot{x}(t) = \max\{v(t), 0\}, \qquad t \in [0, T] \tag{2.5.1}$$
$$\dot{v}(t) = \mathrm{Acc}\big(x(t), \max\{v(t), 0\}, x_\ell(t), v_\ell(t)\big), \qquad t \in [0, T] \tag{2.5.2}$$

and call the model the ***velocity projected IDM****.*

Theorem 2.5.1 (Existence and uniqueness of solutions for small times)**.** *Given assumption (1) the velocity projected IDM in definition 2.5.1 admits on a sufficiently small time horizon $T^* \in \mathbb{R}_{>0}$ a unique solution $(x, v) \in W^{1,\infty}((0, T^*))^2$.*

Proof. The proof is almost identical to the proof of theorem 2.2.1 when recalling that the right hand side is still locally Lipschitz-continuous. We do not go into details. □

However, as we will see the model has some drawbacks:

Example 2.5.2 (The following vehicle waits for too long to start driving). Assume that the constants and initial data as in example 2.3.1 with $\varepsilon < s_0$. Then, the leading vehicle's trajectory can be computed as

$$x_\ell(t) = x_{\ell,0} + v_{\ell,0}t + \tfrac{u}{2}t^2, \ t \in [0, T],$$

and the leading vehicle's velocity can be computed as

$$v_\ell(t) = v_{\ell,0} + ut, \ t \in [0, T].$$

Plugging this into the change of the vehicle's velocity we obtain the following system of ODEs

$$\begin{aligned}
\dot{x}(t) &= \max\{v(t), 0\} \\
\dot{v}(t) &= a\left(1 - \left(\tfrac{\max\{v(t),0\}}{v_{\text{free}}}\right)^{\delta} - \left(\tfrac{2\sqrt{ab}(s_0+\max\{v(t),0\}\tau)+\max\{v(t),0\}(\max\{v(t),0\}-v_\ell(t))}{2\sqrt{ab}(x_\ell(t)-x_{\ell,0}+\varepsilon-\int_0^t \max\{v(s),0\}\,\mathrm{d}s)}\right)^2\right) \\
x(0) &= x_{\ell,0} - l - \varepsilon \\
v(0) &= 0.
\end{aligned}$$

Note that

$$\dot{v}(0) = a\left(1 - \left(\tfrac{s_0}{\varepsilon}\right)^2\right) < 0,$$

therefore, there exists some small time interval $[0, t_1]$ such that for every $t \in [0, t_1]$, $v(t) < 0$. During the time interval $[0, t_1]$, the distance between the two vehicles is

$$l + \varepsilon + x_\ell(t) - x_{\ell,0} = l + \varepsilon + v_{\ell,0}t + \tfrac{u}{2}t^2, \quad t \in [0, t_1].$$

Thus, for every $t \in [0, t_1]$,

$$\dot{v}(t) = a\left(1 - \left(\tfrac{s_0}{\varepsilon + v_{\ell,0}t + \frac{u}{2}t^2}\right)^2\right).$$

Note that $\dot{v}\colon [0, t_1] \mapsto \mathbb{R}$ is strictly increasing. Without loss of generality, we assume that the initial velocity of the leading vehicle is $v_{\ell,0} = 0$ and the acceleration of the leading vehicle is $u = 2$. Then for every $t \in [0, t_1]$,

$$v(t) = \int_0^t a\left(1 - \left(\tfrac{s_0}{\varepsilon+s^2}\right)^2\right)\mathrm{d}s = at - 4as_0^2\int_0^t \left(\tfrac{1}{s^2+\varepsilon}\right)^2 \mathrm{d}s = at - 4as_0^2\left(\tfrac{\frac{\sqrt{\varepsilon}t}{\varepsilon+t^2} + \arctan\left(\frac{t}{\sqrt{\varepsilon}}\right)}{2\varepsilon^{\frac{3}{2}}}\right).$$

In particular, as illustrated in fig. 2.8, we have that t_1 increases as ε decreases. That is, the smaller the initial distance between the two vehicles, the longer it takes the following vehicle to recover its positive velocity. Another example illustrates the projected velocity model numerically with regard to other scenarios:

Example 2.5.3 (Velocity projected IDM). As can be observed the actual velocity in all the three different scenarios is bounded from below by zero and the solution exists on the entire time horizon considered. However, the projection operator leads to the problem that the follower waits too long until they speed up. This can be observed in particular in figs. 2.9 and 2.10 where the distance of the two vehicles after both have started speeding up ($t \approx 5$) is approximately around 8.5 which is quite far from the comfortable vehicle distance s_0 and thus leading to a too large distance. Here we use the free-flow acceleration as following

$$\dot{v}(t) = a - a\left(\tfrac{\max\{v(t),0\}}{v_{\text{free}}}\right)^{\delta} \ \forall t \in [0, T]. \tag{2.5.3}$$

Same can be observed in fig. 2.11 for smaller time.

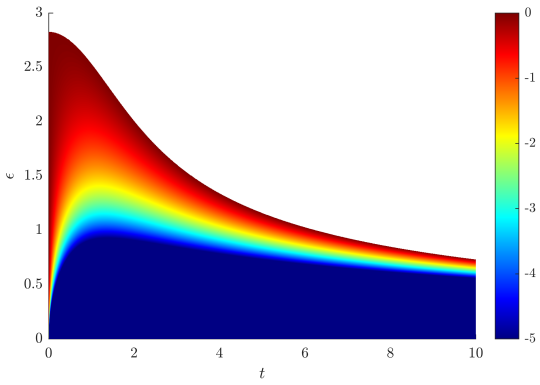

Figure 2.8: Velocity dependent on epsilon and time. The dark blue indicates values less or equal -5 and the white area positive function values, so that the red curve separating the white and colored region can be seen as the values where the velocity is actually zero. In particular, as the initial distance between two vehicles ε increases, the time t_1 when the following vehicle recovers its positive velocity decreases.

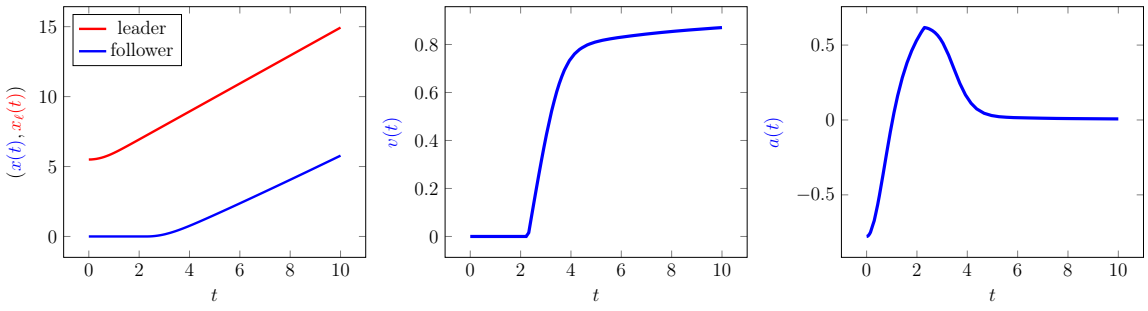

Figure 2.9: The IDM with projection as in definition 2.5.1 and same parameters as in fig. 2.2 with $x_0 = 0$, $x_{\ell,0} = l + 1.5 < l + s_0$. **Left:** the positions of the vehicles, **middle:** the velocity of the follower, and **right:** the acceleration of the follower. The leader follows the free-flow acceleration as in eq. (2.5.3). The follower stays still and waits until there is a safe space to speed up.

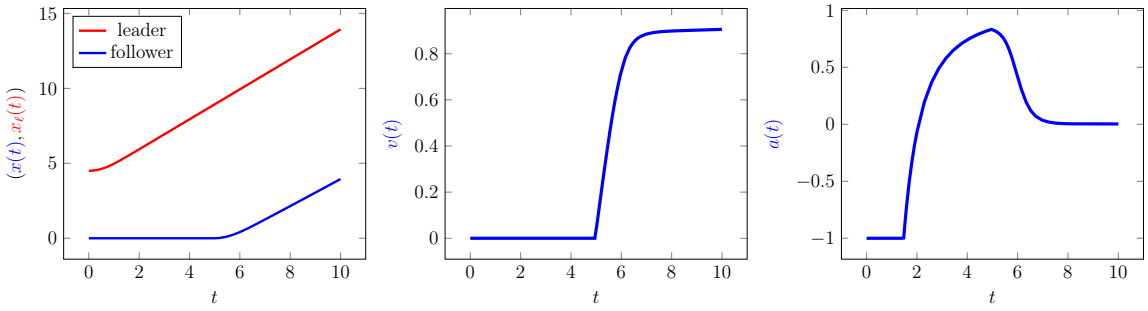

Figure 2.10: The IDM with projection, with the same parameters as in fig. 2.2 and $x_0 = 0,\ x_{\ell,0} = l + 0.5 < l + s_0,\ v_0 = 0 = v_{\ell,0} = 0$. **Left:** vehicles' positions, **middle:** the follower's velocity and **right:** the follower's acceleration. The leader follows the free flow acceleration as in eq. (2.5.3). The follower stays still and waits until there is a safe space to speed up.

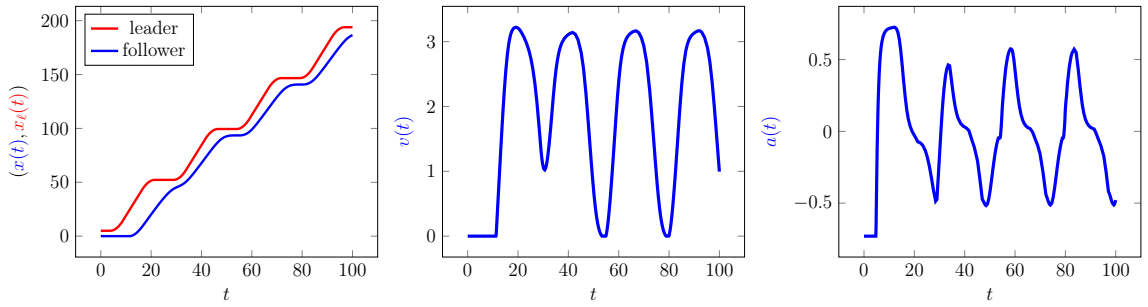

Figure 2.11: The IDM with projection as in definition 2.5.1 and initial data $x_0 = 0,\ x_{\ell,0} = l + 1 < l + s_0,\ v_0 = v_{\ell,0} = 0$. **Left:** the position of the vehicles, **middle:** the velocity of the follower and **right:** the acceleration of the follower. The leader follows the acceleration profile in fig. 2.5. The velocities remain positive, however the waiting time for the follower until speeding up is large.

Projection to nonnegative velocities with bounded deceleration

Another improvement for this is projecting the acceleration to prevent it from becoming too negative. Then, the corresponding model reads as

Definition 2.5.2 (IDM with projection to nonnegative velocities and bounded deceleration)**.** *Given assumption (1), we replace the acceleration in definition 2.2.1 and velocity for the IDM model in definition 2.2.3 by*

$$\begin{aligned} \dot{x}(t) &= \max\{v(t), 0\}, && t \in [0, T] \\ \dot{v}(t) &= \max\{\mathrm{Acc}(x(t), \max\{v(t), 0\}, x_\ell(t), v_\ell(t)), -a_{\min}\}, && t \in [0, T] \end{aligned}$$

*with a parameter $a_{\min} \in \mathbb{R}_{>0}$ be given and call the model the **acceleration projected IDM**.*

Theorem 2.5.2 (Global existence and uniqueness of solutions)**.** *Given assumption (1) the acceleration projected IDM in definition 2.5.2 admits for every $T \in \mathbb{R}_{>0}$ a unique solution $(x, v) \in W^{1,\infty}((0,T))$.*

Proof. The proof of existence and uniqueness for small time is almost identical to the proof of theorem 2.2.1 when recalling that the right hand side is still locally Lipschitz-continuous. We do not go into details.

So it remains to show that we can find uniform estimates for $(x(t), v(t)),\ t \in [0,T]$. Obviously,

$$v(t) \geq v_0 - a_{\min} t \quad \forall t \in [0,T].$$

Thanks to the structure of Acc (see definition 2.2.1) we also obtain as a bound from above

$$v(t) \leq v_0 + at \quad \forall t \in [0,T].$$

As v is uniformly bounded on every finite time horizon, so is x and we are done. □

However, although the previous change of the acceleration profile in definition 2.5.2 looks promising as according to theorem 2.5.2 a solution exists on every finite time horizon, the physical representation, the model itself is unreasonable as the car behind can overtake the leading car – or differently put, the car behind can bump into the leading car without the model noticing it. This is detailed in the following example 2.5.4.

Example 2.5.4 (Physical unreasonability). As the deceleration of the following vehicle is bounded from below by $-a_{\min}$, we can always chose an initial velocity of the follower which leads to the fact that $x_\ell(t) - x(t) - l \to 0$ in finite time.

In formulae, assume for simplicity that the leading vehicle has the following trajectory

$$x_\ell(t) = x_{\ell 0} + v_{\ell 0} t + \tfrac{1}{2} u_{\text{lead}} t^2, \qquad t \in [0,T].$$

with $u_{\text{lead}} \in \mathbb{R}_{\geq 0}$ and $(x_{\ell 0}, v_{\ell 0}) \in \mathbb{R} \times \mathbb{R}_{>0}$. Then, we take the difference of the vehicles position with car length $l \in \mathbb{R}_{>0}$ and have for $t \in [0,T]$

$$\begin{aligned}
&x_\ell(t) - x(t) - l \\
&\leq x_{\ell 0} + v_{\ell 0} t - l + \tfrac{1}{2} u_{\text{lead}} t^2 - x_0 - \int_0^t \max\{v(s), 0\} \,\mathrm{d}s \\
&\leq x_{\ell 0} + v_{\ell 0} t - l + \tfrac{1}{2} u_{\text{lead}} t^2 - x_0 - \int_0^t v(s) \,\mathrm{d}s \\
&\leq x_{\ell 0} + v_{\ell 0} t - l + \tfrac{1}{2} u_{\text{lead}} t^2 - x_0 \\
&\qquad - \int_0^t v_0 + \int_0^s \max\{\mathrm{Acc}(x(\tau), \max\{0, v(\tau)\}, x_\ell(\tau), v_\ell(\tau)), -a_{\min}\} \,\mathrm{d}\tau \,\mathrm{d}s \\
&\leq x_{\ell 0} + v_{\ell 0} t - l + \tfrac{1}{2} u_{\text{lead}} t^2 - x_0 - t v_0 + \int_0^t \int_0^s a_{\min} \,\mathrm{d}\tau \,\mathrm{d}s
\end{aligned}$$

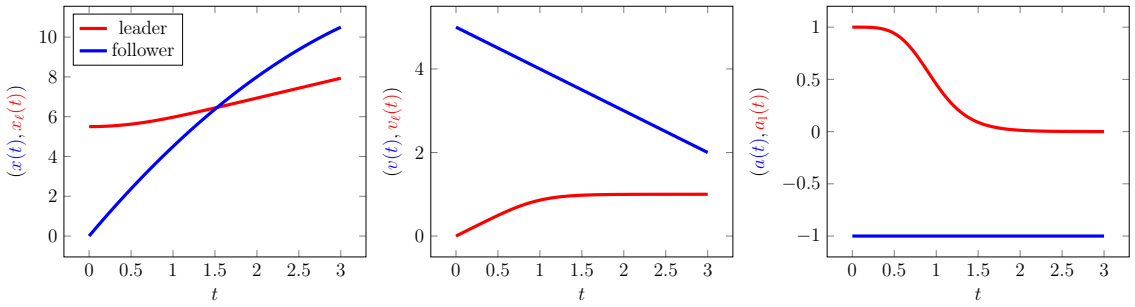

Figure 2.12: Illustration of the improvement in definition 2.5.2 and its physical unreasonability as shown in example 2.5.4. The parameters are $a = a_{\min} = 1$, $b = 2$, $v_{\text{free}} = 1$, $\tau = 1.6$, $l = 4$, $s_0 = 2$, $d = 4$ and datum $x_0 = 0$, $x_{\ell,0} = l + 1.5$, $v_0 = 5$, $v_{\ell,0} = 0$. **Left** Vehicles' positions, **middle** vehicles' velocities, **right** vehicles' acceleration. The follower overtakes the leader in finite time, although the follower breaks constantly.

$$\leq x_{\ell 0} - x_0 - l + (v_{\ell 0} - v_0)t + \tfrac{1}{2}(u_{\text{lead}} + a_{\min})t^2.$$

Obviously, for v_0 sufficiently large, we obtain for small time that $x_\ell(t) - x(t) < l$. An extreme case for this is illustrated in fig. 2.12 where not only the vehicles get closer than l but the follower (in blue) entirely overtakes the leader (in red).

Another velocity projection improvement

Another improvement which had been mentioned in the literature in [100] (however, it goes back to a website of Martin Treiber which is not available anymore, is shortly investigated in this section. Not the entire third part in the IDM acceleration definition 2.2.1 is projected, but only a specific part. This is detailed as follows:

Definition 2.5.3 (Partially projected acceleration)**.** *Let assumption (1) and* Acc *as in definition 2.2.1 be given. Then, replacing in definition 2.2.3 the acceleration of the follower in the following way*

$$\text{Acc}_{ppa} : \begin{cases} \mathcal{A} & \to \mathbb{R} \\ (x, v, x_\ell, v_\ell) & \mapsto a - a\left(\frac{|v|}{v_0}\right)^\delta - a\left(\frac{s_0 + \max\left\{0, v\tau + \frac{v(v_\ell - v)}{2\sqrt{ab}}\right\}}{x_\ell - x - l}\right)^2 \end{cases}$$

we call the resulting car following model the IDM with ***p****artially* ***p****rojected* ***a****cceleration.*

However, as can be seen it does not prevent negative velocity in the case that $x_\ell - x - l < s_0$ as the acceleration then becomes negative if the current follower's speed is zero, i.e., $v = 0$. Thus, we do not study it further.

Velocity regularized acceleration

Another improvement of the IDM is to add a regularization term which will make the third term in the acceleration function definition 2.2.1 of the IDM in definition 2.2.3 become zero if the corresponding velocity approaches zero.

Definition 2.5.4 (IDM with velocity regularized acceleration)**.** *Given assumption (1), we replace acceleration in definition 2.2.1 in definition 2.2.3 by*

$$\mathrm{Acc}_{vra} : \begin{cases} \mathcal{A} & \to \mathbb{R} \\ (x, v, x_\ell, v_\ell) & \mapsto a\left(1 - \left(\frac{|v|}{v_{free}}\right)^\delta - h(v)\left(\frac{2\sqrt{ab}(s_0+v\tau)+v(v-v_\ell)}{2\sqrt{ab}(x_\ell-x-l)}\right)^2\right) \end{cases}$$

*with $\mathcal{A}$ as in definition 2.2.1 and regularization $h \in W^{1,\infty}(\mathbb{R};\mathbb{R}_{\geq 0})$ be a monotonically increasing function satisfying $h(0) = 0$ and – for a given $\varepsilon \in \mathbb{R}_{>0}$ – $h(v) = 1\ \forall v \in \mathbb{R}_{\geq\varepsilon}$. We call this the **velocity regularized acceleration IDM**.*

Theorem 2.5.3 (Existence and Uniqueness of solutions on arbitrary time horizon)**.** *Given assumption (1) and in addition assume that*

$$\exists v_{\min} \in \mathbb{R}_{>0} : \ v_\ell(t) \geq v_{\min}\ \forall t \in [0,T] \ \wedge \ h(v_{\min}) > 0$$

the velocity regularized IDM in definition 2.5.4 admits on every finite time horizon $T \in \mathbb{R}_{\geq 0}$ a unique solution satisfying $x \in W^{2,\infty}((0,T))$

$$x_\ell(t) - x(t) - l \geq \min\left\{x_{\ell,0} - x_0 - l, \sqrt{\tfrac{as_0^2 h(v_{\min})}{-B}}, \tfrac{-A+\sqrt{A^2+4aBh(v_{\min})s_0^2}}{2B}\right\} \qquad \forall t \in [0,T]$$

with

$$\begin{aligned} A &\coloneqq \tfrac{1}{2}(v_{\ell,0} - v_0)^2 - B(x_{\ell,0} - x_0 - l) + a\tfrac{h(v_{\min})s_0^2}{x_{\ell,0}-x_0-l} \\ B &\coloneqq \operatorname*{ess\text{-}inf}_{t\in[0,T]} u_{lead}(t) - a \end{aligned} \tag{2.5.4}$$

and additionally

$$\max\{v_{free}, v_0\} \geqq \dot{x} \equiv v \geqq 0 \quad \text{on } [0,T].$$

If $v_0 > 0$, it even holds

$$v(t) > 0 \quad \forall t \in [0,T].$$

Proof. To show the well-posedness it suffices to make sure that

- $\exists C \in \mathbb{R}_{>0} : x_{\ell,0} - x_0 - l > 0$ implies that $x_\ell(t) - x(t) - l \geq C$, $\forall t \in [0,T]$. Take the difference of the change of the leader's acceleration and the follower's to obtain and mimic somewhat the proof of theorem 2.4.1

$$\ddot{x}_\ell(t) - \ddot{x}(t) \geq u_{\text{lead}}(t) - a + ah(v(t))\left(\frac{2\sqrt{ab}(s_0+v(t)\tau)+v(t)(v(t)-v_\ell(t))}{2\sqrt{ab}\left(x_\ell(t)-x(t)-l\right)}\right)^2$$

assuming without loss of generality $v_\ell(t) - v(t) \leq 0$, i.e., $v(t) \geq v_\ell(t)$ on a certain time interval and as we have $\inf_t v_\ell(t) \geq v_{\min} > 0$, $h \geqq 0$

$$\geq \operatorname*{ess\text{-}inf}_{s\in[0,t]} u_{\text{lead}}(s) - a + as_0^2 h\big(v_{\min}\big)\Big(\tfrac{1}{x_\ell(t)-x(t)-l}\Big)^2$$

and multiplying with $v_\ell(t) - v(t) = \dot{x}_\ell(t) - \dot{x}(t) \leq 0$

$$\Big(\ddot{x}_\ell(t) - \ddot{x}(t)\Big)(\dot{x}_\ell(t) - \dot{x}(t)) \leq \operatorname*{ess\text{-}inf}_{s\in[0,t]} u_{\text{lead}}(s)(\dot{x}_\ell(t) - \dot{x}(t)) \tag{2.5.5}$$

$$- a(\dot{x}_\ell(t) - \dot{x}(t)) + ah\big(v_{\min}\big)s_0^2 \tfrac{\dot{x}_\ell(t)-\dot{x}(t)}{\big(x_\ell(t)-x(t)-l\big)^2}. \tag{2.5.6}$$

Integrating over $(0, t)$ leads to

$$\tfrac{1}{2}(\dot{x}_\ell(t) - \dot{x}(t))^2 \leq \Big(\operatorname*{ess\text{-}inf}_{s\in[0,t]} u_{\text{lead}}(s) - a\Big)\Big(\big(x_\ell(t) - x(t) - l\big) - \big(x_{\ell,0} - x_0 - l\big)\Big)$$
$$+ \tfrac{1}{2}(v_{\ell,0} - v_0)^2 - ah\big(v_{\min}\big)s_0^2\Big(\tfrac{1}{x_\ell(t)-x(t)-l} - \tfrac{1}{x_{\ell,0}-x_0-l}\Big)$$

or in shorter notation $g :\equiv x_\ell - x - l$

$$\tfrac{1}{2}\big(g'(t)\big)^2 \leq A + Bg(t) - a\tfrac{h(v_{\min})s_0^2}{g(t)}$$

with A, B as in eq. (2.5.4). Following the identical steps as in the proof of theorem 2.4.1, particularly noticing that the left hand side is always nonnegative while the right hand side would go to $-\infty$ if $g \to 0$ we obtain the claimed lower bound on the distance.

- $\dot{x}(t) \geq 0\ \forall t \in [0, T]$. We know by the Picard-Lindelöf theorem ([28, Chapter 4] or [27, Thm 1.3]) that there exists a solution on a significantly small time horizon $[0, T^*]$ with $T^* \in \mathbb{R}_{>0}$. Assume that the velocity of a given vehicle $\dot{x}$ becomes zero at a given time $T^{**} \in \mathbb{R}_{>0}$. Then, by continuity of the velocity and due to the nonnegativity of the initial velocity there exists a first time $t \in [0, T^{**})$ so that $v(t) = \dot{x}(t) = 0$. Plugging this into the corresponding acceleration we obtain at that time

$$\ddot{x}(t) = \dot{v}(t) = \text{Acc}_{\text{vra}}\big(x(t), \dot{x}(t), x_\ell(t), \dot{x}_\ell(t)\big) = \text{Acc}_{\text{vra}}\big(x(t), 0, x_\ell(t), \dot{x}_\ell(t)\big) = a > 0,$$

thanks to the assumption on h in definition 2.5.4, namely $h(0) = 0$. This means that whenever the velocity approaches zero, the derivative is strictly positive so that the velocity can never become zero. Assume that for some $t \in [0, T]$ we have $v(t) \geq v_{\text{free}}$. Then, by the velocity regularized acceleration in definition 2.5.4, we have $\dot{v}(t) < 0$ and can conclude

$$v(t) \leq \max\{v_{\text{free}}, v_0\} \quad \forall t \in [0, T].$$

This gives the claim.

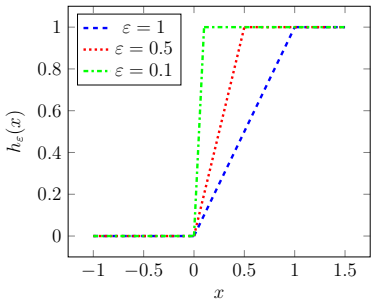

Figure 2.13: Different choices of the "saturation" function h_ε for $\varepsilon \in \{1, 0.5, 0.1\}$ as suggested in eq. (2.5.7).

□

Remark 2.5.1 (Proper choice of the regularization h)**.** *A proper choice for h consists for $\varepsilon \in \mathbb{R}_{>0}$ of*

$$h_\varepsilon : \begin{cases} \mathbb{R} & \to [0,1] \\ v & \mapsto \frac{v}{\varepsilon}\mathbb{1}_{\mathbb{R}_{\geq 0}}(v) \cdot \mathbb{1}_{\mathbb{R}_{\leq \varepsilon}}(v) + \mathbb{1}_{\mathbb{R}_{>\varepsilon}}(v). \end{cases} \tag{2.5.7}$$

This is illustrated in the following fig. 2.13. As can be seen this "saturation" function is only continuous, resulting in an acceleration function which is not differentiable. Obviously, this could be changed by smoothing h_ε. We do not go into details.

We illustrate the model in the following

Example 2.5.5 (Velocity regularized acceleration). As can be seen in figs. 2.14 to 2.16, with this fix the spacing between the two vehicles is not getting large as had been observed in figs. 2.9 to 2.11 but the follower speeds up immediately when there is enough safe distance to do so. The clipping due to the function h_ε can be observed in particular in the acceleration profile which is nonsmooth. In all figs. 2.14 to 2.16 we choose $\varepsilon = 0.1$.

A discontinuous improvement to prevent negative velocity

Our last potential improvement for the IDM which had also been suggested a lot (see for instance [88]) is an improvement which will become active only if the velocity becomes zero and the corresponding acceleration at the time where the velocity is zero is negative. In this way, the following improvement is the most natural one. We state it in the following definition 2.5.5.

Definition 2.5.5 (IDM with discontinuous acceleration)**.** *Let assumption (1) and* Acc *as in definition 2.2.1 be given. Then, replacing in definition 2.2.3 the acceleration of the follower*

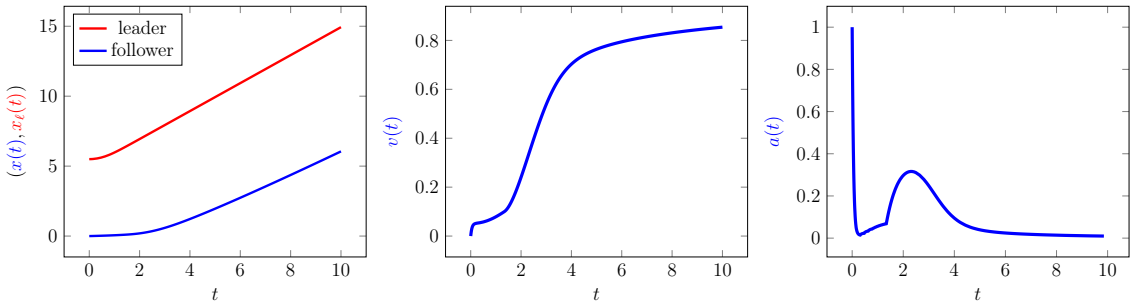

Figure 2.14: The IDM with velocity regularized acceleration as in definition 2.5.4 and parameters as in fig. 2.2. Initial data are $x_0 = 0,\ x_{\ell,0} = l + 1.5 < l + s_0,\ v_0 = v_{\ell,0} = 0$. **Left:** the vehicles' position, **middle:** the vehicles' velicities, and **right:** the vehicles acceleration. The leader follows the free flow acceleration. The follower stays still and waits until there is a safe space to speed up.

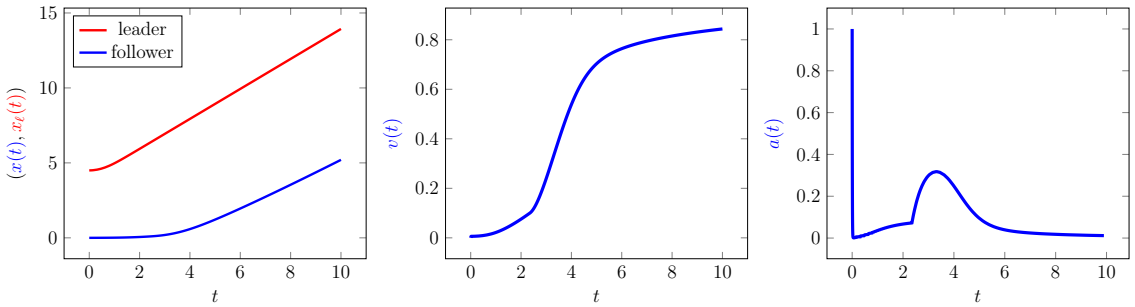

Figure 2.15: The IDM with velocity regularized acceleration, with initial gap equal 0.5 and same parameters as in fig. 2.2. Both vehicles start with 0 velocity, and the leader follows the free flow IDM dynamics. **Left:** $x_0 = 0,\ x_{\ell,0} = l + 0.5 < l + s_0,\ v_0 = 0 = v_{\ell,0} = 0$. The follower stays still and waits until there is a safe space to speed up. **Right:** the follower remains still in the initial phase.

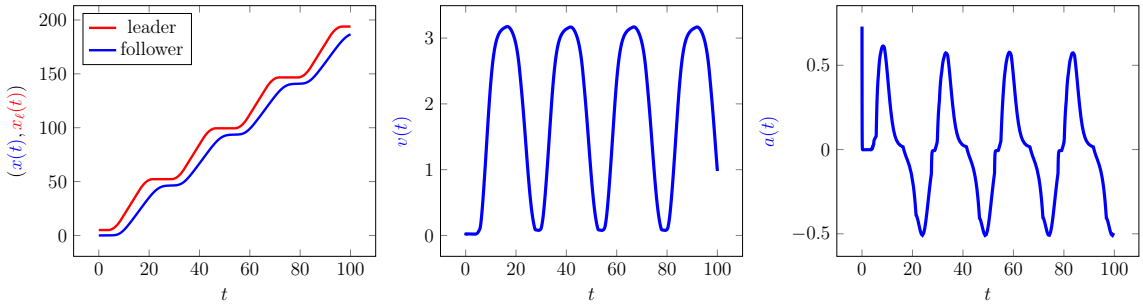

Figure 2.16: The IDM with velocity regularized acceleration, with initial gap equal 1. Both vehicles start with 0 velocity, and the leader follows the acceleration profile in figure fig. 2.5. **Left:** $x_0 = 0,\ x_{\ell,0} = l + 1 < l + s_0,\ v_0 = 0 = v_{\ell,0} = 0$. **Right:** again, the velocity always stays nonnegative.

in the following discontinuous way as

$$\dot{v}(t) = \begin{cases} \mathrm{Acc}(x(t), v(t), x_\ell(t), v_\ell(t)) & \text{if } v(t) > 0 \\ \mathrm{Acc}(x(t), v(t), x_\ell(t), v_\ell(t)) & \text{if } v(t) = 0 \ \wedge \ x_\ell(t) - x(t) - l \geq s_0 \ , \\ 0 & \text{if } v(t) = 0 \ \wedge \ x_\ell(t) - x(t) - l < s_0 \end{cases} \tag{2.5.8}$$

we call this the ***discontinuous IDM****.*

Although one might expect that the introduction of the discontinuity in eq. (2.5.8) might prohibit a solution to exist for all times or also might destroy uniqueness, it actually does not as the following theorem 2.5.4 states:

Theorem 2.5.4 (Well-posedness of the discontinuously fixed IDM in definition 2.5.5)**.** *Given assumption (1) and assuming that the velocity of the leader is only zero at finitely many intervals, the discontinuous improvement of the IDM as in definition 2.5.5 admits a unique solution on every finite time horizon $T \in \mathbb{R}_{>0}$ and satisfies*

$$x \in W^{2,\infty}((0,T)) : \ \dot{x} \geqq 0.$$

In addition, the lower bound on the distance between follower and leader as in theorem 2.4.1 holds.

Proof. We consider several different cases:

- Assume that at $t = 0$ we have $v(0) = c > 0$. Obviously, for small time the solution of the system is unique as the right hand side is locally Lipschitz-continuous then. Either, $v(t) > 0 \ \forall t \in [0, T]$. Then, there is nothing more to do as we never run into the discontinuity or $\exists t^* \in (0, T] : v(t^*) = 0$. We distinguish two cases:

  $x_\ell(t^*) - x(t^*) - l \geq s_0$**:** However, in this case the right hand side has not changed so that the solution still exists and is unique. As at that time, the velocity is zero and as the leading car never moves backwards (by the assumption on the leader's velocity/acceleration, we can never go into the third case where it would hold $x_\ell(t) - x(t) - l < s_0$ but only back into the first case with strictly positive velocity. In this case, the solution exists and is unique.

  $x_\ell(t^*) - x(t^*) - l < s_0$**:** Then, the velocity of the follower is zero and we can only switch into the second case when the leader's position x_ℓ increases, we are automatically left with the case that either we stay in the third case or that we move back to the second case. The second case, however, was already treated previously.

- Assume that we have $v(0) = 0$. Then, we are either in item one or two of the previous case and are done.

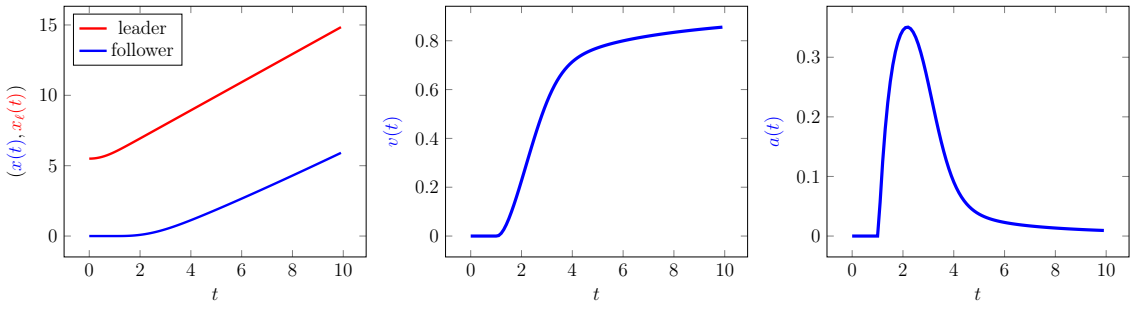

Figure 2.17: The discontinuous improvement of the IDM, with initial gap equal 1.5 and same parameters as in fig. 2.2. Both vehicles start with 0 velocity, and the leader follows the acceleration profile in figure fig. 2.5. **Left:** $x_0 = 0,\ x_{\ell,0} = l + 1.5 < l + s_0,\ v_0 = 0 = v_{\ell,0} = 0$. **Right:** again, the velocity always stays nonnegative.

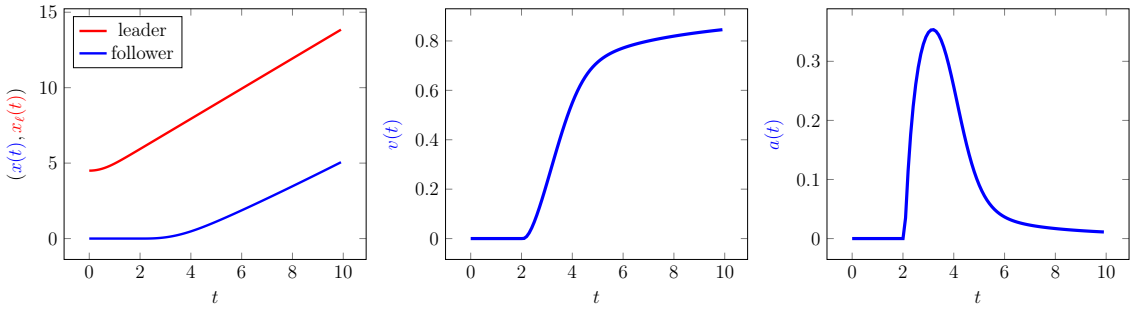

Figure 2.18: The discontinuous improvement of the IDM, with initial gap equal 0.5 and same parameters as in fig. 2.2. Both vehicles start with 0 velocity, and the leader follows the acceleration profile in figure fig. 2.5. **Left:** $x_0 = 0,\ x_{\ell,0} = l + 0.5 < l + s_0,\ v_0 = v_{\ell,0} = 0$. **Right:** again, the velocity always stays nonnegative.

As all of these changes only depend on the leader's trajectory x_ℓ and velocity v_ℓ which is given independent on the status of the follower, and we can conclude the existence and uniqueness of a solution.

The lower bound on the distance follows by the argument that the distance between follower and leader can only decrease if the followers velocity is not zero. However, then, we are in the "classical" IDM model and can apply exactly the reasoning of the proof of theorem 2.4.1. □

Example 2.5.6 (Discontinuous improvement). In figs. 2.17 to 2.19 we illustrate the dynamics of leader and follower for the discontinuous improvement proposed in theorem 2.5.4. Here, the velocity can become zero and stay zero for an amount of time dependent on the leaders velocity/position, but remains nonnegative. If the spacing between the two cars is large enough, the follower immediately speeds up and does not let the gap increase too much.

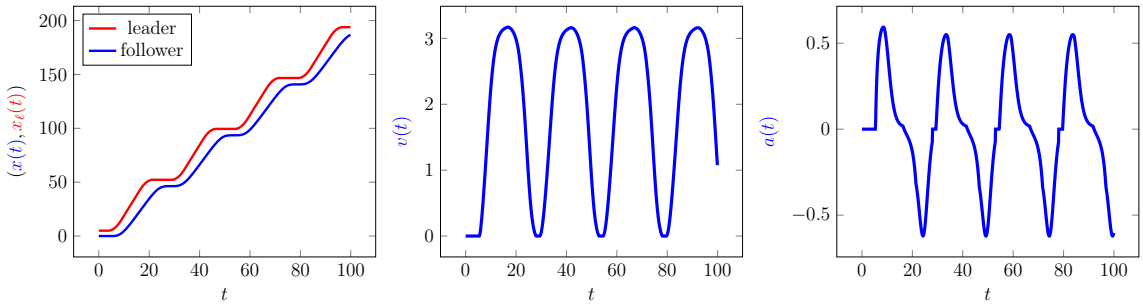

Figure 2.19: The discontinuous improvement of the IDM, with initial gap equal 1. Both vehicles start with 0 velocity, and the leader follows the acceleration profile in figure fig. 2.5. **Left:** $x_0 = 0,\ x_{\ell,0} = l + 1 < l + s_0,\ v_0 = v_{\ell,0} = 0$. **Middle:** again, the velocity always stays nonnegative. **Right:** acceleration

Comparisons among modifications

We herein summarize the strength and weakness of each modification.

- The acceleration projected IDM in definition 2.5.2 is the most straightforward modification to fix the negative velocities. However as shown in figs. 2.9 and 2.10, it suffers from the fact that the follower waits too long to start driving. It may also lead to physical unreasonability issue with certain initial datum as we point out in example 2.5.4.
- The velocity regularized IDM in definition 2.5.4 is capable of preventing negative velocity, and the follower speeds up immediately when it observes safe distance. However in this modification one needs to specify the regularization functions h, which might require extra parameter tuning.
- The discontinuous improvement of the IDM as in definition 2.5.5 prohibits negative velocities, without the need to introduce extra saturation functions.

In order to quantitatively compare the modifications, we compute the average distance (as well as the variance) between the leader and follower over time in table 2.2 on three different scenarios we tested. As it turns out the differences between the latter two modifications are minimal in all scenarios and both mean/variance. On the other hand, the acceleration projected IDM has greater average distance and variance, verifying the potential issue that with the modification, the following vehicle waits for too long to start driving, and reacts to the leader's velocity change in a slower manner.

2.6 Generalization to many cars

In the proposed framework, we have only studied the case where we have one leader and one follower and the leader (in most cases) satisfies an acceleration profile where their velocity is

Table 2.2: The average distance between the leader and follower (and the variance reported in the parenthesis)

Average distance (variance)	item 1	item 2	item 3
acceleration projected IDM definition 2.5.2	7.99 (1.19)	8.09 (3.55)	14.94 (54.99)
velocity regularized IDM definition 2.5.4	7.76 (1.00)	7.24 (1.70)	12.81 (25.51)
discontinuous IDM definition 2.5.5	7.75 (1.01)	7.31 (1.75)	12.39 (25.18)

nonnegative. However, as this is somewhat arbitrary, all proposed results and all "improvements" remain valid as long as the velocity of the follower remains non-negative when we generalize this to more than two cars. We make this precise in the following definition 2.6.1 but first introduce the number of cars as well as some physical reasonable assumption on the input datum:

Assumption 2 (Input datum for multiple cars)**.** *Let $N \in \mathbb{N}_{\geq 1}$ be given. We assume that the parameters of the* Acc *satisfy what we have assumed in assumption (1) as well as the leaders acceleration u_{lead}. Additionally, we assume for the initial datum (position and velocity)*

$$\boldsymbol{x}_0 \in \mathbb{R}^N : \boldsymbol{x}_{0,i} - \boldsymbol{x}_{0,i+1} > l \ \forall i \in \{1, \dots, N-1\} \ \wedge \ \boldsymbol{v}_0 \in \mathbb{R}^N_{\geq 0}.$$

Definition 2.6.1 (The car-following model for many cars)**.** *Given assumption (2), definition 2.2.1 and assumption (1). Then, for $u_{lead} \in \mathcal{U}_{lead}$ the dynamics for the IDM with many vehicles $N \in \mathbb{N}_{\geq 1}$ read in $(\boldsymbol{x}, \boldsymbol{v}) : [0, T] \to \mathbb{R}^N \times \mathbb{R}^N$ as*

$$\begin{aligned}
\dot{\boldsymbol{x}}_1(t) &= \boldsymbol{v}_1(t), && && t \in [0,T] \\
\dot{\boldsymbol{v}}_1(t) &= u_{lead}(t), && && t \in [0,T] \\
\dot{\boldsymbol{x}}_i(t) &= \boldsymbol{v}_i(t), && i \in \{2, \dots, N\} && t \in [0,T] \\
\dot{\boldsymbol{v}}_i(t) &= \mathrm{Acc}(\boldsymbol{x}_i(t), \boldsymbol{v}_i(t), \boldsymbol{x}_{i-1}(t), \boldsymbol{v}_{i-1}(t)), && i \in \{2, \dots, N\} && t \in [0,T] \\
\boldsymbol{x}(0) &= \boldsymbol{x}_0, \\
\boldsymbol{v}(0) &= \boldsymbol{v}_0.
\end{aligned} \tag{2.6.1}$$

The system for many cars is illustrated in fig. 2.20. Having the definition, we obtain the following general result on the well-posedness when applying the proper acceleration functions – IDM improvements – introduced before:

Theorem 2.6.1 (Well-posedness of some of the previously discussed models)**.** *Let assumption (2) hold and consider as "improvement" of the IDM either the*

- *the* ***velocity regularized acceleration*** *in definition 2.5.4 with the additional assumption that there exists $v_{min} \in \mathbb{R}_{>0}$ such that $v_\ell \geqq v_{\min}$ on $[0, T]$ and $\boldsymbol{v}_0 \in \mathbb{R}^N_{>0}$*
- *the* ***discontinuous improvement*** *in definition 2.5.5.*

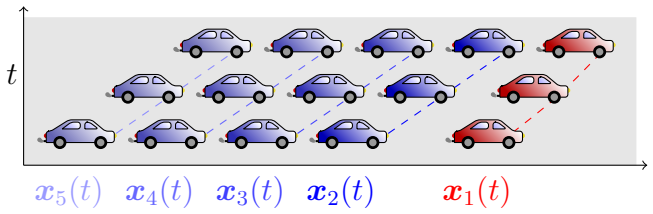

Figure 2.20: The leader $x_1(t)$ with its dynamics determined by the acceleration $u_{\text{lead}}(t)$ and the following cars $x_2(t)$, $x_3(t)$, $x_4(t)$, $x_5(t)$ with its dynamics governed by the classical IDM definition 2.2.3. The overall dynamics is stated in definition 2.6.1.

Then, the system of $2N$ *coupled initial value problems* ($N \in \mathbb{N}_{\geq 1}$) *admits a unique solution on every given time horizon* $T \in \mathbb{R}_{>0}$ *and the solution satisfies for the* ***velocity regularized acceleration***

$$\boldsymbol{x} \in W^{2,\infty}\big((0,T);\mathbb{R}^N\big) : \ \dot{\boldsymbol{x}} :\equiv \boldsymbol{v} > \boldsymbol{0} \ \textit{on} \ [0,T]$$

and for the ***discontinuous improvement***

$$\boldsymbol{x} \in W^{2,\infty}\big((0,T);\mathbb{R}^N\big) : \ \dot{\boldsymbol{x}} :\equiv \boldsymbol{v} \geqq \boldsymbol{0} \ \textit{on} \ [0,T].$$

Proof. The proof consists of recalling that the proofs of the corresponding improvements all work for any leaders acceleration proposed in assumption (2) as long as the corresponding velocity would remain nonnegative/strictly positive. As the dynamics are only "one-directionally" coupled, i.e. the dynamics of the follower depend on the leader but not vice versa, we can use an inductive argument and first look on the dynamics for $\boldsymbol{x}_1, \boldsymbol{x}_2$. According to theorem 2.5.3 and theorem 2.5.4 we obtain the well-posedness. However, additionally also that the velocity $\boldsymbol{v}_2$ is nonnegative/strictly greater than zero. As a next step, we can thus consider the dynamics of $\boldsymbol{x}_2, \boldsymbol{x}_3$. As $\boldsymbol{x}_2$ satisfies the non-negativity/strict positivity of the velocity we can again apply the stated well-posedness results for two vehicles as in theorem 2.5.3 and theorem 2.5.4. This procedure can be iterated until we have reached $\boldsymbol{x}_N$ and we conclude with the existence and uniqueness of solutions and the nonnegativity/strict positivity of the velocities. □

2.7 Conclusions and future work

In this contribution, we have demonstrated the ill-posedness of the rather often used **intelligent driver model** (IDM) for specific initial datum and have presented some improvements to avoid these problems. The proposed work builds a solid foundation for future work on **1)** Multi-lane traffic with lane-changing. The lane-changing requires to know under which condition a car can change lane and how the well-posedness is affected by the lane change. For optimizing lane-changing to smooth traffic and avoid stop and go waves (thus saving

energy) we will next consider a suitable hybrid optimal control problem based on the proposed dynamics. **2)** Signalized junctions/intersection modelled with a form of the IDM also requires the proposed well-posedness in particular as a red traffic light necessitates the vehicles in front of it to stop (velocity becomes zero). **3)** Stability of solutions with regard to the model parameters and comparison of stability for the different suggested improvements. **4)** Implementations of the models presented in this article. While the numerical work presented above results from `matlab` [97] implementations and the use of `ODE45` and similar routines, it would be interesting to also theoretically study the discretization of these equations with standard finite difference schemes to see what guarantees can be provided for the numerical solutions (for example order of the numerical schemes, error bounds on the numerical solution etc.). **5)** It would also be of great interest for the improvements of the IDM model presented here to validate them against field data, or to see if the resulting microsimulation implementations (SUMO [89], Aimsun [1], etc.) match experimental data for specific choices of numerical parameters. In particular, it would be interesting to measure discrepancies with the prior IDM improvements in their implementation, and compare their respective performances. **6)** Finally, obtaining a general well-posedness result for the original IDM when restricting specific parameters and input data would be important and will be subject to further study to justify many already available simulation results a posteriori.

Chapter 3

Design of a Basis-based Feedback Controller with Optimal Control

3.1 Introduction

The development in technology and concepts in terms of vehicle on-board sensors and actuators, as well as for infrastructures, open an unprecedented research direction for the management of vehicular traffic. Researchers are granted with the capability of collecting real-time traffic data with on-board electronic devices with high accuracy in position and velocity measurements [51], the solution to data fidelity and timeliness through interfacing the optimized software and off-the-shelf hardware for data acquisition in real-time [21], and the availability of testbeds evaluating modern Close-Circuit Television (CCTV) camera systems for possible deployment on roadside poles for traffic observation and fast vehicle tracking computer vision algorithms [45]. Those made possible controlling the overall traffic with automated vehicles immersed in the bulk traffic stream.

The mixed autonomy system considered has both controlled- and human-driven-vehicles in the loop. To understand the impact of human driving behavior on the traffic, we refer to [134] for an illustration of the instability of traffic state caused by the enhancement of fluctuations, exhibiting "phantom jams" in which a traffic jam emerges from the collective behavior of drivers. The inclusion of automated vehicles can potentially dissipate the traffic waves, and in fact in [133] the authors show traffic jams could be effectively smoothed out with a single automated vehicle on a ring of more than 20 other human drivers, improving the throughput and energy efficiency.

Both deep learning based and mathematical approaches are proposed in the effort of alleviating ill traffic conditions and reduce fuel consumption. In the realm of machine learning methods, [66, 147, 156] leverage deep-RL policies to decongest stop-and-go waves and validate metrics to quantify the reduction in fuel consumption with the employment of automated vehicle. [146] studies the ability of autonomous vehicles to improve the throughput of a bottleneck using a fully decentralized control scheme in a mixed autonomy setting.

[85] demonstrates optimization of fuel economy in a large, calibrated model using a low penetration rate of decentralized controlled autonomous vehicles.

In the domain of mathematical approaches, PDE models are developed to characterize the traffic waves and simulate highway traffic under a variant of scenarios in [142, 87, 114, 5]. The authors of [137] study the initial-boundary value problem for a scalar nonlinear conservation law to determine the minimum time control problem of how to control the upstream vehicular flow appropriately to regulate the downstream traffic into a constant free flow state in minimum time. [136] investigates the well-posedness networked scalar semilinear balance laws with appropriate design of nonlinear boundary control operators. [81] introduces a model dealing with conservation laws on networks and coupled boundary conditions at the junctions. At the microscopic level, the authors of [140, 20, 8, 9] leverage ODE to model the car-following longitudinal dynamics. For the modeling of lateral dynamics, stochastic jump systems are used in [157] to model the lane-changing behavior. Queueing models for road traffic flow at intersections are developed and discussed in [101, 49, 151]. In order to smooth out the ill pattern in traffic, optimal control designs are advised in [133] where model-based control laws incorporating the knowledge of the traffic environment. Other common optimal control approaches include ACC [135, 59, 144], CACC [128, 112, 91, 127] and MPC [62]. In [82] the authors integrate vehicle dynamics and energy modeling into a single framework, and also develop a high fidelity simulator that allows users to quickly implement and test automated vehicle control schemes in complex traffic environments to assess their capacity to smooth waves and improve energy consumption.

Researchers also propose hybrid control scheme. In [158] the authors introduce a triple-mode hybrid control scheme by combining an efficient linear quadratic regulator, an efficient deep learning neural network, and a costly, fail-safe MPC.

Most of the modeling and optimal control effort, however, lack a theoretical study of the performance bound, due to the complexity of the model structure.

The aim of this contribution

The previous efforts in mathematical approaches to mobile traffic control lack a theoretical characterization to the actuations function space. This characterization is, however, essential as a guideline to the systematic design of traffic controllers. This chapter aims to attempt a primitive understanding of the actuation function space from an approximation theory point of view, where the acceleration functions can be characterized by a linear combination of well-chosen feedback basis coupled with a nonlinear transformation function.

Structure of this chapter

The chapter is organized in the following way. In section (3.2) we introduce the design of basis-based feedback controllers and define the optimal basis-based feedback controller as the solution of a finite dimensional constrained optimization problem. We discuss the choice

of basis functions in section (3.3). Section (3.4) collects a list of typical choices of the objective function. In the subsection (3.4) we also describe the multi-objective optimization problem and the linear scalarization. The setup of the numerical experiments and the numerical results are provided in section (3.5, where we define the Legendre polynomial basis in subsection (3.5) and specify the objective function in the numerics in subsection (3.5). The test trajectories analysis is conducted in subsection (3.5), and we study the equal velocities plots and phase plots in subsection (3.5). Finally in section (3.6) we conclude our work and mention future research directions opened by this contribution.

3.2 Problem Formulation: Optimal Basis-based Feedback Controller

Assume that we have a time-dependent leader vehicle trajectory $x_\ell \in C^2([0,T])$ be given for a considered finite time horizon $T \in \mathbb{R}_{>0}$. For the vehicle trajectory to be physically feasible and for the well-posedness of the ODE system we will define in the optimization problems (3.2.2), (3.5.5), (3.5.6), we make some additional assumptions on the trajectory.

Assumption 3 (Assumptions on the leader vehicle trajectory)**.** *We assume that for the leader vehicle trajectory* $x_\ell \in C^2([0,T])$
Physical feasibility of the velocity: $\dot{x_\ell} \geqq 0$.
Boundness of position and velocity: $(x_\ell, \dot{x_\ell}) \in L^\infty([0,T])^2$

We want to determine the best feedback controller (for the ego vehicle's position abbreviated here with x, ego vehicle's velocity abbreviated here with v) to optimize an objective function.

In order to address the problem stated above, we make a fundamental assumption on the function space of the ego vehicle's acceleration profile.

Assumption 4 (Controlled vehicle acceleration function space)**.** *We assume the function space of the ego vehicle's acceleration profile is a subspace of the Banach space* $\left(W^{1,\infty}(\mathbb{R}^3;\mathbb{R}), \|\cdot\|_{1,\infty}\right)$*, with a Schauder basis sequence* $\left\{\varphi_i \in W^{1,\infty}_{loc}(\mathbb{R}^3;\mathbb{R}), i \in \mathbb{N}\right\}$ *and a non-decreasing function* $A \in W^{1,\infty}(\mathbb{R}) \Subset L^\infty(\mathbb{R})$ *such that for every element* φ *in the acceleration function space there exists a unique sequence* $\left\{b_i \in \mathbb{R}, i \in \mathbb{N}\right\}$ *so that*

$$\varphi = A\left(\sum_{i=0}^{\infty} b_i \varphi_i\right) \tag{3.2.1}$$

where the convergence is understood with respect to the $\|\cdot\|_{1,\infty}$ *topology.*

For a review of the Schauder basis approximation theory and results, we refer to [98]. In reality, however, it is barely possible to implement the function characterization with a

countably infinite Schauder basis. A common alternative is to approximate the function based on a finite basis truncation. As our feedback controller is intended for real-world applications, we define the basis-based feedback controller with the finite truncation approximation, and we use the word *basis functions* to refer to the corresponding finitely truncated basis functions set. More specifically, we define the basis-based feedback controller as follows.

Definition 3.2.1 (Basis-based Feedback Controller)**.** *For a given set of basis functions* $\left\{\varphi_i \in W^{1,\infty}_{loc}(\mathbb{R}^3;\mathbb{R}), i \in \{1,\dots,N\}\right\}$*, a given coefficient vector* $\boldsymbol{b} \in \mathbb{R}^N$*, and a given non-decreasing function* $A \in W^{1,\infty}(\mathbb{R})$*, the* ***basis-based feedback controller*** *is defined as the acceleration profile*

$$\mathrm{Acc}[\boldsymbol{b}] : \begin{cases} \mathbb{R}_{\geq 0} \times \mathbb{R} \times \mathbb{R}_{\geq 0} & \to \mathbb{R} \\ (x_\ell - x, \dot{x_\ell} - v, v) & \mapsto A\left(\sum_{i\in\{1,\dots,N\}} b_i \varphi_i\big(x_\ell - x, \dot{x_\ell} - v, v\big)\right). \end{cases}$$

Remark 3.2.1 (The inclusion of the non-decreasing function $A \in W^{1,\infty}(\mathbb{R}) \Subset L^\infty(\mathbb{R})$)**.** *In real-world applications, it is desirable that the controlled vehicle has a bounded acceleration considering passenger comfort and hardware limitation. Therefore it is reasonable to use a monotonically non-decreasing and bounded transform function A to guarantee the boundness of the basis-based feedback controller, as well as to preserve the monotonicity property of the linear combination of basis functions.*

Having defined the acceleration function of our controller, we are ready to present the optimal basis-based feedback controller.

Definition 3.2.2 (Optimal Basis-based feedback controller)**.** *Let* $T \in \mathbb{R}_{>0}$ *be fixed. For a given trajectory* $x_\ell \in C^2([0,T])$ *satisfying assumption (3), a given objective functional* $J : \big(C^2([0,T]) \times C^1([0,T]) \times C^0([0,T]) \times \mathbb{R}^N\big) \mapsto \mathbb{R}$*, a non-decreasing function* $A \in W^{1,\infty}(\mathbb{R})$*, and a set of basis functions* $\left\{\varphi_i \in W^{1,\infty}_{loc}(\mathbb{R}^3;\mathbb{R}), i \in \{1,\dots,N\}\right\}$*, an* ***optimal basis-based feedback controller*** *is defined as the basis-based feedback controller where the coefficient vector* $\boldsymbol{b} \in \mathbb{R}^N$ *is an optimal solution of the following finite dimensional optimization problem*

$$\begin{aligned} \min_{b_i\in\mathbb{R},\ i\in\{1,\dots,N\}} \ & J(x[\boldsymbol{b}], v[\boldsymbol{b}], \dot{v}[\boldsymbol{b}], \boldsymbol{b}) \\ \dot{x}(t) &= v(t) && \forall t \in [0,T] \\ \dot{v}(t) &= \mathrm{Acc}[\boldsymbol{b}]\big(x_\ell(t) - x(t), \dot{x_\ell}(t) - v(t), v(t)\big) && \forall t \in [0,T] \\ x(0) &= x_0 \\ v(0) &= v_0 \\ x_\ell(t) - x(t) - l &\geq 0 && \forall t \in [0,T] \\ v(t) &\geq 0 && \forall t \in [0,T] \end{aligned} \tag{3.2.2}$$

with $(x_0, v_0) \in \mathbb{R} \times \mathbb{R}_{\geq 0}$ *being the initial position and velocity of the ego vehicle and* $l \in \mathbb{R}_{>0}$ *being the car length.*

For the optimization problem to be feasible, we make the following assumption on the initial datum.

Assumption 5 (Physical relevant initial datum)**.** *We assume the initial position and velocity provided in the definition (3.2.2) satisfies*

$$x_\ell(0) - x_0 - l \geq 0, \quad v_0 \geq 0. \tag{3.2.3}$$

Theorem 3.2.1 (Well-posedness of the ODE system)**.** *Assuming (3), given the* Acc *in definition (3.2.1) and a finite time horizon $T \in \mathbb{R}_{>0}$, the ODE system*

$$\begin{aligned} \dot{x}(t) &= v(t) && \forall t \in [0,T] \\ \dot{v}(t) &= \mathrm{Acc}[\boldsymbol{b}]\big(x_\ell(t) - x(t), \dot{x_\ell}(t) - v(t), v(t)\big) && \forall t \in [0,T] \\ x(0) &= x_0 \\ v(0) &= v_0 \end{aligned} \tag{3.2.4}$$

admits a unique solution $x \in W^{2,\infty}([0,T])$ for each choice of the coefficient vector $\boldsymbol{b} \in \mathbb{R}^N$.

Proof. We aim to prove the map $\mathrm{Acc}[\boldsymbol{b}] \in W^{1,\infty}(\mathcal{I};\mathbb{R})$ where $\mathcal{I} = \big\{(x_\ell - x, \dot{x_\ell} - v, v)\big\} \subseteq \mathbb{R}^3$ is the input space, under the assumption (3). First, $A \in W^{1,\infty}(\mathbb{R}) \Subset L^\infty(\mathbb{R})$ implies there exists a constant $B_0 \in \mathbb{R}_{>0}$ such that $\big|A\big| \leqq B_0$. Hence the $|v|$ can be upper bounded by the estimate

$$\begin{aligned} \big|v(t)\big| &= \left|v(0) + \int_0^t \mathrm{Acc}[\boldsymbol{b}]\big(x_\ell(\tau) - x(\tau), \dot{x_\ell}(\tau) - v(\tau), v(\tau)\big)\,\mathrm{d}\tau\right| \\ &\leq \big|v_0\big| + \int_0^t \left|A\left(\sum_{i\in\{1,\dots,N\}} b_i \varphi_i\big(x_\ell - x, \dot{x_\ell} - v, v\big)\right)\right| \mathrm{d}\tau \\ &\leq \big|v_0\big| + \int_0^T B_0\,\mathrm{d}\tau && (3.2.5) \\ &\leq \big|v_0\big| + B_0\,T && \forall t \in [0,T] \end{aligned}$$

where inequality (3.2.5) is due to the global upper bound for $|A|$. A global upper bound for $|x|$ can be derived by

$$\begin{aligned} \big|x(t)\big| &= \left|x(0) + \int_0^t v(\tau)\,\mathrm{d}\tau\right| \\ &\leq \big|x(0)\big| + \int_0^t \big|v(\tau)\big|\,\mathrm{d}\tau \\ &\leq \big|x(0)\big| + \int_0^T \big(\big|v_0\big| + B_0\,T\big)\,\mathrm{d}\tau && (3.2.6) \\ &\leq \big|x(0)\big| + \big(\big|v_0\big| + B_0\,T\big)\,T && \forall t \in [0,T] \end{aligned}$$

where inequality (3.2.6) is because of the global bound for $|v|$ derived before.

Combined with assumption (3), which implies the existence of a constant $B_1 \in \mathbb{R}_{>0}$ such that $\big|x_\ell\big| \leqq B_1$ and $\big|\dot{x_\ell}\big| \leqq B_1$, we now show the compactness of the input space $\mathcal{I}$ of basis functions φ_i as below,

$$\begin{aligned}\big|x_\ell - x\big| &\leq \big|x_\ell\big| + \big|x\big| \leq B_1 + \big|x(0)\big| + \big(\big|v_0\big| + B_0\,T\big)\,T,\\ \big|\dot{x_\ell} - v\big| &\leq \big|\dot{x_\ell}\big| + \big|v\big| \leq B_1 + \big|v_0\big| + B_0\,T,\\ \big|v\big| &\leq \big|v_0\big| + B_0\,T,\end{aligned}$$

hence the input space $\mathcal{I}$ is bounded in $\mathbb{R}^3$. The input space $\mathcal{I}$ is also closed in terms of the typical $\mathbb{R}^3$ topology. We therefore conclude the compactness of the input space $\mathcal{I}$ of basis functions φ_i in $\mathbb{R}^3$. The compactness of $\mathcal{I}$ and $\varphi_i \in W^{1,\infty}_{\text{loc}}(\mathbb{R}^3;\mathbb{R})$ implies $\varphi_i \in W^{1,\infty}(\mathcal{I};\mathbb{R})$. Finally as the map $\text{Acc}[\boldsymbol{b}]$ is the composition of $A \in W^{1,\infty}(\mathbb{R};\mathbb{R})$ and $\sum_{i\in\{1,\dots,N\}} b_i\varphi_i\big(x_\ell - x, \dot{x_\ell} - v, v\big) \in W^{1,\infty}(\mathcal{I};\mathbb{R})$ for each choice of the coefficient vector $\boldsymbol{b} \in \mathbb{R}^N$, $\text{Acc}[\boldsymbol{b}] \in W^{1,\infty}(\mathcal{I};\mathbb{R})$. Therefore the right hand sides of the ODE system are lipschitz continuous, and the existence and uniqueness of a global solution on the time interval $[0,T]$ follows by the Picard-Lindelöf Theorem ([[28], Chapter 4] or [[27], Thm 1.3).

□

Note that we do not incorporate the impact of our controller on cars behind. However, this could also be done by specifying the dynamics model of the follower vehicles. The generalization to more than 2 cars does not add more complexity to the problem formulation, as we can characterize the human-driven vehicles' dynamics by some specific car-following model, and we can characterize the controlled vehicles' dynamics by basis-based optimal controllers. The system dynamics can then be obtained by solving the ODEs sequentially from the leader to the followers.

3.3 Basis Functions

We now discuss the choices for basis functions $\Big\{\varphi_i \in W^{1,\infty}_{\text{loc}}(\mathbb{R}^3;\mathbb{R}), i \in \{1,\dots,N\}\Big\}$. Some typical choices for basis functions include

- **Polynomial basis functions:** $\{1, x_1, x_2, x_3, x_1x_2, x_1x_3, x_2x_3, x_1^2, x_2^2, x_3^2, \dots\}$.
- **Sinusoidal basis functions:** $\big\{\cos(2\pi\frac{n}{P}x_j), \sin(2\pi\frac{n}{P}x_j) : n \in \mathbb{Z}, P \in \mathbb{R}_{>0}, j = 1,2,3\big\}$, where $\frac{n}{P}$ is the frequency of the harmonic.
- **Radial basis functions:** $\big\{\exp(-\frac{1}{r}\|\boldsymbol{x} - \boldsymbol{\mu}_i\|_2^2) : i \in \mathbb{N}, \boldsymbol{\mu}_i \in \mathbb{R}^N, r \in \mathbb{R}_{>0}\big\}$ where N is the dimension of the input space (i.e., the dimension of x), $\boldsymbol{\mu}_i$ are the bump centers of the basis functions, and r determines the rate of decay.
- **Hyperbolic tangent functions:** $\{\tanh\left(a_i(x_j - b_i)\right) : i \in \mathbb{N}, a_i, b_i \in \mathbb{R}, j = 1,2,3\}$.

- **Splines:** piecewise polynomial functions satisfying smoothing conditions on the knots.

All basis functions above are plausible options and we do not know a priori how such basis functions for the acceleration function space should look like.

3.4 Objective Functional

Definition of objective functions

In this section we discuss potential choices of objective functions. To simplify the notation in this section, we denote $x := x[\boldsymbol{b}], v := v[\boldsymbol{b}], \dot{v} := \dot{v}[\boldsymbol{b}]$ but one should keep in mind they are really $\boldsymbol{b}$ dependent. In general functions $J : (C^2([0,T]) \times C^1([0,T]) \times C^0([0,T]) \times \mathbb{R}^N) \mapsto \mathbb{R}$ are candidates for the objective functions. In order to improve energy consumption or smooth the stop-and-go waves, some typical choices for the objective functional include

- **Cumulative fuel consumption function**: as devised in [82], we consider the instantaneous fuel consumption function $E : \mathbb{R}_{\geq 0} \times \mathbb{R} \mapsto \mathbb{R}$

$$\begin{aligned} E(v, \dot{v}) \coloneqq\ & C_0 + C_1 v + C_2 v^2 + C_3 v^3 \\ & + p_0 \dot{v} + p_1 \dot{v} \cdot v + p_2 \dot{v} \cdot v^2 \\ & + q_0 \max(\dot{v}, 0)^2 + q_1 \max(\dot{v}, 0)^2 v \end{aligned} \tag{3.4.1}$$

  where $v, \dot{v}$ denotes the velocity and acceleration respectively, $(C_0, C_1, C_2, C_3, p_0, p_1, p_2, q_0, q_1) \in \mathbb{R}^9$ are vehicle-specific model parameters. The cumulative fuel consumption cost is computed as

$$J_{\mathrm{E}}(x, v, \dot{v}, \boldsymbol{b}) \coloneqq \int_0^T E(v(t), \dot{v}(t))\, \mathrm{d}t. \tag{3.4.2}$$

  The inclusion of (3.4.2) in the cost function of (3.2.2) encourages the controlled vehicle to drive in a fuel-consumption-minimization way.

- **Miles-per-gallon (MPG):** the negative MPG cost is defined as

$$J_{\mathrm{MPG}}(x, v, \dot{v}, \boldsymbol{b}) \coloneqq -\frac{x(T) - x(0)}{\int_0^T E(v(t), \dot{v}(t))\, \mathrm{d}t}. \tag{3.4.3}$$

  The inclusion of (3.4.3) in the cost function of (3.2.2) induces a fuel-consumption-efficient driving behavior of the controlled vehicle, i.e., maximizing the travel distance for unit fuel consumption.

- **Two-second-rule:** the two-second-rule cost is defined as

$$J_{\text{2-sec-rule}}(x, v, \dot{v}, \boldsymbol{b}) \coloneqq \int_0^T |x_\ell(t) - x(t) - l - 2 \cdot v(t)|^2\, \mathrm{d}t \tag{3.4.4}$$

where $l \in \mathbb{R}_{>0}$ is the car length.
The two-second-rule can be generalized in two ways. We can generalize to the n-second-rule where $n \in \mathbb{R}_{>0}$, and we can generalize the L_2-norm penalization to L_p-norm penalization where $p \in [1, \infty)$, i.e. we define the general n-second-rule as

$$J_{\text{n-sec-rule}}(x, v, \dot{v}, \boldsymbol{b}) \coloneqq \left(\int_0^T |x_\ell(t) - x(t) - l - 2 \cdot v(t)|^p \, \mathrm{d}t \right)^{\frac{1}{p}}. \tag{3.4.5}$$

The inclusion of (3.4.5) in the cost function of (3.2.2) encourages the controlled vehicle to keep a n seconds time headway.

- **Acceleration:** the acceleration cost is defined as

$$J_{\text{acceleration}}(x, v, \dot{v}, \boldsymbol{b}) \coloneqq \left(\int_0^T |\dot{v}(t)|^p \, \mathrm{d}t \right)^{\frac{1}{p}} \tag{3.4.6}$$

where $p \in [1, \infty)$. The inclusion of (3.4.6) in the cost function of (3.2.2) penalizes rapid changes in the velocity of the controlled vehicle.

- **Travel distance:** the negative total distance travelled is defined as

$$J_{\text{distance}}(x, v, \dot{v}, \boldsymbol{b}) \coloneqq -\left(x(T) - x(0)\right) = -\int_0^T v(t) \, \mathrm{d}t, \tag{3.4.7}$$

which can be generalized to

$$J_{\text{distance}}(x, v, \dot{v}, \boldsymbol{b}) \coloneqq \left(\int_0^T v(t)^p \, \mathrm{d}t \right)^{\frac{1}{p}} \tag{3.4.8}$$

where $p \in [1, \infty)$. The inclusion of (3.4.8) in the cost function of (3.2.2) encourages the controlled vehicle to drive with a large feasible velocity.

- **Regularization:** the regularization penalty cost is defined as

$$J_{\text{regularization}}(x, v, \dot{v}, \boldsymbol{b}) \coloneqq \|\boldsymbol{b}\|^p = \left(\sum_{i=1}^N |b_i|^p \right)^{\frac{1}{p}} \tag{3.4.9}$$

where $\boldsymbol{b} \in \mathbb{R}^N$ is the coefficient vector, $p \in [1, \infty)$. The inclusion of (3.4.9) in the cost function of (3.2.2) improves the test performance by balancing the bias-variance trade-off and alleviating over-fitting.

The multi-objective optimization problem

In practice we would like to consider an optimization problem involving multiple objective functions to be optimized simultaneously. For example, we want to maximize the total distance travelled whilst to minimize the cumulative fuel consumption. Oftentimes we need to make a balance among conflicting objective functions. One a priori method to deal with the multi-objective optimization problem is **scalarizing the objective functions**. Specifically we consider the linear scalarization of the multiple objective functions.

Definition 3.4.1 (Linear scalarization)**.** *Given a set of objectives* $\left\{J_i :, i \in \{1, \dots, M\}\right\}$ *and the weights of the objectives* $\left\{\boldsymbol{w} \in \mathbb{R}^M_{\geq 0} : \sum_{i=1}^M w_i = 1\right\}$*, the* ***linear scalarization*** *of the multi-objective function on the set of objectives is defined as*

$$J \coloneqq \sum_{i=1}^{M} w_i J_i. \tag{3.4.10}$$

In the numerics section (3.5) we will experiment with specific choices of the weights in the linear scalarization of multi-objective optimization problem. Note that with different weights for the scalarization, different optimal solutions of (3.2.2) are produced. One needs to choose the weights with the goal of the specific problem in mind, weighting more the main metrics.

3.5 Numerical Results

In this section we provide numerical results and discuss differences in controlled vehicle's driving behavior with

- different choice of basis functions, and
- different choice of the weights for linear scalarization in the multi-objective optimization problem.

Choice of basis functions

For the numerical experiments we choose the polynomial functions as the basis functions for the acceleration function space. Specifically we define the Legendre polynomial basis below.

Definition 3.5.1 (Legendre polynomial basis)**.** *Consider the Legendre polynomials where the degree* $n \in \mathbb{N}$ *polynomial* $P_n(x)$ *is defined as*

$$P_n(x) \coloneqq \frac{1}{2^n\, n!} \frac{\mathrm{d}^n}{\mathrm{d}x^n} (x^2 - 1)^n.$$

*The **Legendre polynomial basis** up to degree $D \in \mathbb{N}$ is defined as the set of functions $\varphi_{ijk} \in C^\infty(\mathbb{R}^3; \mathbb{R})$ such that*

$$\varphi_{ijk}\big(x_\ell - x, v_\ell - v, v\big) := P_i\Big(\frac{x_\ell - x}{L}\Big) P_j\Big(\frac{v_\ell - v}{L}\Big) P_k\Big(\frac{v}{L}\Big), \;\; i+j+k \leq D, \;\; i,j,k \in \mathbb{N} \quad (3.5.1)$$

where $L \in \mathbb{R}_{>0}$ is a scaling factor.

Note that one motivation of choosing Legendre polynomials over monomials is because the Legendre polynomials are mutually orthogonal in the Hilbert space $W^{2,2}([-1,1];\mathbb{R}) \subseteq W^{1,\infty}([-1,1];\mathbb{R})$.

Example 3.5.1 (Legendre polynomial basis with $D = 2, L = 1$). For $D = 2$, the Legendre polynomials up to degree 2 are

$$\begin{aligned} P_0(x) &= 1, \\ P_1(x) &= x, \\ P_2(x) &= \tfrac{1}{2}\left(3x^2 - 1\right), \end{aligned}$$

and the set of Legendre polynomial basis consists of 10 functions

$$\begin{aligned} \Big\{ & P_0(x_\ell - x),\, P_1(x_\ell - x),\, P_2(x_\ell - x), P_1(v_\ell - v),\, P_2(v_\ell - v),\, P_1(v),\, P_2(v), \\ & P_1(x_\ell - x)P_1(v_\ell - v),\, P_1(x_\ell - x)P_1(v),\, P_1(v_\ell - v)P_1(v) \Big\}. \end{aligned}$$

Choice of objective functions

We experiment and compare two linear scalarizations of the multi-objective optimization problem (3.2.2), which both aim to maximize MPG whilst minimize the two-second-rule.

Definition 3.5.2 (Objective functions with and without regularization)**.** *Consider a set of objectives*

$$\Big\{ J_{MPG}, J_{2\text{-sec-rule}}, J_{regularization} \Big\}$$

*where the objective functional are defined in (3.4). The linear scalarization of the multi-objective function on the set of objectives **without** regularization is defined as*

$$J_{un\text{-}regularized} \coloneqq w_1 J_{MPG} + w_2 J_{2\text{-sec-rule}} \quad (3.5.2)$$

*and the linear scalarization of the multi-objective function on the set of objectives **with** regularization is defined as*

$$J_{regularized} \coloneqq w_1 J_{MPG} + w_2 J_{2\text{-sec-rule}} + w_3 J_{regularization}, \quad (3.5.3)$$

where $w_1, w_2, w_3 \in R_{>0}$.

Training trajectory data and choice of hyperparameters

- **Training data for the leader trajectories:** we take the real-world vehicle trajectories from I-24 dataset [102] as the data for leader trajectories x_ℓ. We divide the dataset into training data and test data, where we use the 61 training trajectories $x_{\ell_\mathrm{i}}^{\mathrm{train}}, i \in \{1, \dots, 61\}$ to train the optimal controller coefficient, and we use the 4 test trajectories $x_{\ell_\mathrm{i}}^{\mathrm{test}}, i \in \{1, \dots, 4\}$ to evaluate the performance of the optimal controller.

- **Hyperparameters:** in the experiments we let $D = 3$ and $L = 500$ in the Legendre polynomial basis (3.5.1), which results in a set of 35 basis functions. We choose $w_1 \propto 10^3, w_2 \propto 10^{-1}, w_3 \propto 10^{-6}$ for the weights in the objective functions in (3.5.2). We use $T = 200$ as the time horizon, $l = 1$ as the car length in the objective functions (3.4.3) and (3.4.4).

- **Non-decreasing function A:** for the function A in (3.2.1), we let

$$A(x) \coloneqq \tfrac{6}{\pi} \arctan(x). \tag{3.5.4}$$

  Note that $A(x) \in [-3, 3]$, therefore the controlled vehicle's acceleration is bounded between -3 and 3.

- **Optimization involving multiple training trajectories:** we train the optimal controller coefficient $\boldsymbol{b}$ on multiple training trajectories $x_{\ell_\mathrm{i}}^{\mathrm{train}}, i \in \{1, \dots, N^{\mathrm{train}}\}$ as the solution of the following optimization problem

$$\begin{aligned}
&\sum_{i=1}^{N^{\mathrm{train}}} \min_{b_j \in \mathbb{R},\ j \in \{1,\dots,N\}} J(x_\mathrm{i}[\boldsymbol{b}], v_\mathrm{i}[\boldsymbol{b}], \dot{v}_\mathrm{i}[\boldsymbol{b}], \boldsymbol{b}) \\
&\dot{x}_\mathrm{i}(t) = v_\mathrm{i}(t) && i \in \{1, \dots, N^{\mathrm{train}}\}, \forall t \in [0, T] \\
&\dot{v}_\mathrm{i}(t) = \mathrm{Acc}[\boldsymbol{b}]\big(x_{\ell_\mathrm{i}}^{\mathrm{train}}(t) - x_\mathrm{i}(t), \dot{x}_{\ell_\mathrm{i}}^{\mathrm{train}}(t) - v_\mathrm{i}(t), v_\mathrm{i}(t)\big) && i \in \{1, \dots, N^{\mathrm{train}}\}, \forall t \in [0, T] \\
&x_\mathrm{i}(0) = x_{\mathrm{i},0} && i \in \{1, \dots, N^{\mathrm{train}}\} \\
&v_\mathrm{i}(0) = v_{\mathrm{i},0} && i \in \{1, \dots, N^{\mathrm{train}}\} \\
&0 \le x_{\ell_\mathrm{i}}^{\mathrm{train}}(t) - x_\mathrm{i}(t) - l && i \in \{1, \dots, N^{\mathrm{train}}\}, \forall t \in [0, T] \\
&v_\mathrm{i}(t) \ge 0 && i \in \{1, \dots, N^{\mathrm{train}}\}, \forall t \in [0, T]
\end{aligned} \tag{3.5.5}$$

  where initial datum are $x_{\mathrm{i},0} \coloneqq x_{\ell_\mathrm{i}}^{\mathrm{train}}(0) - l - 2 \cdot \dot{x}_{\ell_\mathrm{i}}^{\mathrm{train}}(0)$ and $v_{\mathrm{i},0} \coloneqq \dot{x}_{\ell_\mathrm{i}}^{\mathrm{train}}(0)$, i.e., initially at $t = 0$ the controlled vehicle drive at the same speed as the leader, and start with a exact 2 second time headway.

- **Constraints in the optimization function:** the two constraints in the optimization problem (3.2.2) are essential to guarantee the feasibility of the controlled vehicle's trajectory, i.e., the controlled follower vehicle must not overtake the leader vehicle, and must not have negative speed. The constraints are potentially nonlinear in the

parameter vector $\boldsymbol{b}$ due to the nonlinearity of $A(\cdot)$, therefore we use **the method of Lagrange multipliers** to enforce the nonlinear constraints.

Definition 3.5.3 (Optimization problem with Lagrange function)**.** *Let the barrier function* $h_\varepsilon(y) := \Big(\log\big(\max\big(\varepsilon, \min(1, y+1)\big)\big)\Big)^2$*, with a small constant* $\varepsilon \in \mathbb{R}_{>0}$*. Let* $g_1(x_\ell, x) := h_\varepsilon(x_\ell - x - l)$ *and* $g_2(v) := h_\varepsilon(v)$*. The optimal feedback controller with* ***optimization problem in Lagrange function*** $\boldsymbol{b}_{Lagrange} \in \mathbb{R}^N$ *is defined as an optimal solution of the following optimization problem*

$$
\begin{aligned}
&\min_{\substack{b_i \in \mathbb{R} \\ i \in \{1,\dots,N\}}} J(x[\boldsymbol{b}], v[\boldsymbol{b}], \dot{v}[\boldsymbol{b}], \boldsymbol{b}) + \mu_1 \int_0^T g_1(x_\ell(t), x(t))\mathrm{d}t + \mu_2 \int_0^T g_2(v(t))\mathrm{d}t \\
&\dot{x}(t) = v(t) && \forall t \in [0,T] \\
&\dot{v}(t) = \mathrm{Acc}[\boldsymbol{b}]\big(x_\ell(t) - x(t), \dot{x_\ell}(t) - v(t), v(t)\big) && \forall t \in [0,T] \\
&x(0) = x_0 \\
&v(0) = v_0
\end{aligned}
\tag{3.5.6}
$$

where $\mu_1, \mu_2 \in \mathbb{R}_{>0}$*.*

Remark 3.5.1 (Nonconvexity of the optimization problem)**.** *There is no guarantee of the convexity of the optimization problem (3.5.3), due to our generic choice of objective function J and the non-linear traffic dynamics. Therefore one can only expect* ***local*** *optimum when optimizing using gradient decent methods.*

Remark 3.5.2 (Theoretical and numerical methods to compute gradient directions)**.** *We discuss the optimization routines with both the time-continuous optimization system (3.5.3) and the corresponding fully discretized system.*

- ***Time-continuous optimization system.*** *To resolve optimal control problems, i.e. optimization problems involving dynamic constraints, classical approaches such as Pontryagin's Maximum Principle [65] provide necessary conditions from the calculus of variations. The gradient directions can be obtained and updated by solving a coupled forward-backward ODE system.*
- ***Fully discretized optimization system.*** *For the fully discretized system, the gradient descent direction can be estimated by finite difference approximations.*

Finally, note that since we aim to keep a moderate size of the dimension of our coefficient vector $\boldsymbol{b}$*, numerical finite difference approximations of the gradient direction is computationally efficient. The PMP solution to our problem is not as efficient since the optimization coefficient* $\boldsymbol{b}$ *is not time-dependent while the computation of gradient directions requires solving the backward equations.*

Figure (3.1) shows the plots of the barrier functions $h_\varepsilon(\cdot)$ for multiple ε. The barrier only penalizes negative values, and the more negative the more penalization incurred. Also we see the smaller the ε, the larger the penalty. In the numerical experiments, we take $\mu_1 = \mu_2 \propto 10^6$ and $\varepsilon = 10^{-15}$.

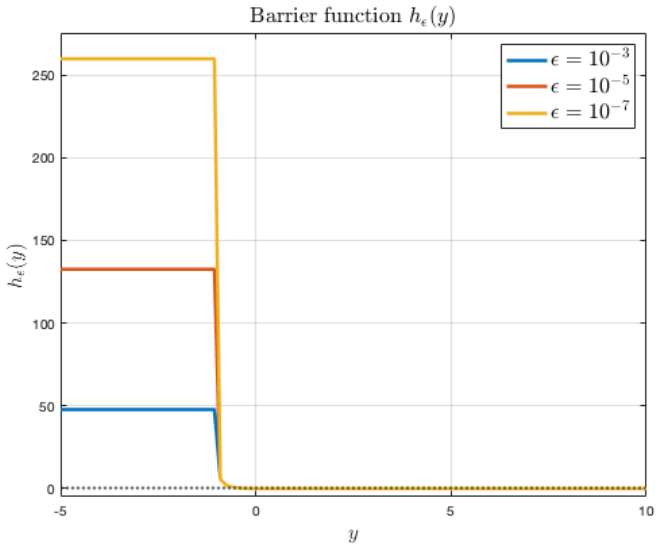

Figure 3.1: The barrier functions $h_\varepsilon(y)$ for different ε.

- **Matlab solvers and time discretization:** in order to solve the optimization problem with Lagrange function in (3.5.3), we use the nonlinear optimization solver `fmincon`$(\cdot)$ to find the minimum of constrained nonlinear multi-variable function. In order to numerically solve the ODEs in (3.5.3), we use the Runge–Kutta method with order 5 and non-adaptive time discretization, with time size chosen as 0.25.

Numerical results on test trajectories

We first look at the test results both with and without regularization. For the optimization problem (3.5.6), let $\boldsymbol{b}_{\text{un-regularized}}$ denote the optimal solution with $J = J_{\text{un-regularized}}$ and let $\boldsymbol{b}_{\text{regularized}}$ denote the optimal solution with $J = J_{\text{regularized}}$.

- **Norm of the optimal coefficient vector:** we first compare the L_2-norm of the optimal coefficient vectors,

$$\|\boldsymbol{b}_{\text{un-regularized}}\|_2 = 496.53, \quad \|\boldsymbol{b}_{\text{regularized}}\|_2 = 133.15,$$

where we see the inclusion of regularization cost in the objective function indeed reduces the norm of the coefficient vector.

- **Comparison between metrics:** we compute and compare the values of MPG and 2-second-rule with the two optimal coefficient vectors. The results are summarized in the table (3.1).
  - **The MPG metric:** the MPG metric is computed as $-J_{\text{MPG}}(x, v, \dot{v})$ where the negative MPG cost is defined in (3.4.3). For the MPG metric, the larger the value the better the performance (the controlled vehicle drives more miles with unit gallon of fuel consumption). One can observe that the MPG metrics of the two optimal controllers are close, with the regularized controller $\boldsymbol{b}_{\text{regularized}}$ performing moderately better and obtaining a slightly larger MPG compared to the unregularized controller $\boldsymbol{b}_{\text{un-regularized}}$ with 3 out of the 4 test trajectories.
  - **The 2-second-rule metric:** the 2-second-rule metric is computed as $J_{\text{2-sec-rule}}(x, v, \dot{v})$ where the 2-second-rule cost is defined in (3.4.4).In terms of the 2-second-rule metric, the smaller the value the more closely the controlled vehicle keeps a 2-second time headway from the leader vehicle. We see the regularized controller $\boldsymbol{b}_{\text{regularized}}$ obtains a uniformly smaller 2-second-rule cost compared to the ones obtained by the unregularized controller $\boldsymbol{b}_{\text{un-regularized}}$ with all 4 test trajectories.

Metrics	**MPG,** $\boldsymbol{b}_{\text{un-regularized}}$	**MPG,** $\boldsymbol{b}_{\text{regularized}}$	**2-sec-rule,** $\boldsymbol{b}_{\text{un-regularized}}$	**2-sec-rule,** $\boldsymbol{b}_{\text{regularized}}$
Trajectory #1	5.1102	5.1008	8798.1	3512.8
Trajectory #2	6.5066	6.5712	3007.8	1946.6
Trajectory #3	6.1075	6.1257	302.4	189.13
Trajectory #4	5.2975	5.2984	1666.9	803.1

Table 3.1: The comparison between MPG and 2-second-rule with and without regularization on the 4 test trajectories.

- **Optimal controlled trajectories:** In figure (3.2) and (3.3), we take a closer look at the optimal controlled trajectories generated by the two optimal controllers. Specifically, we compute
  - the **position trajectories** of the leader vehicle $\{x_\ell(t) : t \in [0, T]\}$ and the follower/controlled vehicle $\{x(t) : t \in [0, T]\}$
  - the **velocity trajectories** of the leader vehicle $\{\dot{x_\ell}(t) : t \in [0, T]\}$ and the follower/controlled vehicle $\{v(t) : t \in [0, T]\}$
  - the **headway trajectory** $\{x_\ell(t) - x(t) : t \in [0, T]\}$
  - the **instantaneous energy consumption trajectory of the controlled vehicle** $\{E(v(t), \dot{v}(t)) : t \in [0, T]\}$ with the function $E(\cdot, \cdot)$ defined in (3.4.1)
  - the **2-second-rule trajectory** $\{x_\ell(t) - x(t) - l - 2 \cdot v(t) : t \in [0, T]\}$

- the **acceleration trajectories** of the leader vehicle $\{\ddot{x}_\ell(t) : t \in [0, T]\}$ and the follower/controlled vehicle $\{\dot{v}(t) : t \in [0, T]\}$

Key observations include

- **Both optimal controllers smooth the leader's acceleration trajectories:** in the acceleration trajectories plots, we see the controllers stabilize the oscillations in the leader vehicles' acceleration, leading to smoother controlled acceleration trajectories. This is a desired behavior as smoother acceleration and braking implies less energy consumption and can potentially smooth the stop-and-go waves.
- **Both optimal controllers track the leader's velocity trajectories:** in the velocity trajectories plots, we see the controlled vehicle's velocity trajectories tend to imitate the one's of its leader's.
- **No violation of the feasibility of the controlled vehicles' trajectories:** in the velocity and the headway trajectories plots, we see there is no negative velocity or negative headway. This is a desired behavior of our controller and the barrier penalties are deactivated.
- **Extreme initial acceleration for the un-regularized optimal controller:** although in general the un-regularized controller determined by the $\boldsymbol{b}_{\text{un-regularized}}$ smooths the leaders' acceleration trajectories, we observe near $t = 0$ the controlled vehicle can have extreme acceleration or braking close to the maximal/minimal allowed acceleration. This is an undesired property of the optimal controller as this might lead to large instantaneous energy consumption near $t = 0$, and since we initialize the controlled vehicle with equal speed as the leader's speed and a 2-second headway, the extreme acceleration/braking seems unnecessary. In comparison, the regularized controller determined by the $\boldsymbol{b}_{\text{regularized}}$ manages to alleviate the initial extreme acceleration.

The results listed above are remarkable as the number of basis functions is relatively low. We observe the potential of polynomials up to degree three to capture the general trend of complex traffic trajectories.

Equal velocities plot and phase plots

In this section we study the acceleration profile generated by both controllers, i.e., the map $\text{Acc} : \mathbb{R}_{\geq 0} \times \mathbb{R} \times \mathbb{R}_{\geq 0} \mapsto \mathbb{R}$ as defined in (3.2.1). This map takes in a 3-dimensional input tuple consists of the headway $x_\ell - x$, the relative velocity $v_\ell - v$ and the controlled vehicle's velocity v. In order to visualize this map, we generate two types of plots fixing one of the elements in the input tuple,

- **Acceleration at and near equal velocities:** let the relative velocity be 0, i.e., let $v_\ell = v$. We generate the heatmap where the horizontal-axis is the controlled vehicle's

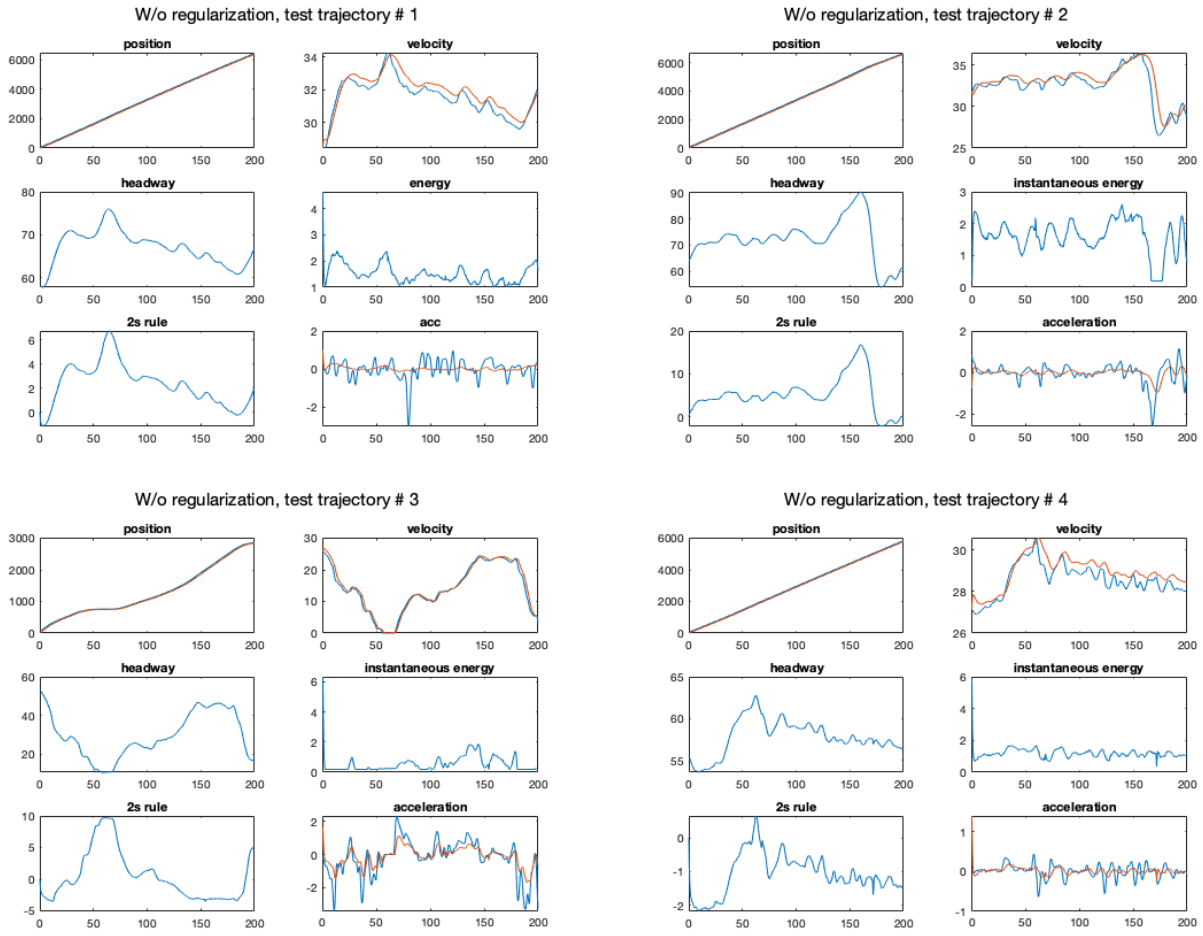

Figure 3.2: The test data result with $J_{\text{un-regularized}}$ as defined in (3.5.2). In the position, velocity and acceleration subplots, the **red** trajectories denote the controlled/follower vehicle's values and **blue** trajectories denote the leader vehicle's values. The energy subplot is the controlled/follower vehicle's instantaneous energy.

speed v, the vertical-axis is the headway $x_\ell - x$, and the color represents the value of the acceleration $\text{Acc}(x_\ell - x, 0, v)$.

- **Acceleration as function of phase space:** let the speed of the controlled vehicle v be fixed. We generate the the heatmap where the horizontal-axis is the leader vehicle's speed v_ℓ, the vertical-axis is the headway $x_\ell - x$, and the color represents the value of the acceleration $\text{Acc}(x_\ell - x, v_\ell - v, v)$ for a range of choice of v.

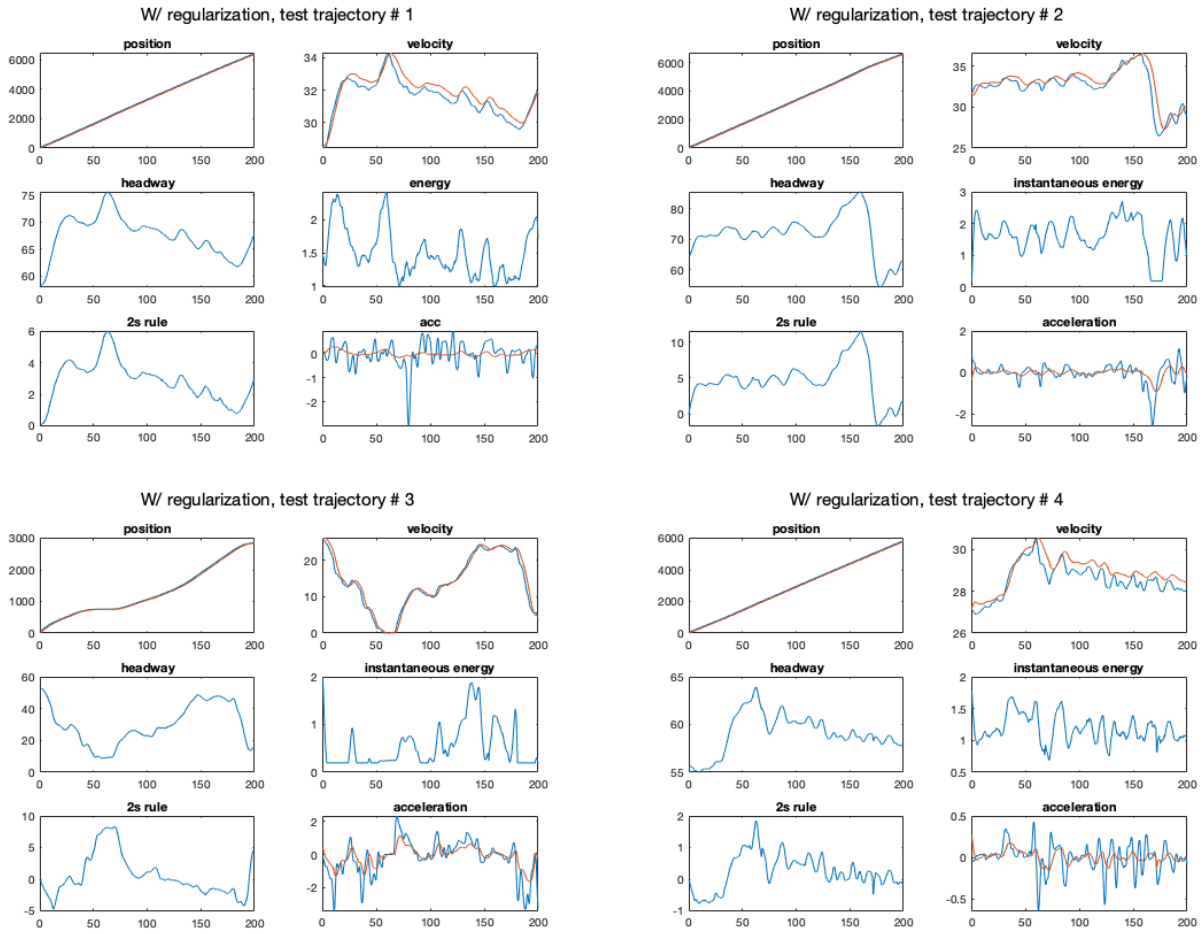

Figure 3.3: The test data result with $J_{\text{regularized}}$ as defined in (3.5.3). In the position, velocity and acceleration subplots, the **red** trajectories denote the controlled/follower vehicle's values and **blue** trajectories denote the leader vehicle's values. The energy subplot is the controlled/follower vehicle's instantaneous energy.

Acceleration at and near equal velocities

In figure (3.4) we show the equal velocities plots for both optimal controllers, where on the left is the plot with the un-regularized optimal controller and on the right is the plot with the regularized optimal controller. Key observations include

- **Both optimal controllers prescribe a roughly 2 second time headway, along with an added safety distance:** we see in both equal velocities plots, the equilibrium gap is unique for each $v \in [0, 30]$. The slope of the equilibrium curve (the sets of points generating zero acceleration) indicates the time headway kept by the controlled vehicle, which roughly equal to 2 seconds and increases slightly at higher speed for both optimal

controllers. The intercept of the equilibrium curve indicates the safe distance kept by the controlled vehicle, which roughly equal to 10 miles for both optimal controllers. This is a reasonable performance of a good optimal controller.

- **Both optimal controllers exhibit reasonable acceleration and braking behavior given the speed-headway pairs:** the controlled vehicle heavily brakes with large speed and small headway, and heavily accelerates with small speed and large headway. The acceleration transits between those two regions.
- **Sharp transition for the un-regularized optimal controller:** in the equal velocities plot for the un-regularized controller determined by $\boldsymbol{b}_{\text{un-regularized}}$, there is only a very slim transition region between maximum acceleration to maximum braking. This is an undesired property for the optimal controller as the controller might be too sensitive to the change in its inputs, posing difficulty to the hardware implementation and diminishing driving comfort. In comparison, with the regularized controller determined by $\boldsymbol{b}_{\text{regularized}}$, the transition in acceleration is smoother.

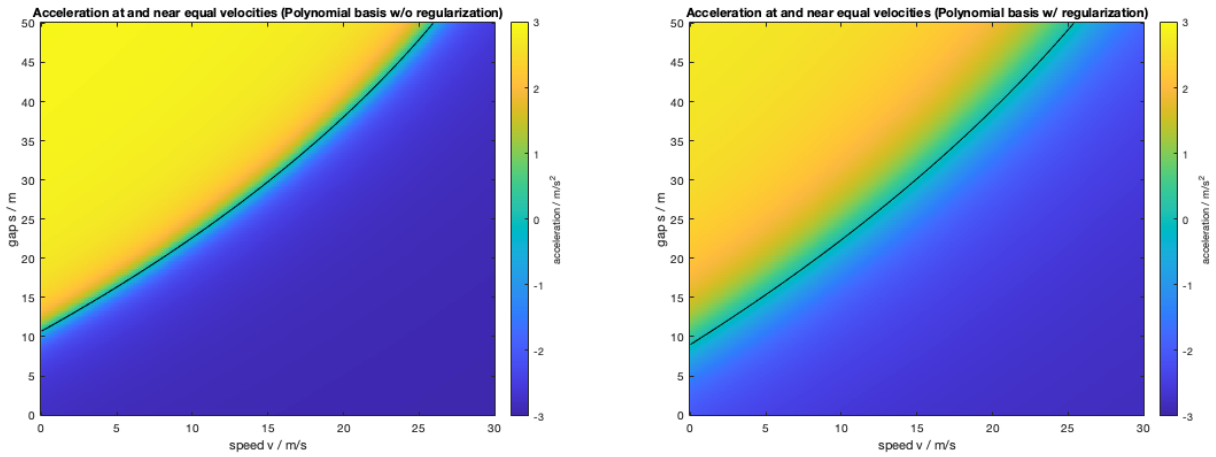

Figure 3.4: The equal velocity plot for both objective functions. Left: un-regularized. Right: regularized. The black curve in the plot is the equilibrium curve, i.e., the points of zero acceleration.

Acceleration as function of phase space

In figure (3.5) we show the phase plots for both optimal controllers, where the upper plots are generated with the un-regularized optimal controller and the lower plots are generated with the regularized optimal controller. Key observations includes

- **Both optimal controllers exhibit reasonable acceleration and braking behavior given the leader speed and headway pairs:** we see in both phase plots,

the equilibrium gap is unique for each $v_\ell \in [0, 30]$, where with fixed controlled vehicle speed v, the equilibrium headway decreases with larger leader speed v_ℓ. With fixed controlled vehicle speed v, the acceleration is negative with small leader speed and small headway, and the acceleration is positive with large leader speed and large headway. The braking region enlarges with larger controlled vehicle speed.

- **Sharp transition for the un-regularized optimal controller:** Again we see a sharp transition in the acceleration with the un-regularized controller determined by $\boldsymbol{b}_{\text{un-regularized}}$. This is an undesired property for the optimal controller for the same reason described in the section (3.5). Again with the regularized controller determined by $\boldsymbol{b}_{\text{regularized}}$, the transition in acceleration becomes smoother.

3.6 Conclusion and Future Work

In this chapter, we introduce the design of **optimal basis-based feedback controllers**. We demonstrate a systematic way to characterize the controlled vehicle's acceleration function space by a linear combination of basis functions and a (nonlinear) transformation function. We define the optimal basis-based feedback controller as the optimal solution of an optimization problem. We discuss the choice of basis functions and objective functions, and show the numerical results with Legendre polynomial basis optimal feedback controllers. We use the equal velocities plot and the phase plot to explore the performance of the optimal controller, to detect potential flaw in the design, and to study the robustness of the optimal basis controller regarding the input tuple.

Future work includes **1)** numerical experiments with basis functions other than polynomials and a systematic comparison among the performance of the optimal controllers with different choices of basis functions, **2)** a study of the impact of the choice of the transformation function $A(\cdot)$, **3)** experimenting and studying the impact of potential inclusion of existing car-following models into the basis functions, **4)** exploring the robustness of the optimal controller regarding the initial datum (x_0, v_0) in the optimization problem (3.2.2).

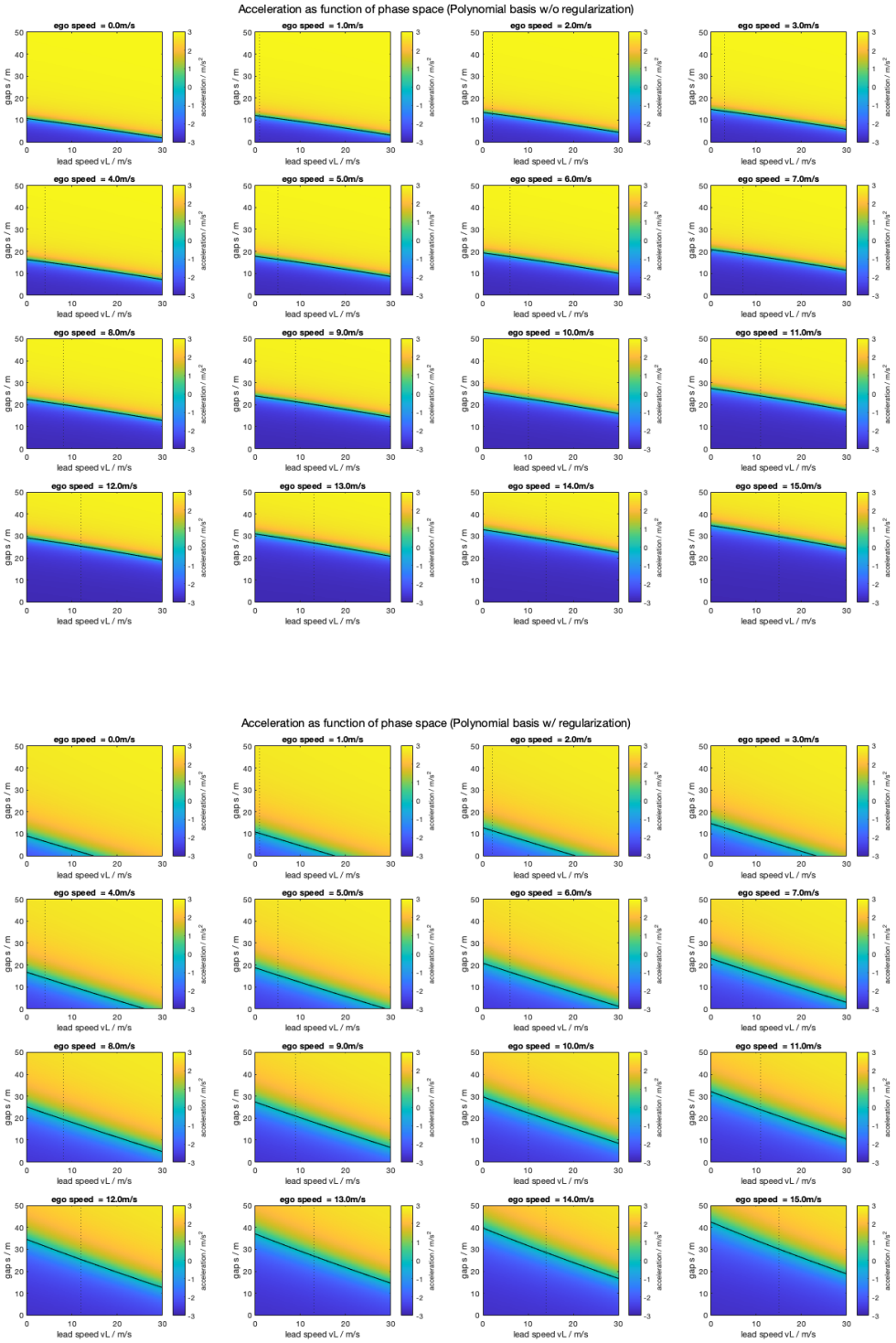

Figure 3.5: The phase plots for both objective functions. Upper: un-regularized. Lower: regularized. The black curve in the plot is the equilibrium curve, i.e., the points of zero acceleration. The dotted vertical line indicates $v_\ell = v$.

Chapter 4

Parallel Network Flow Allocation in Repeated Routing Games via LQR Optimal Control

4.1 Introduction

The routing problem – a problem in which trip-makers route traffic between an origin and destination – is a central and essential component in the study of urban transportation planning. Emerging as an enabler to this problem over the last decade, navigational apps have used solution from the routing problem to provide shortest paths from origin to destination, or identify the paths with the shortest travel time [22]. Due to ubiquitous adoption of navigational apps by motorists (commuters, travelers), TNCs (Lyft/Uber), delivery fleets [58], and many others, these apps are playing even bigger roles in transportation and the significance of their roles are growing [4]. With increased penetration routing app users, navigational apps are starting to "act" as flow allocation mechanisms – having positive effects on some cities travels and negative on others when users use local neighborhood routes to avoid traffic [138]. Thus, it is becoming ever for important to understand the routing game problem, its solutions, and how flow allocation mechanisms (and traffic assignment) are being used in transportation.

The traffic assignment problem is a model framework for aggregated flows of motorists routed through a network from their origins to their destinations. To address the traffic assignment problem, this process has initially been modeled in a static way using notions such as static traffic assignment, for which specific solutions exist like User equilibrium and system optimal [19, 109]. In this static model, we assume the network being studied is close to "steady state", and that the current network capacity is the capacity over the entire analysis period. However, in hopes to move away from this assumption and better model traffic in urban areas, researchers have moved toward dynamic traffic assignment models, which aim to model time-varying networks and demand interactions and changes [26, 126,

93, 19]. Additionally, within the field of traffic control, researchers have used simulation based approaches [107] and some are starting to use big data to further analyze travel behavior [25].

The traffic assignment problem has been modeled using game theory among many other techniques. Specifically, it has been posed in a game theoretic framework called routing game. A routing game is a game in which the players (non-cooperatively) route traffic between an origin and a destination of a proposed network, where the network models a system of roads. After each player chooses routing strategies, each player will incur a cost on the route they choose [103]. One specific kind of game is called "the one-shot" game. The one-shot routing game is a static game[1], where the players make their decision simultaneously and therefore no time history is involved. Within the one-shot game framework, multiple equilibrium models and the corresponding equilibria have played an important role in understanding the inefficiencies of networks (e.g. the price of anarchy [118]), for example the user equilibrium or Nash equilibrium [109]. Properties and the characterizations of the equilibrium solutions are also well-studied, for example, the Nash equilibria are known to be the solution set of the convex Rosenthal potential function [116]. Closely related works include [77, 76], where the authors present a game theoretic framework for studying Nash and Stackelberg routing games on parallel networks with horizontal queues, and in [60] the authors futher study the Stackelberg thresholds with the same problem setup. [37] proposes a heterogeneous routing game in which each driver or vehicle belongs to a certain type, and investigates the existence of a Nash equilibrium in this heterogeneous routing game.

Within routing games, one can also study a dynamic game, where the environment is time varying. The analysis of such games is more difficult from a theoretic standpoint: the notion of dynamic equilibria has to be introduced, and extra ingredients like information acquisition and time ordering of the execution of the actions need to be specified [11]. Therefore, moving towards more dynamical games, we consider repeated games, i.e. a static game iterated over time, as a model of the evolution of the traffic situation. The iteration here can be naturally interpreted as time discretization (e.g. sometimes where traffic conditions are steady over time intervals). In the case of the present work, we follow previous approaches in which the repeated nature of the game encompasses the process of a routing entity (Google, Waze, etc) to learn from day to day from their previous performances. Oftentimes (and it is the case in our formulation), the repeated version is essentially the sequential appreciation of a static game. A natural question to study is the behavior of the dynamics, when the players repeat a static game using past information. Dynamics in a repeated routing game might not converge, and even if it does, convergence might not be quantifiable (e.g. convergence almost everywhere, convergence in the sense of Cesaro means or of the time-averages, etc.). Even when the dynamics sequence converges itself, the equilibria to which it converges to (Nash equilibrium or social optimum) might not be unique [80]. Approaching this question, Krichene et al. estimates the learning dynamics within an online learning model of player dynamics [71] and studies the traffic dynamics under partial control [72]. Discussions of

[1] A static game is played only once with one iteration.

optimization algorithms and the convergence of the learning algorithms to an equilibrium are conducted in [6, 70, 75, 73]. The authors of [34] study the stability property of the optimal in the congestion game under Replicator dynamics. [31] investigates the privacy in the routing game, where the origins and destinations of drivers are considered private.

To better understand the routing game in these systems and provide bigger impacts in transportation, we might also want to leverage concepts from other areas of engineering. Modeling and analysis of conflict, the study of systems, and the study of their equilibria are not unique to the routing game. In fact, very similar concepts and analysis shows up in control theory, which oftentimes, similarly to game theory, models interactions between a system of controllers (the "decision-makers") and their environment [113]. Unsurprisingly, many influences within game theory show up in many areas of controls (differential games, teams games, and distributed control) [94], and many connections can be made between the two. Even though there exists many similarities and influences between game theory and controls, there are many useful control design techniques that exists separate from game theory [47, 2, 10], but are conceptually similar/applicable to designing decision-makers within routing games, especially for routing systems like google.

Therefore, in this chapter, we contribute to the literature of routing games and draw from other areas of engineering to make deeper connections and make use of control techniques for routing. We specifically introduce a new game design framework for routing games using the linear-quadratic regulator (LQR).

Key Contributions

The present chapter focuses on transforming the repeated game problem into a control theoretic problem, and studying the convergence of the game dynamics in this framework. The key contributions of the chapter include the following:

- We provide a game design scheme for repeated routing games through the Linear Quadratic Regulator (LQR).
- We design control dynamics with specific choices of system parameters to respect the conservation of flow and achieve specific convergence results.
- We provide a method for producing piecewise affine optimal routing strategies using explicit model predictive control (MPC) techniques.
- We derive new theoretical results for specific cases of the new design scheme.
- We illustrate a geometric framework for visualizing optimal routing solutions for every feasible state in the routing game.
- We extend the comparison literature between game theory and controls.

Structure of this chapter

This chapter, first, explains the new control theoretic game design scheme in section 4.3, under which we also build up the intuition and understanding of the framework by illustrating an evolution of the game from a one-shot framing (see section 4.3) to a repeated game framing (see section 4.3), and finally to the new control framing (see section 4.3). We further present analogies between the new framework and a classical algorithmic game theory model of routing games within this section (see section 4.3); then, we finally talk about how to design the game (see section 4.3) and its interpretation (see section 4.3). Next, we run through the system analysis and its properties in section 4.4, where we additionally describe a few requirements for the system. In section 4.5, we describe a algorithmic approach to solve the control routing problem using explicit MPC techniques. Finally, in section 4.6 we run through a few numerical simulations and present its results with associated discussions.

4.2 Preliminary

Notation	Description	Type
$\mathcal{G} = (\mathcal{V}, \mathcal{E})$	A parallel network for the routing game made of a set of edges $\mathcal{E}$ (as roads) and a set of vertices $\mathcal{V}$ (one origin and one destination)	A directed graph
$e \in \mathcal{E}$	An edge in the edge set	An element of $\mathcal{E}$
$l_e(\cdot)$	Affine latency function on edge e	$\mathbb{R}_{\geq 0} \mapsto \mathbb{R}_{\geq 0} : l_e(f_e) = a_e f_e + b_e, a_e, b_e \geq 0$
n_e	Number of parallel edges	$\mathbb{N}$
T	Time horizon (total number of rounds in game)	$\mathbb{N}$ (discrete time)
Δ	Probability Simplex	$\Delta := \{f : \sum_{e \in \mathcal{E}} f_e = 1, f_e \geq 0\}$
f	Flow allocation vector on the network	$\Delta, f = (f_e)_{e \in \mathcal{E}}$
l	Latency vector incurred on the network	$\mathbb{R}^{n_e}_{>0}, l = (l_e(f_e))_{e \in \mathcal{E}}$
$\mathbf{x}_t$	System state vector at time t	$\Delta, \mathbf{x}_t = (x_1^t, \ldots, x_{n_e}^t)^\top$
$\mathbf{u}_t$	System input vector at time t	$\Delta, \mathbf{u}_t = (u_1^t, \ldots, u_{n_e}^t)^\top$
$\mathbf{x}^*$	Steady state of the system	Δ
$\mathbf{x}_0$	Initial state of the system	Δ
Q_f	Terminal cost matrix	$\mathbb{R}^{n_e \times n_e}$ positive semi-definite
R	Running cost matrix for inputs	$\mathbb{R}^{n_e \times n_e}$ positive semi-definite
Q	Running cost matrix for states	$\mathbb{R}^{n_e \times n_e}$ positive semi-definite
γ	Weight parameter in the dynamics	$\gamma \in [0, 1]$
A	Mapping from the memory to decision	$\mathbb{R}^{n_e \times n_e}$ left stochastic matrix
B	Mapping from suggested routing to decision	$\mathbb{R}^{n_e \times n_e}$ left stochastic matrix

4.3 LQR Repeated Game Framework for Routing in Parallel Networks

We consider a specific routing game design problem where the routing game is posed with a parallel network, $\mathcal{G}$. $\mathcal{G}$ is modeled as a directed graph $\mathcal{G} = (\mathcal{V}, \mathcal{E})$, where $\mathcal{V}$ is a set containing two nodes (an origin o and a destination d), and $\mathcal{E}$ is an edge set containing n_e edges between each vertex.

One-shot Game Framework

We start by introducing the flow allocation problem, which we will use later as a potential equilibrium point for our repeated game. We will also refer to it as a one-shot game (i.e. a repeated game converging in one iteration).

Definition 4.3.1 (Edge flows)**.** *For each edge $e \in \mathcal{E}$, the edge flow, $f_e \in \mathbb{R}_{\geq 0}$, represents a large collection of non-atomic drivers using edge e on the network. Each edge flow, f_e, represents a portion of traffic in the game (and thus has "mass"), while individual drivers themselves do not. They are negligible with respect to the total number of drivers present (i.e. the non-atomic framework).*

In the flow allocation problem, all drivers are allocated along the network's edges, and each allocation incurs a latency (i.e., loss), l (this latency is usually labeled as the average travel time each driver took). Each edge's latency l is modeled in the present work as an affine function associated with each edge.

Definition 4.3.2 (Latency function)**.** *Each edge $e \in \mathcal{E}$ has an affine latency function $l_e(\cdot) : \mathbb{R}_{\geq 0} \mapsto \mathbb{R}_{\geq 0}, l_e(f_e) = a_e f_e + b_e, a_e, b_e \geq 0$ that converts the edge flow f_e into the edge latency. The latency functions are nonnegative, nondecreasing and Lipschitz-continuous functions.*

Normally, in the allocation problem, drivers at the origin, o, are allocated strategically to reduce the total travel time the system will incur. The resulting allocation for all of the drivers of total mass 1 in $\mathcal{G}$, is represented as a stochastic vector $f = (f_e)_{e \in \mathcal{E}} \in \mathbb{R}^{n_e}_{\geq 0}$, where each f_e tells us the proportion of flow being allocated on edge e. Specifically,

$$f \in \Delta, \text{ where } \Delta := \{f : \sum_{e \in \mathcal{E}} f_e = 1, f_e \geq 0\} \tag{4.3.1}$$

Nash Equilibrium

If we assume that all drivers act rationally and has access to perfect information, we can describe an equilibrium of the game, known as the ***Nash equilibrium***.

Definition 4.3.3 (Nash equilibrium)**.** *A flow allocation $f \in \Delta$ is a Nash equilibrium (user equilibrium [109], non-atomic equilibrium flow [103], or Wardrop equilibrium [150]) if and only if:*

$$\forall e \in \mathcal{E} \text{ such that } f_e > 0, \quad l_e(f_e) = \min_{e' \in \mathcal{E}} l_{e'}(f_{e'}). \tag{4.3.2}$$

Repeated Game Framework

In order to encompass time-varying changes in the system, one can use "repeated play" or learning models [23]. In this framework, a flow allocator (i.e. Gooogle maps) makes a decision iteratively, as opposed to one time in the one-shot game, and uses the outcome of each iteration to adjust their next decision. Adding a t dependency for time to the aforementioned notation, $f_t \in \Delta$ becomes the flow allocation at time t, $l_t \in \mathbb{R}^{n_e}_{\geq 0}$ becomes a vector of latencies produced from functions $l_e(\cdot)$ at time t, and throughout the game, the flow allocator iteratively chooses f_t and then observes l_t. In this framework, designing learning models of player decisions and whether the resulting dynamics asymptotically converges to equilibrium is one of the objectives of our article. Furthermore, we are also interested in situations in which convergence happens in one shot. Previous research has been done to characterize classes of learning algorithms that converge to different sets of equilibria [17, 94, 48]. Specifically, different models of learning algorithms and their associated convergence guarantees has been studied for the routing game [71, 72, 74].

LQR Framework

Table (4.1) sets the framework for the proposed work. The right column defines the repeated game framework previously described (using example designs from previous work [69]), while the left column defines the classical control framework used later for LQR control. Both frameworks present obvious mathematical analogies [94, 95].

We re-frame the routing problem under the repeated game framework into the LQR framework and solve for/analyze player strategies using existing control techniques. We will essentially aim to do the same game theoretical analysis within linear/nonlinear controls. In the right column of the table, we list the setup under the repeated game framework. The goal of the routing problem there is to design algorithms that dictate strategies for players (the flow allocator). At each time step t, the algorithm updates the flow allocation f_{t+1} based on the players' memory f_t and the loss on the edge l_t induced by the traffic [74, 72, 68, 117]. The goal is to guarantee a sub-linear regret and a convergence to the set of Nash equilibria.

We start from the repeated games setup, and cast the repeated game problem in a control theoretic framework. We keep the authoritative central decision maker $\mathbf{u}$ as the flow allocator, but we differentiate between the "player" and the "decision-maker" as coined in the original game theoretic setup. Here, the "players" will refer to the drivers in the network

	Control problem	**Repeated game (online learning)**
Notation	$\mathbf{x}_t$ state, $\mathbf{u}_t$ control at time t	f_t flow allocation, l_t loss at time t
Entities involved	• Central decision maker: flow allocator • Players: drivers	• Central decision maker: flow allocator • Players: flow allocator
Design	$\mathbf{u}_t(\cdot)$ s.t. $\mathbf{x}_{t+1} = g(\mathbf{x}_t, \mathbf{u}_t)$ is stable, where $g(\cdot,\cdot)$ is the recurrence relation defining the dynamics.	$h(\cdot,\cdot)$ s.t. $f_{t+1} = h(f_t, l_t)$ defines the dynamics for the routing game.
Example designs	$\mathbf{u}_t(\mathbf{x}_t) = K\mathbf{x}_t$ and $g(\mathbf{x}_t, \mathbf{u}_t) = A\mathbf{x}_t + B\mathbf{u}_t \implies \mathbf{x}_{t+1} = (A+BK)\mathbf{x}_t$, where (A, B) is stabilizable, and $A + BK$ is asymptotically stable.	$h(f_t, l_t) = \operatorname{argmin}_{f\in\Delta} l_t^\top (f - f_t) + \frac{1}{\eta_t} D_\Psi(f, f_t)$, where η_t is the learning rate at time t, $D_\Psi(\cdot,\cdot)$ is the Bregman divergence induced by a strongly convex function Ψ defined as $D_\Psi(x, y) = \Psi(x) - \Psi(y) - \nabla\Psi(y)^\top(x - y)$. This is called the **mirror descent algorithm** with Bregman divergence D_Ψ.
Objective function (to minimize)	Cumulative cost, $\sum_{t=0}^{T-1} c_1(\mathbf{x}_t, \mathbf{u}_t) + c_{1,T}(\mathbf{x}_T)$	Cumulative regret, $\sum_{t=0}^{T} c_2(f_t, l_t) - \min_{f\in\Delta} \sum_{t=0}^{T} c_2(f, l_t)$
Example objective functions	$c_1(\mathbf{x}_t, \mathbf{u}_t) = \mathbf{x}_t^\top Q\mathbf{x}_t + \mathbf{u}_t^\top R\mathbf{u}_t$, $c_{1,T}(\mathbf{x}_t) = \mathbf{x}_t^\top Q_f \mathbf{x}_t$, $Q, Q_f \succeq 0, R \succ 0$	$c_2(f_t, l_t) = f_t^\top l_t$

Table 4.1: The framework for the proposed work.

flow being routed. In our framework, the "players" do not play; they are only considered by the routing system and the model. The central decision maker is what we want to design in this framework. It has full access to the flow allocation $\mathbf{x}$ on the network, and aims to achieve a certain routing goal (e.g., steer the network flow to a target flow distribution, or minimize the average travel time). The central decision maker embeds the routing goal in the cumulative cost function $\sum_{t=0}^{T-1} c_1(\mathbf{x}_t, \mathbf{u}_t) + c_{1,T}(\mathbf{x}_T)$. The players now update their routing decision $\mathbf{x}_{t+1}$ by leveraging their memory $\mathbf{x}_t$ and the central decision maker's suggested routing distribution $\mathbf{u}_t$ at each time step. The target flow allocations $\mathbf{x}^*$ are characterized as the steady states of the controlled system, and the central decision maker chooses the optimal controls $\{\mathbf{u}_t\}$ to minimize the cumulative cost function and stabilizes the system to its steady states.

The choice of LQR is motivated by the observation that a potential game with affine latency and a parallel network can be naturally framed as a **quadratic** cost and **linear** dynamic problem, leveraging the convex formulation of the Rosenthal potential:

$$\underset{\mathbf{u}_t, t=0,\ldots,T-1}{\text{minimize}} \quad \sum_{t=0}^{T-1} \left(\mathbf{x}_t^\top Q\mathbf{x}_t + \mathbf{u}_t^\top R\mathbf{u}_t\right) + \mathbf{x}_T^\top Q_f \mathbf{x}_T \tag{4.3.3}$$

$$\text{subject to} \qquad \mathbf{x}_{t+1} = A\mathbf{x}_t + B\mathbf{u}_t, t = 0, 1, \ldots, T-1 \tag{4.3.4}$$

$$\mathbf{x}_0 = \mathbf{x}(0) \tag{4.3.5}$$

where $\mathbf{x}_t \in \mathbb{R}^{n_x}$ is the state of the system at time t and $\mathbf{u}_t \in \mathbb{R}^{n_u}$ is the action of the decision-maker at time t, with appropriate matrices A, B, Q, R, Q_f. Within this framework, we can leverage known optimal control techniques to formulate optimal strategies and inherent known properties for the system. Furthermore, definition (4.3.3) for the context here becomes:

Nash Equilibrium

Definition 4.3.4 (Nash equilibrium)**.** *A state of the system $\mathbf{x} \in \Delta$ is a Nash equilibrium if and only if:*

$$\forall e \in \mathcal{E} \text{ such that } \mathbf{x}_e > 0, \quad l_e(\mathbf{x}_e) = \min_{e' \in \mathcal{E}} l_{e'}(\mathbf{x}_{e'}). \tag{4.3.6}$$

We reiterate the key differences between the repeated game framework and our control theoretic framework:

1. In repeated games for parallel networks, the two entities involved, the player and the central decision maker are the same (a flow allocator). However, in our control theoretic framework, the two entities are different – **players being the drivers** (in the present case aggregated as non-atomic along the edges) and **the central decision-maker being the flow allocator**.

2. In repeated games, the players update their flow allocation based on their memory f_t and the incurred loss l_t on the network. In our control theoretic framework, the players update their flow allocation based on **their memory $\mathbf{x}_t$** and **the central decision maker's suggested routing decision $\mathbf{u}_t$**.

3. In repeated games, one possible goal of the non-atomic player, the flow allocator, (see for example [68, 67]) is to update their flow allocation in order to converge to the set of Nash equilibria and to achieve sub-linear regret. In our control theoretic framework, **the goal of the central decision maker is to steer the flow allocation to a target flow distribution, by inputting suggestions to the system's players (drivers)**.

Designing Games with LQR

We now describe our control routing model.

1. States and controls: the *state* of the LQR at time t is the flow vector $\mathbf{x}_t$, consisting of the flow on each edge at time t, and the *control* at time t is the flow allocation $\mathbf{u}_t$

given by the decision maker, i.e.,

$$\mathbf{x}_t = (x_1^t, \ldots, x_{n_e}^t)^\top, t = 0, \ldots, T \tag{4.3.7}$$
$$\mathbf{u}_t = (u_1^t, \ldots, u_{n_e}^t)^\top, t = 0, \ldots, T-1. \tag{4.3.8}$$

We model both $\mathbf{x}_t, \mathbf{u}_t \in \Delta$ at each time step t.

2. Equation for the dynamics: we assume the dynamics of the flow update is described using a linear time invariant difference equation

$$\mathbf{x}_{t+1} = \gamma A\mathbf{x}_t + (1-\gamma)B\mathbf{u}_t, t = 0, 1, \ldots, T-1 \tag{4.3.9}$$

where $\gamma \in [0, 1]$ is a design parameter that weights the contribution of $\mathbf{x}_t$ and $\mathbf{u}_t$ in the update rule, and $A, B \in \mathbb{R}^{n_e \times n_e}$ are two design matrices deciding how the flow vectors $\mathbf{x}_t$ and $\mathbf{u}_t$ will affect the drivers' routing decision in the subsequent time step respectively.

3. Cost function: the cost function of our control problem is a summation of quadratic functions

$$\sum_{t=0}^{T-1} \left(\mathbf{x}_t^\top Q\mathbf{x}_t + \mathbf{u}_t^\top R\mathbf{u}_t\right) + \mathbf{x}_T^\top Q_f \mathbf{x}_T \tag{4.3.10}$$

where $Q, Q_f, R \succeq 0$.

The resulting control problem is

$$\underset{\mathbf{u}_t, t=0,\ldots,T-1}{\text{minimize}} \quad \sum_{t=0}^{T-1} \left(\mathbf{x}_t^\top Q\mathbf{x}_t + \mathbf{u}_t^\top R\mathbf{u}_t\right) + \mathbf{x}_T^\top Q_f \mathbf{x}_T \tag{4.3.11}$$

$$\text{subject to} \quad \mathbf{x}_{t+1} = \gamma A\mathbf{x}_t + (1-\gamma)B\mathbf{u}_t, t = 0, 1, \ldots, T-1 \tag{4.3.12}$$
$$\mathbf{x}_t \in \Delta, t = 0, \ldots, T \tag{4.3.13}$$
$$\mathbf{u}_t \in \Delta, t = 0, \ldots, T-1 \tag{4.3.14}$$

Interpretation of the Framework

We now provide interpretations for the design of the control system.

1. States $\mathbf{x}_t$: the interpretation of the state $\mathbf{x}_t$ is twofold: (1) one could interpret it as the routing decision made by the drivers from one day to another, and (2) it is also the *actual flow distribution* on the network, incurred by the drivers. We assume all drivers comply with a routing decision which depends at the same time on the past state, and the control.

2. Controls $\mathbf{u}_t$: One could interpret the control $\mathbf{u}_t$ as the recommended routing decision from the central decision maker.

3. The $A\mathbf{x}_t$ term in the dynamics represents the mapping from the drivers' memory (past state inherited from the day before) to their flow allocation decision.

4. The $B\mathbf{u}_t$ term in the dynamics represents the mapping from the central decision maker's suggested routing distribution to the players' flow allocation decision.

5. When updating their flow allocation decision, the drivers leverage their memory $\mathbf{x}_t$ and the suggested routing distribution $\mathbf{u}_t$ from the decision maker. $\gamma \in [0, 1]$ is the design parameter that characterizes the trade-off between the two contributions.

6. (Quadratic) Cost function: the design of the quadratic cost function $\mathbf{x}_t^\top Q\mathbf{x}_t + \mathbf{u}_t^\top R\mathbf{u}_t$ is motivated by the observation that the Rosenthal potential function and the cost function associated to social welfare in a potential game are both quadratic for linear latency functions [116].

Definition 4.3.5 (Rosenthal potential)**.** *The Rosenthal potential function of a potential game, with a flow vector* $\mathbf{x}$*, is defined as*

$$\mathcal{J}_1(\mathbf{x}) = \sum_{e\in\mathcal{E}} \int_0^{x_e} l_e(y)\,\mathrm{d}y. \tag{4.3.15}$$

Definition 4.3.6 (Social Welfare)**.** *The cost function associated to social welfare is defined as*

$$\mathcal{J}_2(\mathbf{x}) = \sum_{e\in\mathcal{E}} x_e \cdot l_e(x_e),$$

The importance of the Rosenthal potential and the social welfare is that the Nash equilibrium and social optimal of the routing game can be characterized as the local minimizers of these functions respectively, respecting the conservation of flow. With linear latency parallel networks,

$$\mathcal{J}_1(\mathbf{x}) = \sum_{i=1}^{n_e} \int_0^{x_i} (a_i y + b_i)\,\mathrm{d}y = \sum_{i=1}^{n_e} \frac{a_i x_i^2}{2} + b_i x_i = \mathbf{x}^\top \tilde{Q}\mathbf{x} + \mathbf{b}^\top \mathbf{x}, \tag{4.3.16}$$

where $\tilde{Q} = \mathrm{diag}(\frac{a_1}{2}, \ldots, \frac{a_{n_e}}{2}), \mathbf{b} = (b_1, \ldots, b_{n_e})^\top$ and

$$\mathcal{J}_2(\mathbf{x}) = \sum_{i=1}^{n_e} x_i(a_i x_i + b_i) = \sum_{i=1}^{n_e} a_i x_i^2 + b_i x_i = 2\mathbf{x}^\top \tilde{Q}\mathbf{x} + \mathbf{b}^\top \mathbf{x}, \tag{4.3.17}$$

with the $\tilde{Q}, \mathbf{b}$ defined as the same as above. Note that $\tilde{Q}$ and $\mathbf{b}$ are used to construct Q and Q_f of the cost function.

7. Design of the matrix A in the dynamics: since the $A\mathbf{x}_t$ is the mapping from the memory to the flow allocation decision, the matrix A should reflect how the drivers take the memory into account when updating their routing decisions.

8. Design of the matrix B in the dynamics: since the $B\mathbf{u}_t$ is the mapping from the suggested routing distribution to the flow allocation decision, the matrix B should reflect how the drivers take the central decision maker's suggested flow into account when updating their routing decisions.

4.4 System Analysis and System Properties

One of the contributions of the work is about how to design specific A and B matrices to produce various convergence results.

1. Construction of A, B: when designing the matrices A, B in the dynamics, we need to take the conservation of flow into account. More specifically, A, B have to be chosen such that the following property holds

$$\mathbf{x}_t, \mathbf{u}_t \in \Delta \quad \Longrightarrow \quad \gamma A\mathbf{x}_t + (1-\gamma)B\mathbf{u}_t = \mathbf{x}_{t+1} \in \Delta. \tag{4.4.1}$$

   One way to ensure the conservation of flow on the network is to construct *left stochastic* A, B.

Definition 4.4.1. *A matrix $P = (\mathbf{p}_1, \ldots, \mathbf{p}_{n_e}) \in \mathbb{R}^{n_e \times n_e}$ is left stochastic if $\mathbf{p}_i \in \Delta, i = 1, \ldots, n_e$.*

Remark 4.4.1 (The notation $\mathbb{I}$)**.** *Throughout this chapter, we use the notation $\mathbb{I}$ to denote all-ones vectors with proper dimensions, i.e., $\mathbb{I} = (1, 1, \ldots, 1)^\top$.*

Lemma 4.4.1. *If $A, B \in \mathbb{R}^{n_e \times n_e}$ are left stochastic, and $\mathbf{x}_0, \mathbf{u}_t \in \Delta, t = 0, \ldots, T-1$, then $\gamma A\mathbf{x}_t + (1-\gamma)B\mathbf{u}_t = \mathbf{x}_{t+1} \in \Delta, t = 0, \ldots, T-1$.*

Proof. We will show that if $\mathbf{x}_t, \mathbf{u}_t \in \Delta$, then $\gamma A\mathbf{x}_t + (1-\gamma)B\mathbf{u}_t = \mathbf{x}_{t+1} \in \Delta$. The proof is then complete by induction on t.
First observe that $\mathbf{x}_{t+1}$ has non-negative entries due to the non-negativity of the entries in $A, B, \mathbf{x}_t, \mathbf{u}_t$. Furthermore,

$$\begin{aligned} \mathbb{I}^\top \mathbf{x}_{t+1} &= \gamma \mathbb{I}^\top A\mathbf{x}_t + (1-\gamma)\mathbb{I}^\top B\mathbf{u}_t && (4.4.2)\\ &= \gamma \mathbb{I}^\top \mathbf{x}_t + (1-\gamma)\mathbb{I}^\top \mathbf{u}_t && (4.4.3)\\ &= \gamma + (1-\gamma) = 1. && (4.4.4) \end{aligned}$$

□

2. Examples: the analysis of the LQR problem with probability simplex constraints is in general not tractable. In other words, we are not aware of a way to solve the discrete-time algebraic Ricatti equation in a way that preserves (4.4.1). We therefore provide the important special cases where either (1) exact calculations of the steady state and optimal controls are allowed, or (2) interesting behavioral interpretation of the players can be given.

   Example 4.4.1. We first consider the special case where

$$B = \begin{pmatrix} \frac{1}{n_e} & \frac{1}{n_e} & \cdots & \frac{1}{n_e} \\ \frac{1}{n_e} & \frac{1}{n_e} & \cdots & \frac{1}{n_e} \\ \vdots & \vdots & \ddots & \vdots \\ \frac{1}{n_e} & \frac{1}{n_e} & \cdots & \frac{1}{n_e} \end{pmatrix} \in \mathbb{R}^{n_e \times n_e}. \tag{4.4.5}$$

   This choice of B matrix in the dynamics can be interpreted as follows: when the players (drivers) leverage the central decision maker's suggested routing distribution $\mathbf{u}_t$ to update their flow allocation on each edge, they simply average the suggested flow at each time step t, and take only the average $\frac{1}{n_e}\sum_{i=1}^{n_e} u_i^t$ into account.
   We show that when the players (drivers) update their flow allocation in this way, the controller $\mathbf{u}_t$ is essentially "muted", and therefore a target state may not be controllable. The state $\mathbf{x}_t$ will converge to the same equilibrium that is independent of the choice of the cost function.

   Property 4.4.1. *Consider the control problem* (4.3.11)-(4.3.14) *with*

$$B = \begin{pmatrix} \frac{1}{n_e} & \frac{1}{n_e} & \cdots & \frac{1}{n_e} \\ \frac{1}{n_e} & \frac{1}{n_e} & \cdots & \frac{1}{n_e} \\ \vdots & \vdots & \ddots & \vdots \\ \frac{1}{n_e} & \frac{1}{n_e} & \cdots & \frac{1}{n_e} \end{pmatrix}, \gamma \in [0, 1), \text{ and any left stochastic matrix } A, \tag{4.4.6}$$

   then the unique steady state of the system is given by

$$\mathbf{x}^* = \frac{1-\gamma}{n_e}(I_{n_e} - \gamma A)^{-1}\mathbb{I}, \tag{4.4.7}$$

   where I_{n_e} is the n_e-dimensional identity matrix, and $\mathbb{I} = (1, 1, \ldots, 1)^\top \in \mathbb{R}^{n_e}$ is the all-ones vector.

   Proof. The key observation is, with equation (4.4.6), since we have $\mathbf{u}_t \in \Delta, t = 0, \ldots, T-1$,

$$B\mathbf{u}_t = \frac{1}{n_e}\mathbb{I}, \tag{4.4.8}$$

therefore

$$\mathbf{x}_{t+1} = \gamma A\mathbf{x}_t + (1-\gamma)\frac{1}{n_e}\mathbb{I}, \tag{4.4.9}$$

and the steady state should satisfy

$$\mathbf{x}^* = \gamma A\mathbf{x}^* + (1-\gamma)\frac{1}{n_e}\mathbb{I}, \quad \Longrightarrow \quad \mathbf{x}^* = \frac{1-\gamma}{n_e}(I_{n_e} - \gamma A)^{-1}\mathbb{I}, \tag{4.4.10}$$

with the invertibility of $I_{n_e} - \gamma A$ guaranteed by the fact that the spectral radius of any left stochastic matrix is at most 1, and $\gamma < 1$. □

The foregoing property suggests that in the case of equation (4.4.6), the flow allocation on the network does converge to an equilibrium, but the equilibrium depends only on the design parameters A, γ and the number of edges n_e, which can be different from the Nash equilibrium.

Example 4.4.2. We next consider the special case where

$$A = \begin{pmatrix} \frac{1}{n_e} & \frac{1}{n_e} & \cdots & \frac{1}{n_e} \\ \frac{1}{n_e} & \frac{1}{n_e} & \cdots & \frac{1}{n_e} \\ \vdots & \vdots & \ddots & \vdots \\ \frac{1}{n_e} & \frac{1}{n_e} & \cdots & \frac{1}{n_e} \end{pmatrix} \in \mathbb{R}^{n_e \times n_e}. \tag{4.4.11}$$

This choice of A matrix in the dynamics can be interpreted as follows: when the players (drivers) leverage their memory $\mathbf{x}_t$ to update their flow allocation on each edge, they simply average the past flow at each time step t, and take only this average $\frac{1}{n_e}\sum_{i=1}^{n_e} x_i^t$ into account.
We similarly show that when the players (drivers) update their flow allocation in this way, their memory has no impact in the update rule.

Property 4.4.2. *Consider the control problem* (4.3.11)-(4.3.14) *with*

$$A = \begin{pmatrix} \frac{1}{n_e} & \frac{1}{n_e} & \cdots & \frac{1}{n_e} \\ \frac{1}{n_e} & \frac{1}{n_e} & \cdots & \frac{1}{n_e} \\ \vdots & \vdots & \ddots & \vdots \\ \frac{1}{n_e} & \frac{1}{n_e} & \cdots & \frac{1}{n_e} \end{pmatrix} \text{ and any left stochastic matrix } B, \tag{4.4.12}$$

then the optimal controller $\mathbf{u}_t, t = 0, \ldots, T-2$ *is the solution set of the optimization problem*

$$\underset{\mathbf{u}}{\text{minimize}} \quad \left(\frac{\gamma}{n_e}\mathbb{I} + (1-\gamma)B\mathbf{u}\right)^\top Q \left(\frac{\gamma}{n_e}\mathbb{I} + (1-\gamma)B\mathbf{u}\right) + \mathbf{u}^\top R\mathbf{u} \tag{4.4.13}$$

$$\textit{subject to} \quad \mathbf{u} \in \Delta, \tag{4.4.14}$$

and the optimal $\mathbf{u}_{T-1}$ *is the solution set of the optimization problem*

$$\underset{\mathbf{u}}{\textit{minimize}} \quad \left(\frac{\gamma}{n_e}\mathbb{I} + (1-\gamma)B\mathbf{u}\right)^\top Q_f \left(\frac{\gamma}{n_e}\mathbb{I} + (1-\gamma)B\mathbf{u}\right) + \mathbf{u}^\top R\mathbf{u} \tag{4.4.15}$$

$$\textit{subject to} \quad \mathbf{u} \in \Delta. \tag{4.4.16}$$

Proof. The key observation is, with equation (4.4.12), since we have $\mathbf{x}_t \in \Delta, t = 0, \ldots, T-1$,

$$A\mathbf{x}_t = \frac{1}{n_e}\mathbb{I}, \tag{4.4.17}$$

therefore

$$\mathbf{x}_{t+1} = \gamma\frac{1}{n_e}\mathbb{I} + (1-\gamma)B\mathbf{u}_t. \tag{4.4.18}$$

Therefore, the optimal control of problem (4.3.11)-(4.3.14) can be explicitly solved by the optimization problem

$$\begin{aligned}\underset{\mathbf{u}_t, t=0,\ldots T-1}{\text{minimize}} \quad & \mathbf{x}_0^\top Q\mathbf{x}_0 + \sum_{t=0}^{T-2}\left(\left(\frac{\gamma}{n_e}\mathbb{I} + (1-\gamma)B\mathbf{u}_t\right)^\top Q\left(\frac{\gamma}{n_e}\mathbb{I} + (1-\gamma)B\mathbf{u}_t\right) + \mathbf{u}_t^\top R\mathbf{u}_t\right) + \\ & \left(\left(\frac{\gamma}{n_e}\mathbb{I} + (1-\gamma)B\mathbf{u}_{T-1}\right)^\top Q_f\left(\frac{\gamma}{n_e}\mathbb{I} + (1-\gamma)B\mathbf{u}_{T-1}\right) + \mathbf{u}_{T-1}^\top R\mathbf{u}_{T-1}\right)\end{aligned} \tag{4.4.19}$$

$$\text{subject to} \quad \mathbf{u}_t \in \Delta, t = 0, \ldots, T-1, \tag{4.4.20}$$

which is further equivalent to solving the constrained optimization problems

$$\underset{\mathbf{u}}{\text{minimize}} \quad \left(\frac{\gamma}{n_e}\mathbb{I} + (1-\gamma)B\mathbf{u}\right)^\top Q\left(\frac{\gamma}{n_e}\mathbb{I} + (1-\gamma)B\mathbf{u}\right) + \mathbf{u}^\top R\mathbf{u} \tag{4.4.21}$$

$$\text{subject to} \quad \mathbf{u} \in \Delta \tag{4.4.22}$$

and

$$\underset{\mathbf{u}}{\text{minimize}} \quad \left(\frac{\gamma}{n_e}\mathbb{I} + (1-\gamma)B\mathbf{u}\right)^\top Q_f\left(\frac{\gamma}{n_e}\mathbb{I} + (1-\gamma)B\mathbf{u}\right) + \mathbf{u}^\top R\mathbf{u} \tag{4.4.23}$$

$$\text{subject to} \quad \mathbf{u} \in \Delta. \tag{4.4.24}$$

If $Q_f = Q$ and the solution of the above optimization problem exists, the minimizer $\mathbf{u}^*$ characterizes the steady state $\mathbf{x}^* = \frac{\gamma}{n_e}\mathbb{I} + (1-\gamma)B\mathbf{u}^*$. □

Note that in the very specific case where $R = 0$ and Q, Q_f are defined by the Rosenthal potential function, the minimizer of the above optimization problem and steady state of the system $\mathbf{x}^*$ is the Nash equilibrium. If the linear equation system $\mathbf{x}^* = \frac{\gamma}{n_e}\mathbb{I} + (1-\gamma)B\mathbf{u}$ has at least one solution $\mathbf{u}^*$ (e.g., when B is invertible and $\gamma \neq 1$), then the optimal controllers are $\mathbf{u}_t = \mathbf{u}^*, t = 0, \ldots, T-1$.

Example 4.4.3. The third special case we would like to analyze is $A = B = I_{n_e}$. The players update their flow allocation with $\mathbf{x}_{t+1} = \gamma\mathbf{x}_t + (1-\gamma)\mathbf{u}_t$ at each time step t, which is the same as the element-wise update $x_i^{t+1} = \gamma x_i^t + (1-\gamma)u_i^t, i = 1, \ldots, N, t = 0, \ldots, T-1$.
The interpretation of this choice of A, B is that the players update the flow on each edge *independently*: to update the flow on edge i, the players leverage their memory and the suggested routing decision on the edge i only.

4.5 Solutions via Explicit MPC: A Multiparametric Quadratic Programming Approach

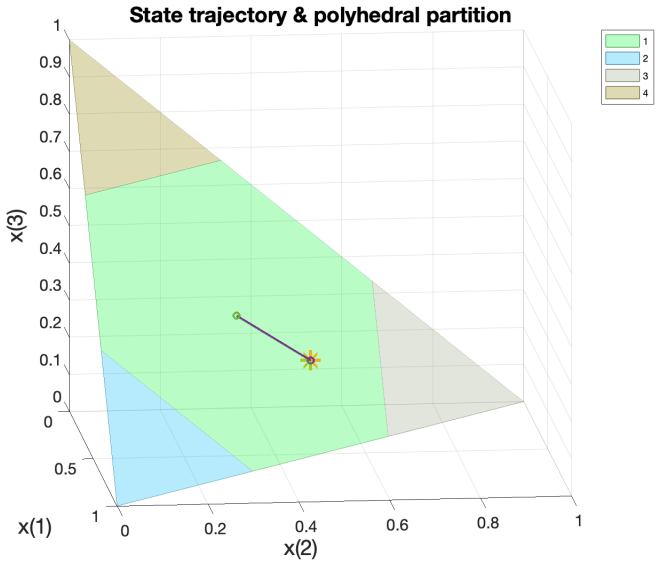

Figure 4.1: Here, the optimal strategy for our player is space-varying and we visualize solutions with respect to the feasible state space of the routing game. Each colored region of the graph represents a unique affine strategy that is optimal for those points in space. For example, region 1 (in green) has the solution $\mathbf{u}_t^*(\mathbf{x}_t) = \begin{pmatrix} -\frac{2}{3} & \frac{1}{3} & \frac{1}{3} \\ \frac{1}{3} & -\frac{2}{3} & \frac{1}{3} \\ \frac{1}{3} & \frac{1}{3} & -\frac{2}{3} \end{pmatrix} \mathbf{x}_t + \begin{pmatrix} \frac{1}{3} \\ \frac{1}{3} \\ \frac{1}{3} \end{pmatrix}$.

At first glance, one might consider using the discrete-time algebraic Ricatti equation to obtain solutions for system (4.3.11)-(4.3.14).

Definition 4.5.1 (Discrete-time Algebraic Ricatti Equation)**.** *The discrete-time algebraic Ricatti equation is a nonlinear equation that gives a solution to the LQR problem presented in equation* (4.3.3)*, described as P_t evolving backwards in time from $P_T = Q_f$ according to*

$$P_{t-1} = Q + A^\top P_t A - A^\top P_t B(R + B^\top Q_f B)^{-1} B^\top P_t A. \tag{4.5.1}$$

However, using the algebraic Riccati equation is not possible in the presence of our flow conservation constraints, as specified in equation (4.4.1). According to lemma (4.4.1), in order to design a flow preserving scheme and guarantee flow conservation, we must be able to guarantee that each $\mathbf{x}_t$ and $\mathbf{u}_t$ vector given by a chosen controller remains on the probability simplex Δ, while the optimal controller given by the algebraic Riccati equation drives the system to the steady state $\mathbf{x}^* = 0$. Therefore, we turn to multiparametric quadratic programming (mpQP), a technique used in explicit MPC to generate explicit piecewise affine controllers. To generate these explicit strategies, we will formulate the LQR problem into a mpQP problem, utilize an mpQP solver proposed in [13] to generate piecewise affine functions for $\mathbf{u}_t$ (the player needs to execute different affine controllers depending on the state), and use (within the solver) a geometric algorithm to plot regions, known as ***critical regions***, on the state space to visualize when players should use which specific optimal strategies. Optimal strategies produced by this technique will be piecewisely-affine with respect to the state of the game, hence, optimal strategies in this context are space-varying (see figure (4.1) for an example).

Algorithm (2) defines the process by which we use mpQP to generate solutions for routing games. Specifically, we consider the optimal control formulation in problem (4.3.11)-(4.3.14). We take the linear flow and input constraints in (4.4.1) and construct them in the form

$$A_u \mathbf{u}_t \leq b_u, \quad A_x \mathbf{x}_t \leq b_x. \tag{4.5.2}$$

To solve for the optimal controls $\mathbf{u}_0, \ldots, \mathbf{u}_{T-1}$, first we condense the problem into a strictly convex quadratic programming problem

$$V^*(x) \triangleq \quad \textit{minimize} \quad \frac{1}{2} z^\top P z + (Fx + c)^\top z + \frac{1}{2} x^\top Y x \tag{4.5.3}$$

$$\textit{subject to} \quad Gz \leq W + Sx \tag{4.5.4}$$

and then use the mpQP algorithm from reference [13] to solve for z where $z := \left(\mathbf{u}_0^\top \ldots \mathbf{u}_{T-1}^\top\right)^\top \in \mathbb{R}^{n_e T}$ is the decision variable.

$P = P^\top \in \mathbb{R}^{n_e T \boldsymbol{y} n_e T}$, $F \in \mathbb{R}^{n_e T \boldsymbol{y} n_e}$, $c \in \mathbb{R}^{n_e T}$, $Y \in \mathbb{R}^{n_e \boldsymbol{y} n_e}$ are defined by the cost matrices, and $G \in \mathbb{R}^{n_e T \boldsymbol{y} q}$, $W \in \mathbb{R}^q$, $S \in \mathbb{R}^{q \boldsymbol{y} n_e}$ define the constraints imposed by (4.3.11)-(4.3.14) in compact form. The following property guarantees the existence of a (piecewise affine) solution of the condensed problem (4.5.3)-(4.5.4).

Property 4.5.1 (Existence of a piecewise affine solution [13]). *Consider* (4.5.3)-(4.5.4) *with* $P = P^\top \succ 0$ *and let* $x \in \mathcal{X} = \mathbb{R}^n$.

1. *The set* $\mathcal{X}_f$ *of states for which the problem is feasible is a polyhedron.*
2. *The optimizer function* $z^* : \mathcal{X}_f \to \mathbb{R}^n$ *is piecewise affine and continuous over* $\mathcal{X}_f$.
3. *If* $\begin{pmatrix} P & \boldsymbol{F}^\top \\ \boldsymbol{F} & Y \end{pmatrix} \succeq 0$ *and symmetric, then the value function* V^* *is continuous, convex, and piecewise quadratic over* $\mathcal{X}_f$.

Definition 4.5.2 (Critical Region [131]). *A critical region is a polyhedron in* $\mathcal{X}$ *for which there exists an optimal solution* $z^*(\cdot)$ *that is affine and optimal for the entire region. Each critical region is defined by a unique set of active constraints* $\mathcal{A}$ *that is common for all points in the region.*

Algorithm 2: mpQP algorithm

Input : Q,R,Q_f,N_c,A,B,A_u,b_u,A_x,b_x
Output: Optimal strategy solutions: $\mathcal{F}$, $\mathcal{G}$
Critical Regions to apply solutions: $\mathcal{R}$, $\mathcal{H}$, $\mathcal{K}$,

$P, F, c, Y, G, W, S \leftarrow$ `Condense`(Q,R,Q_f,N_c,A,B,A_u,b_u,A_x,b_x);
return `MPQPSolver`(P, F, c, Y, G, W, S);

As explained in ([13]), `MPQPSolver`$(\cdot)$ uses a geometrical algorithm (see [131]) to find the critical regions of the feasible state space by understanding when sets of active constraints differs from point to point in the state space. Once it has identified a critical region, the algorithm is able to uncover the optimal solution defined within the region by using KKT conditions (or similar methods) to obtain the piecewise affine solution z^*. Algorithm (2) produces (1) the critical regions $\mathcal{R}$, (2) the matrices to check if a state is in specific critical region, $\mathcal{H} = \{\mathcal{H}_r\}$ and $\mathcal{K} = \{\mathcal{K}_r\}$, and (3) the matrices that characterizes the affine solution $\mathcal{F} = \{\mathcal{F}_r\}$ and $\mathcal{G} = \{\mathcal{G}_r\}$. Therefore, during the routing game, to recover the optimal strategies, the central decision maker executes

$$\text{if } \mathcal{H}_r \mathbf{x}_t \leq \mathcal{K}_r \text{ , then } \mathbf{u}_t^* = \mathcal{F}_r \mathbf{x}_t + \mathcal{G}_r \tag{4.5.5}$$

and $\mathbf{x}_t$ belongs to critical region r.

4.6 Illustration via Simple Numerics

In this section, we plan to provide numerical results and discuss

1. differences in varying A matrices in the dynamics, and the interpretations,

2. changes in γ and its effect on the converging rate,

3. different initial states and its effect on the converging rate,

4. different cost functions to drive the system towards different stable equilibrium.

More specifically, we will compare between

1. $A = \begin{pmatrix} \frac{1}{3} & \frac{1}{3} & \frac{1}{3} \\ \frac{1}{3} & \frac{1}{3} & \frac{1}{3} \\ \frac{1}{3} & \frac{1}{3} & \frac{1}{3} \end{pmatrix}$ and $A = I_3$, with all the other parameters fixed as $B = I_3, Q = Q_f = I_3, R = 0, \gamma = 0.5, \mathbf{x}_0 = (0.3, 0.5, 0.2)^\top$. This means we investigate the differences between the players' routing decision process when they "mute" their memory, and when they leverage their memory on each edge independently (i.e., when x_i^{t+1} depends only on x_i^t in the past state $\mathbf{x}_t$ for $i = 1, \ldots, n_e$).

2. $\gamma = 0.5$ and $\gamma = 0.7$: with all the other parameters fixed as $A = B = I_3, Q = Q_f = \begin{pmatrix} 1 & 0 & 0 \\ 0 & 2 & 0 \\ 0 & 0 & 4 \end{pmatrix}, R = \begin{pmatrix} 0 & 0 & 0 \\ 0 & 0 & 0 \\ 0 & 0 & 0 \end{pmatrix}, \mathbf{x}_0 = (0.3, 0.5, 0.2)^\top$. This means we investigate the differences between the players' routing decision process when they weight equally the their memory and the suggested flow, and when they weight more their memory (and less the suggestions).

3. $\mathbf{x}_0 = (0.3, 0.5, 0.2)^\top$ and $\mathbf{x}_0 = (0, 1, 0)^\top$: with all the other parameters fixed as $A = B = I_3, Q = Q_f = \begin{pmatrix} 1 & 0 & 0 \\ 0 & 2 & 0 \\ 0 & 0 & 4 \end{pmatrix}, R = \begin{pmatrix} 0 & 0 & 0 \\ 0 & 0 & 0 \\ 0 & 0 & 0 \end{pmatrix}, \gamma = 0.5$. This means we investigate the differences between the players' routing decision process when they start with putting partial flow on each edge, and when they start with putting all flow on the second edge.

4. $Q = Q_f = I_3$ and $Q = Q_f = \begin{pmatrix} 1 & 0 & 0 \\ 0 & 2 & 0 \\ 0 & 0 & 4 \end{pmatrix}$: with all the other parameters fixed as $A = B = I_3, R = \begin{pmatrix} 0 & 0 & 0 \\ 0 & 0 & 0 \\ 0 & 0 & 0 \end{pmatrix}, \gamma = 0.5, \mathbf{x}_0 = (0.3, 0.5, 0.2)^\top$. This means we investigate the differences between the players' routing decision process when the central decision maker penalizes equally the flow on the three edges, and when it gradually doubles the penalty on the edges.

We also discuss the *reliability of the solver* by showing one example, where the solver outputs the correct steady state solution only with large enough time horizon T. This example serves as an alert that in order to get the accurate numerical solution with the

`MPQPSolver`$(\cdot)$, one needs to set a large time horizon T, at the price of longer computation time.

Comparisons and Results

For ease of reference, we list below the detailed choice of parameters in each figure. In all experiments we assume no penalty on the controller (i.e., the central decision maker has the freedom to pose any suggested routing decision).

Figure (4.2):

$$Q = Q_f = \begin{pmatrix} 1 & 0 & 0 \\ 0 & 1 & 0 \\ 0 & 0 & 1 \end{pmatrix}, R = \begin{pmatrix} 0 & 0 & 0 \\ 0 & 0 & 0 \\ 0 & 0 & 0 \end{pmatrix}, A = \begin{pmatrix} \frac{1}{3} & \frac{1}{3} & \frac{1}{3} \\ \frac{1}{3} & \frac{1}{3} & \frac{1}{3} \\ \frac{1}{3} & \frac{1}{3} & \frac{1}{3} \end{pmatrix}, B = \begin{pmatrix} 1 & 0 & 0 \\ 0 & 1 & 0 \\ 0 & 0 & 1 \end{pmatrix},$$
$$T = 15, \gamma = 0.5, \mathbf{x}_0 = \begin{pmatrix} 0.3 & 0.5 & 0.2 \end{pmatrix}^\top$$

Figure (4.3):

$$Q = Q_f = \begin{pmatrix} 1 & 0 & 0 \\ 0 & 1 & 0 \\ 0 & 0 & 1 \end{pmatrix}, R = \begin{pmatrix} 0 & 0 & 0 \\ 0 & 0 & 0 \\ 0 & 0 & 0 \end{pmatrix}, A = \begin{pmatrix} 1 & 0 & 0 \\ 0 & 1 & 0 \\ 0 & 0 & 1 \end{pmatrix}, B = \begin{pmatrix} 1 & 0 & 0 \\ 0 & 1 & 0 \\ 0 & 0 & 1 \end{pmatrix},$$
$$T = 15, \gamma = 0.5, \mathbf{x}_0 = \begin{pmatrix} 0.3 & 0.5 & 0.2 \end{pmatrix}^\top$$

Figure (4.4):

$$Q = Q_f = \begin{pmatrix} 1 & 0 & 0 \\ 0 & 2 & 0 \\ 0 & 0 & 4 \end{pmatrix}, R = \begin{pmatrix} 0 & 0 & 0 \\ 0 & 0 & 0 \\ 0 & 0 & 0 \end{pmatrix}, A = \begin{pmatrix} \frac{1}{3} & \frac{1}{3} & \frac{1}{3} \\ \frac{1}{3} & \frac{1}{3} & \frac{1}{3} \\ \frac{1}{3} & \frac{1}{3} & \frac{1}{3} \end{pmatrix}, B = \begin{pmatrix} 1 & 0 & 0 \\ 0 & 1 & 0 \\ 0 & 0 & 1 \end{pmatrix},$$
$$T = 15, \gamma = 0.5, \mathbf{x}_0 = \begin{pmatrix} 0.3 & 0.5 & 0.2 \end{pmatrix}^\top$$

Figure (4.5):

$$Q = Q_f = \begin{pmatrix} 1 & 0 & 0 \\ 0 & 2 & 0 \\ 0 & 0 & 4 \end{pmatrix}, R = \begin{pmatrix} 0 & 0 & 0 \\ 0 & 0 & 0 \\ 0 & 0 & 0 \end{pmatrix}, A = \begin{pmatrix} 1 & 0 & 0 \\ 0 & 1 & 0 \\ 0 & 0 & 1 \end{pmatrix}, B = \begin{pmatrix} 1 & 0 & 0 \\ 0 & 1 & 0 \\ 0 & 0 & 1 \end{pmatrix},$$
$$T = 15, \gamma = 0.5, \mathbf{x}_0 = \begin{pmatrix} 0.3 & 0.5 & 0.2 \end{pmatrix}^\top$$

Figure (4.6):

$$Q = Q_f = \begin{pmatrix} 1 & 0 & 0 \\ 0 & 2 & 0 \\ 0 & 0 & 4 \end{pmatrix}, R = \begin{pmatrix} 0 & 0 & 0 \\ 0 & 0 & 0 \\ 0 & 0 & 0 \end{pmatrix}, A = \begin{pmatrix} 1 & 0 & 0 \\ 0 & 1 & 0 \\ 0 & 0 & 1 \end{pmatrix}, B = \begin{pmatrix} 1 & 0 & 0 \\ 0 & 1 & 0 \\ 0 & 0 & 1 \end{pmatrix},$$

$$T = 15, \gamma = 0.5, \mathbf{x}_0 = \begin{pmatrix} 0 & 1 & 0 \end{pmatrix}^\top$$

Figure (4.7):

$$Q = Q_f = \begin{pmatrix} 1 & 0 & 0 \\ 0 & 2 & 0 \\ 0 & 0 & 4 \end{pmatrix}, R = \begin{pmatrix} 0 & 0 & 0 \\ 0 & 0 & 0 \\ 0 & 0 & 0 \end{pmatrix}, A = \begin{pmatrix} 1 & 0 & 0 \\ 0 & 1 & 0 \\ 0 & 0 & 1 \end{pmatrix}, B = \begin{pmatrix} 1 & 0 & 0 \\ 0 & 1 & 0 \\ 0 & 0 & 1 \end{pmatrix},$$

$$T = 15, \gamma = 0.7, \mathbf{x}_0 = \begin{pmatrix} 0.3 & 0.2 & 0.5 \end{pmatrix}^\top$$

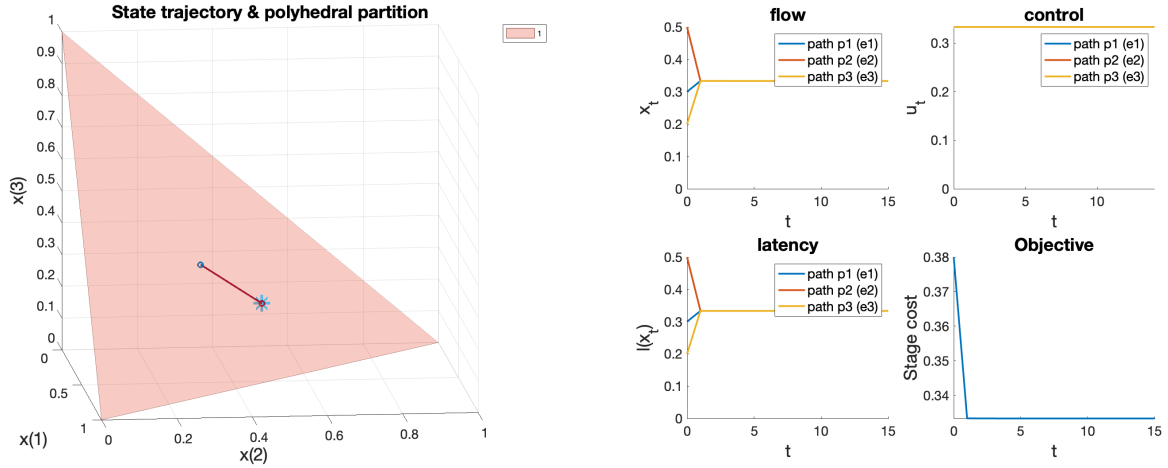

Figure 4.2: Identity Q, Q_f, B, $A = (1/3), \gamma = 0.5$. "*" denotes the initial state.

Discussion: In each figure, we present on the left the probability simplex in $\mathbb{R}^3$, the critical regions in it (recall that within each partition the optimal controller takes different affine expression), and the convergence trajectory of the state $\mathbf{x}_t$ (with the initial state denoted by $*$). On the right we present (1) the value of the flow allocation $\mathbf{x}_t$ on each edge at each time step t, (2) the value of the optimal control (suggested routing decision) $\mathbf{u}_t$ on each edge at each time step t, (3) the incurred latency l_t on each edge at each time step t, and (4) the incurred stage cost $\mathbf{x}_t^\top Q \mathbf{x}_t + \mathbf{u}_t^\top R \mathbf{u}_t, t = 0, \ldots, T-1$ and the terminal cost $\mathbf{x}_T^\top Q_f \mathbf{x}_T$.

1. **Varying A matrices in the dynamics:** To see the differences in changing A, we compare figure (4.2) and figure (4.3).

   - It can be observed that in both scenarios, the controlled system converges to its steady state $\mathbf{x}^* = (1/3, 1/3, 1/3)^\top$ in one step. The numerical results suggest that with the choice of cost matrices being $Q = Q_f = I_3, R = 0$ and the specific setup of other parameters in the numerics, the steady state $\mathbf{x}^*$ coincides with the Nash equilibrium in the parallel network with latency functions $l_1(y) = l_2(y) = l_3(y) = y$.

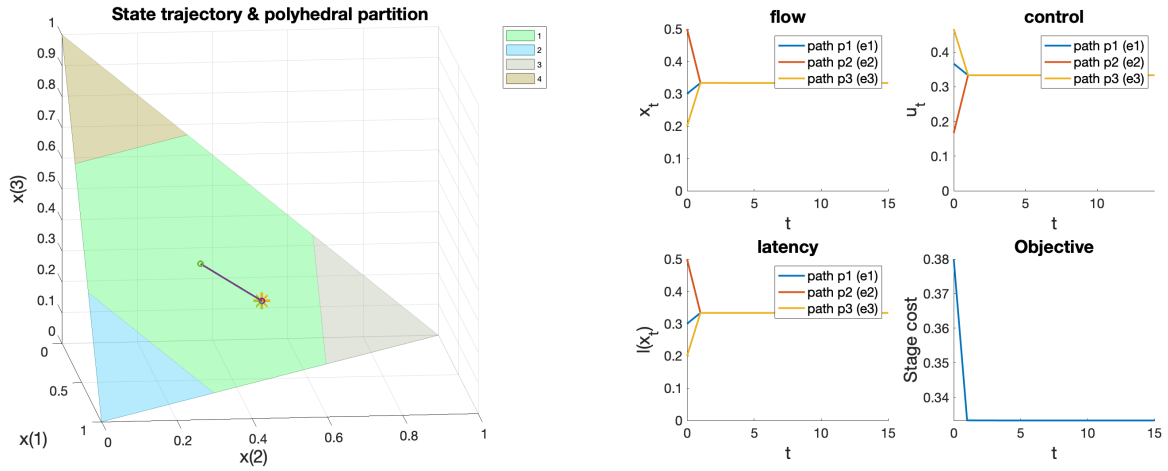

Figure 4.3: Identity Q, Q_f, A, B, $\gamma = 0.5$. "*" denotes the initial state.

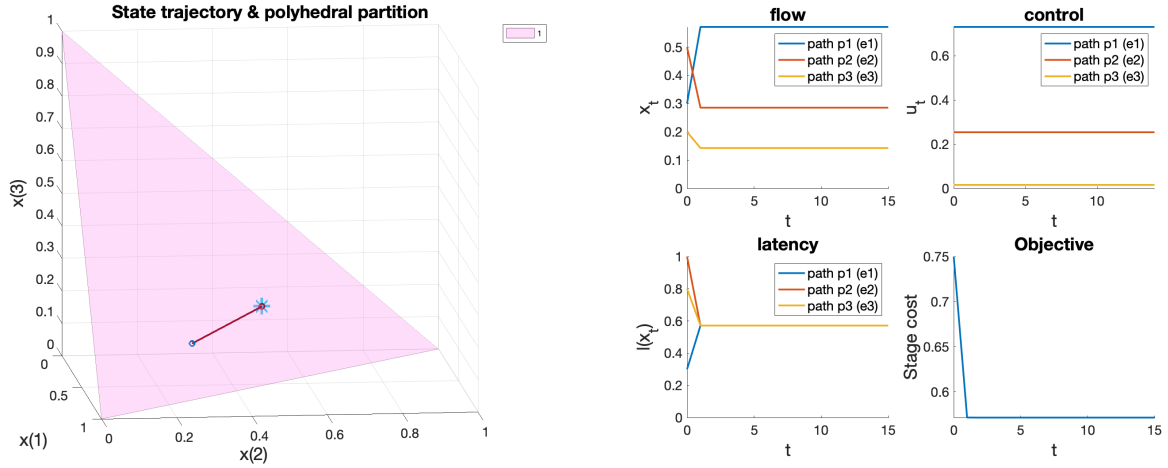

Figure 4.4: Identity B, $A = (1/3), Q = Q_f = \text{diag}(1, 2, 4), \gamma = 0.5$. "*" denotes the initial state.

- Specifically, the fact that the state $\mathbf{x}_t$ converges in one step to the Nash equilibrium with $A = \begin{pmatrix} \frac{1}{3} & \frac{1}{3} & \frac{1}{3} \\ \frac{1}{3} & \frac{1}{3} & \frac{1}{3} \\ \frac{1}{3} & \frac{1}{3} & \frac{1}{3} \end{pmatrix}$ agrees with our analysis in property (4.4.2).
- The polyhedral partitions of the feasible state space Δ are different. In the case of $A = \begin{pmatrix} \frac{1}{3} & \frac{1}{3} & \frac{1}{3} \\ \frac{1}{3} & \frac{1}{3} & \frac{1}{3} \\ \frac{1}{3} & \frac{1}{3} & \frac{1}{3} \end{pmatrix}$ there is no partition of the space, meaning that the optimal controller takes the same affine function over Δ. In the case of $A = I_3$, the feasible

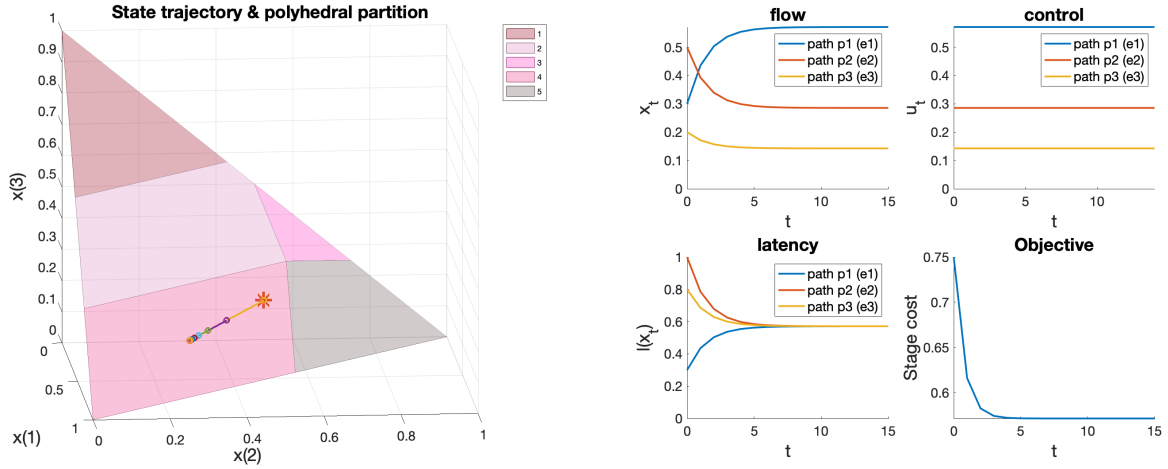

Figure 4.5: Identity A, B, $Q = Q_f = \text{diag}(1, 2, 4), \gamma = 0.5$. "*" denotes the initial state.

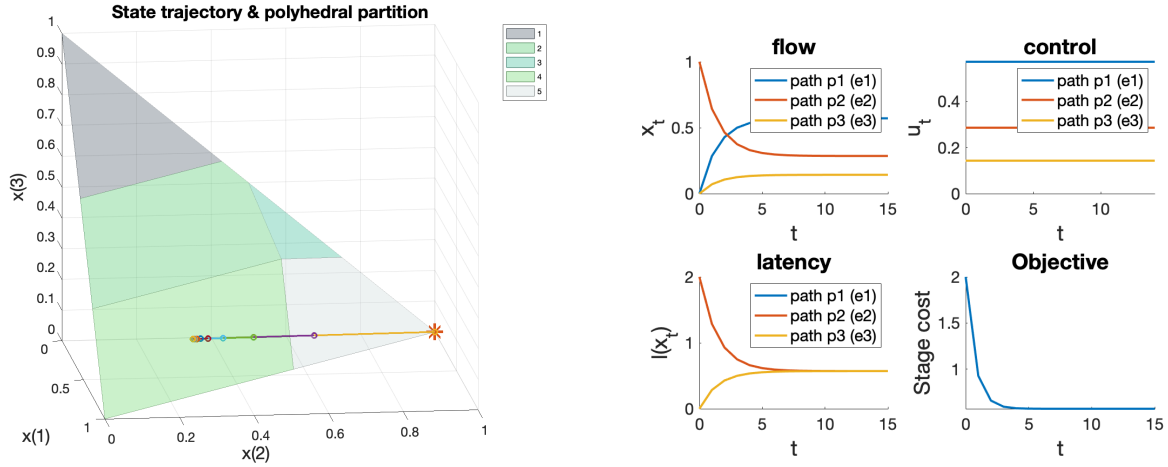

Figure 4.6: Identity A, B, $Q = Q_f = \text{diag}(1, 2, 4), \gamma = 0.5$, initial $(0, 1, 0)$. "*" denotes the initial state.

state space is partitioned into four polyhedral regions, within each taking different expression of affine optimal controllers.

2. **Varying γ in the dynamics:** To see the differences in changing γ, we compare figure (4.5) and figure (4.7).

   - Both controlled systems converge to the steady state $\mathbf{x}^* = (4/7, 2/7, 1/7)^\top$. The numerical results suggest that with the choice of cost matrices being $Q = Q_f =$

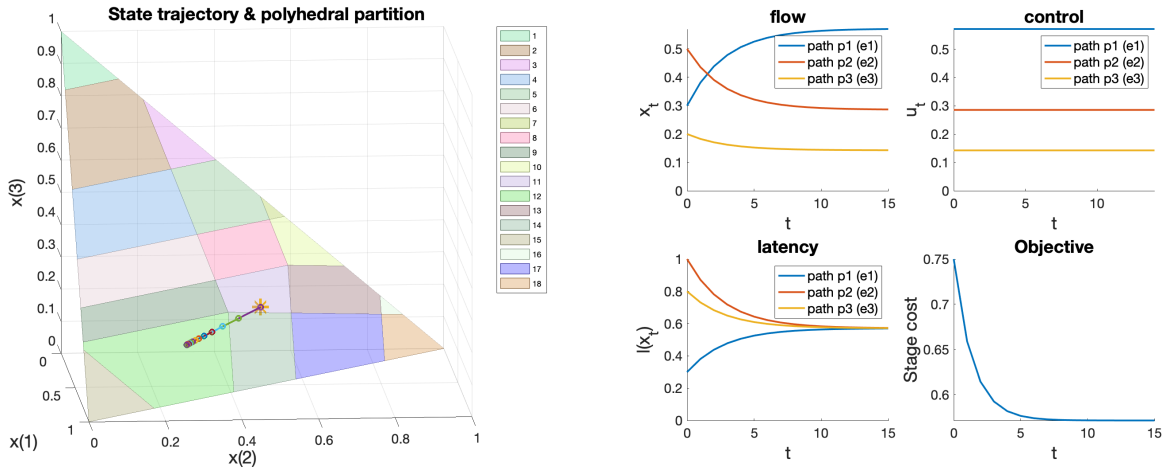

Figure 4.7: Identity A, B, $Q = Q_f = \text{diag}(1, 2, 4), \gamma = 0.7$. "*" denotes the initial state.

$\begin{pmatrix} 1 & 0 & 0 \\ 0 & 2 & 0 \\ 0 & 0 & 4 \end{pmatrix}$, $R = 0$ and the specific setup of other parameters in the numerics, the steady state $\mathbf{x}^*$ coincides with the Nash equilibrium in the parallel network with latency functions $l_1(y) = y, l_2(y) = 2y, l_3(y) = 4y$.

- The polyhedral partitions of the feasible state space Δ are different in the two cases. We observe that with larger $\gamma = 0.7$ (i.e. the players update their flow allocation considering **more** their memory than the central decision maker's suggested routing decision), the feasible state space has way more polyhedral partitions. This intuitively means that: if the players weight less the suggestions from the central decision maker, in order for the central decision maker to drive the traffic to a target flow allocation, it will have to design more complex routing strategy based on the actual flow on the network.
- The convergence rate with larger γ is slower: we see that with $\gamma = 0.5$, the state stabilizes with around 5 time steps, while with $\gamma = 0.7$, the state stabilizes with around 10 time steps. This can be intuitively interpreted as: if the players weight less the suggestions from the central decision maker, the steady state of the system is less controllable and therefore it takes longer for the central decision maker to stabilize the system.

3. **Varying initial states $\mathbf{x}_0$:** To see the differences in changing $\mathbf{x}_0$, we compare figure (4.5) and figure (4.6).

   - Both controlled systems converge to the steady state $\mathbf{x}^* = (4/7, 2/7, 1/7)^\top$, which again coincides with the Nash equilibrium in the parallel network with latency functions $l_1(y) = y, l_2(y) = 2y, l_3(y) = 4y$.

- We would like to point out that with $x_0 = [0, 1, 0]^\top$, the state of the system starts further away from its steady state, and starts within a different polyhedron from where the steady state is located. However with the specific control dynamics in the numerical experiment, the central decision maker still manages to steer the system to the target flow allocation.

4. **Varying cost functions:** To see the differences in changing the cost matrices, we compare figure (4.3) and figure (4.5).

   - Both controlled systems converge, but to the different steady states. More specifically, with $Q = Q_f = I_3$, the steady state is $\mathbf{x}^* = (1/3, 1/3, 1/3)^\top$, which coincides with the Nash equilibrium in the parallel network with latency functions $l_1(y) = l_2(y) = l_3(y) = y$; with $Q = Q_f = \begin{pmatrix} 1 & 0 & 0 \\ 0 & 2 & 0 \\ 0 & 0 & 4 \end{pmatrix}$, the steady state is $\mathbf{x}^* = (4/7, 2/7, 1/7)^\top$, which coincides with the Nash equilibrium in the parallel network with latency functions $l_1(y) = y, l_2(y) = 2y, l_3(y) = 4y$.
   - This justifies the capability of the central decision maker to design different objective functions and steer the controlled system to different target flow allocations.

Reliability of the solver: with the following setting, we show that it is important to set the time horizon T to be large enough so that the algorithm gives the steady state solution.

Let

$$Q = Q_f = \begin{pmatrix} 1 & 0 & 0 \\ 0 & 2 & 0 \\ 0 & 0 & 4 \end{pmatrix}, R = \begin{pmatrix} 0 & 0 & 0 \\ 0 & 0 & 0 \\ 0 & 0 & 0 \end{pmatrix}, A = \begin{pmatrix} 1 & 0 & 0 \\ 0 & 1 & 0 \\ 0 & 0 & 1 \end{pmatrix}, B = \begin{pmatrix} \frac{1}{2} & \frac{1}{2} & 0 \\ 0 & \frac{1}{2} & \frac{1}{2} \\ \frac{1}{2} & 0 & \frac{1}{2} \end{pmatrix},$$

$$\gamma = 0.6, \mathbf{x}_0 = \begin{pmatrix} 0.3 & 0.5 & 0.2 \end{pmatrix}^\top$$

If we set the time horizon $T = 15$, we observe in figure (4.8) that the control system can be oscillating and non-stable, and does not converge to a steady state. However if we set a larger $T = 35$, we see in figure (4.9) that the controlled system is stabilizing – the trajectory of the state converges to a steady state.

4.7 Conclusion

This chapter transformed the dynamic traffic assignment problem into a control theoretic problem, under a simple scenario using a parallel network with affine latency functions on each edge. We started with the routing problem under the repeated game framework, proposed a game design scheme through LQR within the control theoretic framework, and

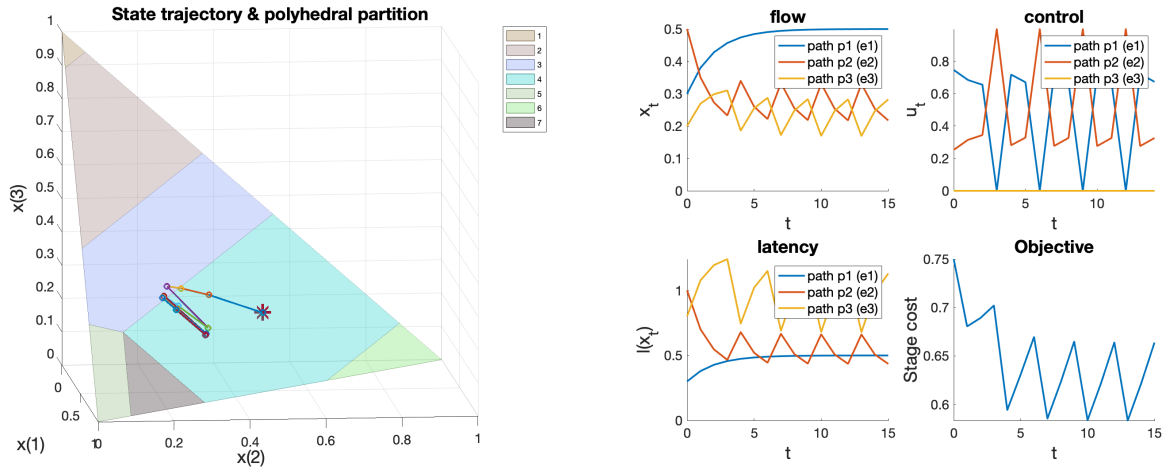

Figure 4.8: Identity A, $B = \begin{pmatrix} 1/2 & 1/2 & 0 \\ 0 & 1/2 & 1/2 \\ 1/2 & 0 & 1/2 \end{pmatrix}$, $Q = Q_f = \mathrm{diag}(1, 2, 4), \gamma = 0.6$, $T = 15$. "*" denotes the initial state.

then leveraged control techniques to analyze convergence/stability of the system with special examples. Within our system analysis, we discovered that the design of A, B in the equation of the dynamics could be chosen to be *left stochastic matrices* so that the conservation of flow is guaranteed. Additionally, the suggested routing allocation $\mathbf{u}$ has to be chosen such that the resulting vector is stochastic, disqualifying certain control technique that can be used in this system (i.e. the algebraic Ricatti equation) and requesting the use of others. Using this fact, we designed an algorithmic solution for the optimal control using a multiparametric quadratic programming approach (explicit MPC), generating explicit strategies and geometric plots to visualize the optimal solutions the central decision maker should take at the feasible states of the game. We discussed the impact of each system parameter on the solution and explained that various structures in A will result in different solution requirements for the central decision maker, while the cost function changes the system's steady state, and $\gamma, \mathbf{x}_0$ influence the rate of convergence.

Future work includes **1)** studying the region of attraction of the LQR routing system via reachability analysis, **2)** extending the present work to more complex network structures (beyond the parallel network), **3)** generalizing the analysis of the convergence behavior of the LQR routing system beyond the special cases considered in the present work, and **4)** leveraging the Reinforcement Learning techniques to approach general routing problems.

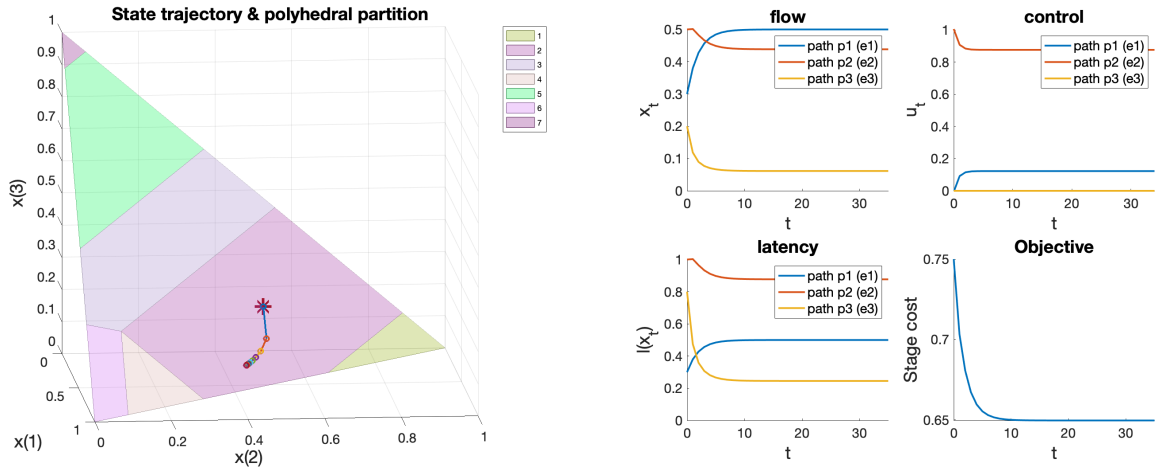

Figure 4.9: Identity A, $B = \begin{pmatrix} 1/2 & 1/2 & 0 \\ 0 & 1/2 & 1/2 \\ 1/2 & 0 & 1/2 \end{pmatrix}$, $Q = Q_f = \mathrm{diag}(1, 2, 4), \gamma = 0.6$, $T = 35$. "*" denotes the initial state.

Chapter 5

Conclusions and Future Steps

Transportation accounts for 28% of energy consumption in the US, with 75% of that occurring on highways. Workers spent on aggregate over three million driver-years commuting to their jobs [32], contributing significantly to the nation-wide congestion. Based on 2012 estimates, US commuters experienced an average of 52 hours of delay in 2011, which amounts to $121 billion of fuel costs and opportunity costs due to delay annually [122]. Estimates project that 4.2% of fuel will be wasted in congestion in 2050 (up from 1.8% in 1998) with the adoption of autonomous vehicles [148]. Mixed autonomy, the intermediate regime between a system with no adoption of autonomy and a system where autonomy is fully employed, is proposed as a potential solution to fuel consumption reduction and flow capacity improvement. However the mixed autonomy system differs from the isolated system or the fully-controlled system, and it may exhibit high complexity and uncertainty. The design and analysis of models and controls are thus challenging. In this thesis we studied the transportation system at three levels: the vehicle level, the mixed autonomy vehicle control level, and the full origin-destination demand routing level.

5.1 Discussion and open problems

At the vehicle level. Chapter 2, Limitations and Improvements of the Intelligent Driver Model (IDM), demonstrated the lack of guarantee of well-posedness for the solution of IDM and closed the theoretical gap by proposing several modifications and rigorously showing the existence and uniqueness of solutions.

Based on the improvements on the original IDM and solid theoretical guarantee on the well-posedness and feasibility of their solutions, one can further work on more complex traffic scenarios such as multi-lane traffic with lane-changing. To improve the overall traffic performance on multi-lanes, we will consider a hybrid system where the continuous longitudinal dynamics can be chosen as one of the IDM modifications and the discrete lateral control is the lane-changing time.

Richer traffic conditions can be integrated with the modified IDM, such as traffic dynam-

ics at the intersection or at the bottleneck. The stability of the solutions in terms of model parameters and initial datum will also be investigated. Furthermore, it would be of great interest to calibrate the modified IDM with simulation and field data, and to compared the simulated results from the calibrated model with the real traffic data.

At the mixed autonomy vehicle control level. Chapter 3, Design of a Basis-based Feedback Controller with Optimal Control, introduced a systematic way to design the basis-based feedback controller. The optimal controller was defined by the solution of a finite-dimensional constrained optimization problem.

The theoretical discussion of the characterization of the actuation function space is, however, still primitive. Due to the complexity of mixed autonomy system and the objective, understanding the actuation space is challenging. Further analysis will be conducted combining prior knowledge from the field data.

The optimal Legendre polynomial basis controller is trained with field data and has been evaluated with simulation data and compared with a range of other mobile traffic controller (including deep-RL methods, MPC, car-following model based controllers and modified FollowerStopper controller). A field experiment of the proposed Legendre polynomial basis controller will be of interest.

Moreover, one will extend the basis-based optimal controller from single lane environment to the more general multi-lane road system. A hybrid system can be considered where the continuous longitudinal dynamics is governed by the basis-based controller, and the discrete lateral controller determines optimal lane-changing behavior.

The approach in this chapter can be combined with other controller designs. For example, we will study the impact on traffic performance with inclusion of car-following based controllers. Finally, it is crucial to further explore the stability of the proposed control scheme with regard to the initial datum, as the transportation system can be noisy.

At the full origin-destination demand routing level. Chapter 4, Parallel Network Flow Allocation in Repeated Routing Games via LQR Optimal Control, studied the repeated routing game problem on a parallel network with affine latency functions on each edge, transforming the dynamic traffic assignment problem into a control-theoretic problem. The impact of model parameters on the traffic performance was theoretically studied, and an algorithmic solution based on explicit MPC was proposed.

Due to the extra flow conservation constraints, an analysis of region of attraction of the LQR routing system is challenging. For the same reason mentioned, theoretical analysis of the convergence behavior of the LQR routing system is limited to special cases. Analytical tools such as reachability analysis [10] are suitable here for a solid discussion on the properties of constrained LQR solutions.

Real roadway networks are way more complicated than the parallel network considered in the present work. In order to employ the flow allocation techniques in this chapter to the real-world applications, one crucial step is to generalize the control-theoretical framework to more complex network topology. As the routing strategies are oftentimes updated online with the sequence of traffic data becomes available, it is essential to further study the time complexity and the rate of convergence of the control algorithm.

5.2 Future Directions

Mixed autonomy is a highly complex system, due to the uncertainty of human performance involved, failure and delay in vehicle-to-vehicle connection, cognitive and irrational perspective in human-vehicle interaction, various designs of the communication protocol potentially limited by hardware implementation and computing power, and uncertainty in the design objective. As a result, mathematical modeling and control of mixed autonomous traffic is extremely challenging. The literature on theoretically solid mixed autonomy modelling and control is still sparse. Further progress would require the development in (non-convex) optimization theory; optimal control theory; mathematical analysis for ODEs/PDEs/stochastic systems; cooperative and non-cooperative, one-shot and dynamical game theory; probabilistic models; and many others. The mission of mixed autonomy is crucial to benefit humanity, and the collaboration and integration of the fields described above have vast potential to improve transportation systems through efficiency, improved safety, and access to mobility.

Bibliography

[1] AIMSUN. *aimsun.* Version Aimsun Next 20. Mar. 6, 2021.

[2] A. Alessio and A. Bemporad. "A survey on explicit model predictive control". In: *Nonlinear model predictive control*. Springer, 2009, pp. 345–369.

[3] A. Alipour-Fanid, M. Dabaghchian, H. Zhang, and K. Zeng. "String stability analysis of cooperative adaptive cruise control under jamming attacks". In: *2017 IEEE 18th International Symposium on High Assurance Systems Engineering (HASE)*. 2017, pp. 157–162.

[4] J. Alonso-Mora, S. Samaranayake, A. Wallar, E. Frazzoli, and D. Rus. "On-demand high-capacity ride-sharing via dynamic trip-vehicle assignment". In: *Proceedings of the National Academy of Sciences* 114.3 (2017), pp. 462–467.

[5] A. Aw and M. Rascle. "Resurrection of "second order" models of traffic flow". In: *SIAM J. Appl. Math.* 60 (2000), pp. 916–938.

[6] M. Balandat, W. Krichene, C. J. Tomlin, and A. M. Bayen. "Minimizing regret on reflexive Banach spaces and Nash equilibria in continuous zero-Sum games". In: *NIPS*. 2016.

[7] M. Bando, K. Hasebe, K. Nakanishi, A. Nakayama, A. Shibata, and Y. Sugiyama. "Phenomenological study of dynamical model of traffic flow". In: *Journal de Physique I* 5.11 (1995), pp. 1389–1399.

[8] M. Bando, K. Hasebe, A. Nakayama, A. Shibata, and Y. Sugiyama. "Dynamical model of traffic congestion and numerical simulation". In: *Phys. Rev. E* 51 (2 Feb. 1995), pp. 1035–1042.

[9] M. Bando, K. Hasebe, A. Nakayama, A. Shibata, and Y. Sugiyama. "Structure stability of congestion in traffic dynamics". In: *Japan Journal of Industrial and Applied Mathematics* 11 (1994), pp. 203–223.

[10] S. Bansal, M. Chen, S. Herbert, and C. J. Tomlin. "Hamilton-Jacobi reachability: A brief overview and recent advances". In: *2017 IEEE 56th Annual Conference on Decision and Control (CDC)*. IEEE. 2017, pp. 2242–2253.

[11] T. Başar and G. J. Olsder. *Dynamic Noncooperative Game Theory, 2nd Edition.* Society for Industrial and Applied Mathematics, 1998.

[12] F. Belletti, D. Haziza, G. B. Gomes, and A. M. Bayen. "Expert level control of ramp metering based on multi-task deep reinforcement learning". In: *IEEE Transactions on Intelligent Transportation Systems* 19 (2018), pp. 1198–1207.

[13] A. Bemporad. "A multiparametric quadratic programming algorithm with polyhedral computations based on nonnegative least squares". In: *IEEE Transactions on Automatic Control* 60.11 (2015), pp. 2892–2903.

[14] S. Bexelius. "An extended model for car-following". In: *Transportation Research* 2.1 (1968), pp. 13–21.

[15] E. Biyik, D. A. Lazar, R. Pedarsani, and D. Sadigh. "Altruistic autonomy: Beating congestion on shared roads". In: *WAFR*. 2018.

[16] E. Biyik, D. A. Lazar, R. Pedarsani, and D. Sadigh. "Incentivizing efficient equilibria in traffic networks with mixed autonomy". In: *IEEE Transactions on Control of Network Systems* 8 (2021), pp. 1717–1729.

[17] A. Blum, E. Even-Dar, and K. Ligett. "Routing without regret: On convergence to Nash equilibria of regret-minimizing algorithms in routing games". In: *Proceedings of the twenty-fifth annual ACM symposium on Principles of distributed computing*. 2006, pp. 45–52.

[18] A. Bobu, A. Bajcsy, J. F. Fisac, and A. D. Dragan. "Learning under misspecified objective spaces". In: *CoRL*. 2018.

[19] S. D. Boyles and S. T. Waller. "Traffic network analysis and design". In: *Wiley Encyclopedia of Operations Research and Management Science* (2010).

[20] M. Brackstone and M. McDonald. "Car-following: A historical review". In: *Transportation Research Part F: Traffic Psychology and Behaviour* 2.4 (1999), pp. 181–196.

[21] M. Bunting, R. K. Bhadani, and J. Sprinkle. "Libpanda: A high performance library for vehicle data collection". In: *Proceedings of the Workshop on Data-Driven and Intelligent Cyber-Physical Systems* (2021).

[22] T. Cabannes, M. A. S. Vincentelli, A. Sundt, H. Signargout, E. Porter, V. Fighiera, J. Ugirumurera, and A. M. Bayen. "The impact of GPS-enabled shortest path routing on mobility: A game theoretic approach". In: 2018.

[23] N. Cesa-Bianchi and G. Lugosi. *Prediction, learning, and games*. Cambridge university press, 2006.

[24] R. E. Chandler, R. Herman, and E. W. Montroll. "Traffic dynamics: Studies in car following". In: *Operations Research* 6 (1958), pp. 165–184.

[25] C. Chen, J. Ma, Y. Susilo, Y. Liu, and M. Wang. "The promises of big data and small data for travel behavior (aka human mobility) analysis". In: *Transportation research part C: emerging technologies* 68 (2016), pp. 285–299.

[26] Y.-C. Chiu, J. Bottom, M. Mahut, A. Paz, R. Balakrishna, T. Waller, and J. Hicks. "Dynamic traffic assignment: A primer". In: *Dynamic Traffic Assignment: A Primer* (2011).

[27] E. A. Coddington and N. Levinson. *Theory of ordinary differential equations*. R.E. Krieger, 1984.

[28] R. Cooke and V. I. Arnold. *Ordinary Differential Equations*. Springer Textbook. Springer Berlin Heidelberg, 1992.

[29] O. Derbel, T. Peter, H. Zebiri, B. Mourllion, and M. Basset. "Modified Intelligent Driver Model for driver safety and traffic stability improvement". In: *IFAC Proceedings Volumes* 46.21 (2013). 7th IFAC Symposium on Advances in Automotive Control, pp. 744–749.

[30] S. E. Shladover Deputy Director. "Review of the State of Development of Advanced Vehicle Control Systems (AVCS)". In: *Vehicle System Dynamics* 24.6-7 (1995), pp. 551–595.

[31] R. Dong, W. Krichene, A. M. Bayen, and S. S. Sastry. "Differential privacy of populations in routing games". In: *2015 54th IEEE Conference on Decision and Control (CDC)*. 2015, pp. 2798–2803.

[32] U. DOT. "National transportation statistics". In: (2016).

[33] K. Dresner and P. Stone. "A multiagent approach to autonomous intersection management". In: *J. Artif. Int. Res.* 31.1 (Mar. 2008), pp. 591–656.

[34] B. Drighès, W. Krichene, and A. M. Bayen. "Stability of Nash equilibria in the congestion game under Replicator dynamics". In: *53rd IEEE Conference on Decision and Control*. 2014, pp. 1923–1929.

[35] Y. Du, O. Watkins, T. Darrell, P. Abbeel, and D. Pathak. "Auto-tuned sim-to-real transfer". In: *2021 IEEE International Conference on Robotics and Automation (ICRA)* (2021), pp. 1290–1296.

[36] J. Eggert, F. Damerow, and S. Klingelschmitt. "The Foresighted Driver Model". In: *2015 IEEE Intelligent Vehicles Symposium (IV)*. 2015, pp. 322–329.

[37] F. Farokhi, W. Krichene, A. M. Bayen, and K. H. Johansson. "A heterogeneous routing game". In: *2013 51st Annual Allerton Conference on Communication, Control, and Computing (Allerton)* (2013), pp. 448–455.

[38] J. F. Fisac, A. Bajcsy, S. L. Herbert, D. Fridovich-Keil, S. Wang, C. J. Tomlin, and A. D. Dragan. "Probabilistically safe robot planning with confidence-based human predictions". In: *Robotics: Science and Systems XIV, Carnegie Mellon University, Pittsburgh, Pennsylvania, USA, June 26-30, 2018*. Ed. by H. Kress-Gazit, S. S. Srinivasa, T. Howard, and N. Atanasov. 2018.

[39] J. F. Fisac, E. Bronstein, E. Stefansson, D. Sadigh, S. S. Sastry, and A. D. Dragan. "Hierarchical game-theoretic planning for autonomous vehicles". In: *2019 International Conference on Robotics and Automation (ICRA)* (2019), pp. 9590–9596.

[40] M. Fornasier, B. Piccoli, and F. Rossi. "Mean-field sparse optimal control". In: *Philosophical Transactions of the Royal Society A: Mathematical, Physical and Engineering Sciences* 372.2028 (2014), p. 20130400.

[41] D. Fridovich-Keil, E. Ratner, L. Peters, A. D. Dragan, and C. J. Tomlin. "Efficient iterative linear-quadratic approximations for nonlinear multi-player general-sum differential games". In: *2020 IEEE International Conference on Robotics and Automation (ICRA)* (2020), pp. 1475–1481.

[42] D. C. Gazis, R. Herman, and R. W. Rothery. "Nonlinear follow-the-leader models of traffic flow". In: *Operations research* 9.4 (1961), pp. 545–567.

[43] J. I. Ge and G. Orosz. "Dynamics of connected vehicle systems with delayed acceleration feedback". In: *Transportation Research Part C-emerging Technologies* 46 (2014), pp. 46–64.

[44] P. G. Gipps. "A behavioural car-following model for computer simulation". In: *Transportation Research Part B: Methodological* 15.2 (1981), pp. 105–111.

[45] D. Gloudemans, W. Barbour, N. Gloudemans, M. Neuendorf, B. Freeze, S. ElSaid, and D. B. Work. "Interstate-24 MOTION: Closing the loop on Smart Mobility". In: *2020 IEEE Workshop on Design Automation for CPS and IoT (DESTION)*. 2020, pp. 49–55.

[46] X. Gong, B. Piccoli, and G. Visconti. "Mean-field limit of a hybrid system for multilane multi-class traffic". In: *arXiv preprint arXiv:2007.14655* (2020).

[47] G. C. Goodwin, S. F. Graebe, and M. E. Salgado. *Control system design*. Upper Saddle River, NJ: Prentice Hall, 2001.

[48] S. Hart and A. Mas-Colell. "A general class of adaptive strategies". In: *Journal of Economic Theory* 98.1 (2001), pp. 26–54.

[49] D. Heidemann. "A queueing theory approach to speed-flow-density relationships". In: 1996.

[50] D. Helbing, A. Hennecke, V. Shvetsov, and M. Treiber. "Micro- and macro-simulation of freeway traffic". In: *Mathematical and Computer Modelling* 35.5 (2002), pp. 517–547.

[51] J. C. Herrera, D. B. Work, R. Herring, X. J. Ban, Q. A. Jacobson, and A. M. Bayen. "Evaluation of traffic data obtained via GPS-enabled mobile phones: The Mobile Century field experiment". In: *Transportation Research Part C-emerging Technologies* 18 (2009), pp. 568–583.

[52] S. Hoermann, D. Stumper, and K. Dietmayer. "Probabilistic long-term prediction for autonomous vehicles". In: *2017 IEEE Intelligent Vehicles Symposium (IV)*. 2017, pp. 237–243.

[53] S. P. Hoogendoorn and P. H. L. Bovy. "State-of-the-art of vehicular traffic flow modelling". In: *Proceedings of the Institution of Mechanical Engineers, Part I: Journal of Systems and Control Engineering* 215.4 (2001), pp. 283–303.

[54] B. K.-P. Horn. "Suppressing traffic flow instabilities". In: *16th International IEEE Conference on Intelligent Transportation Systems (ITSC 2013)*. 2013, pp. 13–20.

[55] K. Hornik. "Approximation capabilities of multilayer feedforward networks". In: *Neural Networks* 4.2 (1991), pp. 251–257.

[56] R. Horowitz. "Automated Highway Systems: The smart way to go". In: *IFAC Proceedings Volumes* 30.8 (1997). 8th IFAC/IFIP/IFORS Symposium on Transportation Systems 1997 (TS '97), Chania, Greece, 16-18 June, pp. 449–460.

[57] R. Horowitz and P. Varaiya. "Control design of an automated highway system". In: *Proceedings of the IEEE* 88.7 (2000), pp. 913–925.

[58] T. Hwang and Y. Ouyang. "Urban freight truck routing under stochastic congestion and emission considerations". In: *Sustainability* 7.6 (2015), pp. 6610–6625.

[59] P. A. Ioannou and C. C. Chien. "Autonomous intelligent cruise control". In: *IEEE Transactions on Vehicular Technology* 42.4 (1993), pp. 657–672.

[60] Y. Jebbari, J. D. Reilly, and A. M. Bayen. "Stackelberg thresholds on parallel networks with horizontal queues". In: *52nd IEEE Conference on Decision and Control*. 2013, pp. 268–274.

[61] T. Jochem and D. Pomerleau. "Life in the fast lane: The evolution of an adaptive vehicle control system". In: *AI Magazine* 17.2 (Mar. 1996), p. 11.

[62] M. A. S. Kamal, J. Imura, T. Hayakawa, A. Ohata, and K. Aihara. "Smart driving of a vehicle using model predictive control for improving traffic flow". In: *IEEE Transactions on Intelligent Transportation Systems* 15 (2014), pp. 878–888.

[63] M. G. Karlaftis and E. I. Vlahogianni. "Statistical methods versus neural networks in transportation research: Differences, similarities and some insights". In: *Transportation Research Part C: Emerging Technologies* 19.3 (2011), pp. 387–399.

[64] A. Kesting, M. Treiber, and D. Helbing. "Enhanced intelligent driver model to access the impact of driving strategies on traffic capacity". In: *Philosophical Transactions of the Royal Society A: Mathematical, Physical and Engineering Sciences* 368.1928 (Oct. 2010), pp. 4585–4605.

[65] D. E Kirk. *Optimal control theory: an introduction*. Springer, 1970.

[66] A. R. Kreidieh, C. Wu, and A. M. Bayen. "Dissipating stop-and-go waves in closed and open networks via deep reinforcement learning". In: *2018 21st International Conference on Intelligent Transportation Systems (ITSC)* (2018), pp. 1475–1480.

[67] S. Krichene, W. Krichene, R. Dong, and A. M. Bayen. "Convergence of heterogeneous distributed learning in stochastic routing games". In: *2015 53rd Annual Allerton Conference on Communication, Control, and Computing (Allerton)*. Sept. 2015, pp. 480–487.

[68] W. Krichene, M. Balandat, C. Tomlin, and A. M. Bayen. "The Hedge algorithm on a continuum". In: *Proceedings of the 32nd International Conference on Machine Learning*. Ed. by Francis Bach and David Blei. Vol. 37. Proceedings of Machine Learning Research. Lille, France: PMLR, June 2015, pp. 824–832.

[69] W. Krichene, A. M. Bayen, and P. L. Bartlett. "Accelerated mirror descent in continuous and discrete time". In: *Advances in Neural Information Processing Systems 28*. Ed. by C. Cortes, N. D. Lawrence, D. D. Lee, M. Sugiyama, and R. Garnett. Curran Associates, Inc., 2015, pp. 2845–2853.

[70] W. Krichene, A. M. Bayen, and P. L. Bartlett. "Adaptive averaging in accelerated descent dynamics". In: *NIPS*. 2016.

[71] W. Krichene, M. C. Bourguiba, K. Lam, and A. M. Bayen. "On learning how players learn: Estimation of learning dynamics in the routing game". In: *ACM Trans. Cyber-Phys. Syst.* 2.1 (Jan. 2018), 6:1–6:23.

[72] W. Krichene, M. S. Castillo, and A. M. Bayen. "On social optimal routing under selfish learning". In: *IEEE Transactions on Control of Network Systems* PP.99 (2016), pp. 1–1.

[73] W. Krichene, B. Drighès, and A. M. Bayen. "On the convergence of no-regret learning in selfish routing". In: *Proceedings of the 31st International Conference on Machine Learning*. Ed. by Eric P. Xing and Tony Jebara. Vol. 32. Proceedings of Machine Learning Research 2. Bejing, China: PMLR, June 2014, pp. 163–171.

[74] W. Krichene, B. Drighès, and A. M. Bayen. "Online learning of Nash equilibria in congestion games". In: *SIAM Journal on Control and Optimization* 53.2 (2015), pp. 1056–1081.

[75] W. Krichene, S. Krichene, and A. M. Bayen. "Convergence of mirror descent dynamics in the routing game". In: *2015 European Control Conference (ECC)*. 2015, pp. 569–574.

[76] W. Krichene, J. D. Reilly, S. Amin, and A. M. Bayen. "On the characterization and computation of Nash equilibria on parallel networks with horizontal queues". In: *2012 IEEE 51st IEEE Conference on Decision and Control (CDC)*. 2012, pp. 7119–7125.

[77] W. Krichene, J. D. Reilly, S. Amin, and A. M. Bayen. "Stackelberg routing on parallel networks with horizontal queues". In: *IEEE Transactions on Automatic Control* 59.3 (2014), pp. 714–727.

[78] M. Kwon, E. Biyik, A. Talati, K. Bhasin, D. P. Losey, and D. Sadigh. "When humans aren't optimal: Robots that collaborate with risk-aware humans". In: *Proceedings of the 2020 ACM/IEEE International Conference on Human-Robot Interaction*. New York, NY, USA: Association for Computing Machinery, 2020, pp. 43–52.

[79] M. Kwon, S. Karamcheti, M.-F. Cuéllar, and D. Sadigh. "Targeted data acquisition for evolving negotiation agents". In: *ArXiv* abs/2106.07728 (2021).

[80] K. Lam, W. Krichene, and A. M. Bayen. "On learning how players learn: Estimation of learning dynamics in the routing game". In: *2016 ACM/IEEE 7th International Conference on Cyber-Physical Systems (ICCPS)*. 2016, pp. 1–10.

[81] N. Laurent-Brouty, A. Keimer, P. Goatin, and A. M. Bayen. "A macroscopic traffic flow model with finite buffers on networks: well-posedness by means of Hamilton–Jacobi equations". In: *Communications in Mathematical Sciences* 18 (2020), pp. 1569–1604.

[82] J. W. Lee et al. "Integrated framework of vehicle dynamics, instabilities, energy models, and sparse flow smoothing controllers". In: *Proceedings of the Workshop on Data-Driven and Intelligent Cyber-Physical Systems*. DI-CPS'21. Nashville, TN, USA: Association for Computing Machinery, 2021, pp. 41–47.

[83] L. Li, Y. Lv, and F.-Y. Wang. "Traffic signal timing via deep reinforcement learning". In: *IEEE/CAA Journal of Automatica Sinica* 3.3 (2016), pp. 247–254.

[84] Z. Li, W. Li, S. Xu, and Y. Qian. "Stability analysis of an extended intelligent driver model and its simulations under open boundary condition". In: *Physica A: Statistical Mechanics and its Applications* 419 (2015), pp. 526–536.

[85] N. Lichtlé, E. Vinitsky, G. Gunter, A. Velu, and A. M. Bayen. "Fuel consumption reduction of multi-lane road networks using decentralized mixed-autonomy control". In: *2021 IEEE International Intelligent Transportation Systems Conference (ITSC)*. 2021, pp. 2068–2073.

[86] M. Liebner, M. Baumann, F. Klanner, and C. Stiller. "Driver intent inference at urban intersections using the intelligent driver model". In: *2012 IEEE Intelligent Vehicles Symposium*. 2012, pp. 1162–1167.

[87] M. J. Lighthill and G. B. Whitham. "On kinematic waves II. A theory of traffic flow on long crowded roads". In: *Proceedings of the Royal Society of London. Series A. Mathematical and Physical Sciences* 229.1178 (1955), pp. 317–345.

[88] *Longitudinal Traffic model: The IDM*. `https://mtreiber.de/MicroApplet/IDM.html#IDMparameters`. Accessed: 2021-01-21.

[89] P. A. Lopez, M. Behrisch, L. Bieker-Walz, J. Erdmann, Y.-P. Flötteröd, R. Hilbrich, L. Lücken, J. Rummel, P. Wagner, and E. Wießner. "Microscopic traffic simulation using SUMO". In: *The 21st IEEE International Conference on Intelligent Transportation Systems*. IEEE, 2018.

[90] D. P. Losey, M. Li, J. Bohg, and D. Sadigh. "Learning from my partner's actions: Roles in decentralized robot teams". In: *CoRR* abs/1910.07613 (2019).

[91] X.-Y. Lu, S. Shladover, and J. K. Hedrick. "Heavy-duty truck control: Short inter-vehicle distance following". In: *Proceedings of the 2004 American Control Conference*. Vol. 5. 2004, 4722–4727 vol.5.

[92] Y. Lv, Y. Duan, W. Kang, Z. Li, and F.-Y. Wang. "Traffic flow prediction with big data: A deep learning approach". In: *IEEE Transactions on Intelligent Transportation Systems* 16.2 (2015), pp. 865–873.

[93] H. S. Mahmassani. "Dynamic network traffic assignment and simulation methodology for advanced system management applications". In: *Networks and spatial economics* 1.3-4 (2001), pp. 267–292.

[94] J. R. Marden and J. S. Shamma. "Game theory and control". In: *Annual Review of Control, Robotics, and Autonomous Systems* 1 (2018), pp. 105–134.

[95] J. R. Marden and J. S. Shamma. "Game theory and distributed control". In: *Handbook of game theory with economic applications*. Vol. 4. Elsevier, 2015, pp. 861–899.

[96] B. N. Matcha, S. Namasivayam, M. H. Fouladi, K. C. Ng, S. Sivanesan, and S. Y. E. Noum. "Simulation strategies for mixed traffic conditions: A review of car-following models and simulation frameworks". In: *The Journal of Engineering* 2020 (2020), p. 8231930.

[97] MATLAB. *9.8.0.1359463 (R2020a)*. Natick, Massachusetts: The MathWorks Inc., 2021.

[98] C. W. Mcarthur. "Developments in Schauder basis theory". In: *Bulletin of the American Mathematical Society* 78 (1972), pp. 877–908.

[99] D. Miculescu and S. Karaman. "Polling-systems-based autonomous vehicle coordination in traffic intersections with no traffic signals". In: *IEEE Transactions on Automatic Control* 65.2 (2020), pp. 680–694.

[100] V. Milanés and S. E. Shladover. "Modeling cooperative and autonomous adaptive cruise control dynamic responses using experimental data". In: *Transportation Research Part C: Emerging Technologies* 48 (2014), pp. 285–300.

[101] A. J. Miller. "A queueing model for road traffic flow". In: *Journal of the Royal Statistical Society. Series B (Methodological)* 23.1 (1961), pp. 64–90.

[102] M. Nice et al. *The I-24 Trajectory Dataset*. Version 1.0.0. Zenodo, Sept. 2021.

[103] N. Nisam, T. Roughgarden, E. Tardos, and V. Vazirani. *Algorithmic game theory*. Cambridge University Press, 2007.

[104] G. Orosz, B. Krauskopf, and R. E. Wilson. "Bifurcations and multiple traffic jams in a car-following model with reaction-time delay". In: *Physica D: Nonlinear Phenomena* 211.3-4 (2005), pp. 277–293.

[105] G. Orosz, J. Moehlis, and F. Bullo. "Delayed car-following dynamics for human and robotic drivers". In: 2011.

[106] G. Orosz and G. Stépán. "Subcritical Hopf bifurcations in a car-following model with reaction-time delay". In: *Proceedings of the Royal Society A: Mathematical, Physical and Engineering Sciences* 462.2073 (2006), pp. 2643–2670.

[107] C. Osorio and M. Bierlaire. *A simulation-based optimization framework for urban traffic control*. Tech. rep. 2010.

[108] M. Papageorgiou, C. Diakaki, V. Dinopoulou, A. Kotsialos, and Y. Wang. "Review of road traffic control strategies". In: *Proceedings of the IEEE* 91.12 (2003), pp. 2043–2067.

[109] M. Patriksson. *The traffic assignment problem: models and methods*. Courier Dover Publications, 2015.

[110] H. J. Payne. "FREFLO: A macroscopic simulation model of freeway traffic". In: *Transportation Research Record* (1979).

[111] N. G. Polson and V. O. Sokolov. "Deep learning for short-term traffic flow prediction". In: *Transportation Research Part C: Emerging Technologies* 79 (2017), pp. 1–17.

[112] R. Rajamani and C. Zhu. "Semi-autonomous adaptive cruise control systems". In: *IEEE Transactions on Vehicular Technology* 51.5 (2002), pp. 1186–1192.

[113] B. Recht. "A tour of reinforcement learning: The view from continuous control". In: *Annual Review of Control, Robotics, and Autonomous Systems* 2 (2019), pp. 253–279.

[114] P. I. Richards. "Shock waves on the highway". In: *Operations Research* 4.1 (1956), pp. 42–51.

[115] J. H. Rillings. "Automated highways". In: *Scientific American* 277.4 (1997), pp. 80–85.

[116] R. W. Rosenthal. "A class of games possessing pure-strategy Nash equilibria". In: *International Journal of Game Theory* 2 (1973), pp. 65–67.

[117] T. Roughgarden. "Algorithmic game theory". In: *Communications of the ACM* 53.7 (2010), pp. 78–86.

[118] T. Roughgarden and É. Tardos. "How bad is selfish routing?" In: *J. ACM* 49.2 (Mar. 2002), pp. 236–259.

[119] D. Sadigh, A. D. Dragan, S. S. Sastry, and S. A. Seshia. "Active preference-based learning of reward functions". In: *Robotics: Science and Systems*. 2017.

[120] D. Sadigh, S. S. Sastry, S. A. Seshia, and A. Dragan. "Information gathering actions over human internal state". In: *Proceedings of the IEEE, /RSJ, International Conference on Intelligent Robots and Systems (IROS)*. IEEE, Oct. 2016, pp. 66–73.

[121] D. Sadigh, S. S. Sastry, S. A. Seshia, and A. D. Dragan. "Planning for autonomous cars that leverage effects on human actions". In: *Robotics: Science and Systems*. 2016.

[122] D. Schrank, B. Eisele, and T. Lomax. "Ttis 2012 urban mobility report". In: *Texas AM Transportation Inst., the Texas AM Univ. System* (2012).

[123] J. Schulz, C. Hubmann, J. Löchner, and D. Burschka. "Interaction-aware probabilistic behavior prediction in urban environments". In: *2018 IEEE/RSJ International Conference on Intelligent Robots and Systems (IROS)* (2018), pp. 3999–4006.

[124] J. Schulz, C. Hubmann, J. Löchner, and D. Burschka. "Multiple model unscented Kalman filtering in dynamic Bayesian networks for intention estimation and trajectory prediction". In: *2018 21st International Conference on Intelligent Transportation Systems (ITSC)* (2018), pp. 1467–1474.

[125] T. Seo, A. M. Bayen, T. Kusakabe, and Y. Asakura. "Traffic state estimation on highway: A comprehensive survey". In: *Annu. Rev. Control.* 43 (2017), pp. 128–151.

[126] S. Shafiei, Z. Gu, and M. Saberi. "Calibration and validation of a simulation-based dynamic traffic assignment model for a large-scale congested network". In: *Simulation Modelling Practice and Theory* 86 (2018), pp. 169–186.

[127] S. Sheikholeslam and C. A. Desoer. "Longitudinal control of a platoon of vehicles with no communication of lead vehicle information: a system level study". In: *IEEE Transactions on Vehicular Technology* 42.4 (1993), pp. 546–554.

[128] S. E. Shladover. "Automated vehicles for highway operations (automated highway systems)". In: *Proceedings of the Institution of Mechanical Engineers, Part I: Journal of Systems and Control Engineering* 219.1 (2005), pp. 53–75.

[129] S. Singh. *The DARPA urban challenge: Autonomous vehicles in city traffic*. Nov. 2009.

[130] K. Spieser, K. Treleaven, R. Zhang, E. Frazzoli, D. Morton, and M. Pavone. "Toward a systematic approach to the design and evaluation of automated mobility-on-demand systems: A case study in Singapore". In: *Road Vehicle Automation*. Ed. by Gereon Meyer and Sven Beiker. Cham: Springer International Publishing, 2014, pp. 229–245.

[131] J. SpjøTvold, E. C. Kerrigan, C. N. Jones, P. TøNdel, and T. A. Johansen. "On the facet-to-facet property of solutions to convex parametric quadratic programs". In: *Automatica* 42.12 (2006), pp. 2209–2214.

[132] E. Stefansson, J. Fisac, D. Sadigh, S. S. Sastry, and K. H. Johansson. "Human-robot interaction for truck platooning using hierarchical dynamic games". In: *European Control Conference (ECC)*. June 2019.

[133] R. E. Stern, S. Cui, M. L. Delle Monache, R. K. Bhadani, M. Bunting, M. Churchill, N. Hamilton, R. Haulcy, H. Pohlmann, F. Wu, B. Piccoli, B. Seibold, J. Sprinkle, and D. B. Work. "Dissipation of stop-and-go waves via control of autonomous vehicles: Field experiments". In: *ArXiv* abs/1705.01693 (2017).

[134] Y. Sugiyama, M. Fukui, M. Kikuchi, K. Hasebe, A. Nakayama, K. Nishinari, S.-i. Tadaki, and S. Yukawa. "Traffic jams without bottlenecks—experimental evidence for the physical mechanism of the formation of a jam". In: *New Journal of Physics* 10 (2008), p. 033001.

[135] Technical Committee ISO/TC 204 Intelligent transport systems. "Intelligent transport systems — Adaptive cruise control systems — Performance requirements and test procedures". In: *ISO* (2010).

[136] S.-X. Tang, A. Keimer, and A. M. Bayen. "Well-posedness of networked scalar semilinear balance laws subject to nonlinear boundary control operators". In: *2019 IEEE 58th Conference on Decision and Control (CDC)*. 2019, pp. 4011–4016.

[137] S.-X. Tang, A. Keimer, P. Goatin, and A. M. Bayen. "A study on minimum time regulation of a bounded congested road with upstream flow control". In: *2019 IEEE 58th Conference on Decision and Control (CDC)*. 2019, pp. 4097–4102.

[138] J. Thai, N. Laurent-Brouty, and A. M. Bayen. "Negative externalities of GPS-enabled routing applications: A game theoretical approach". In: *2016 IEEE 19th International Conference on Intelligent Transportation Systems (ITSC)*. IEEE. 2016, pp. 595–601.

[139] S. Thrun et al. "Stanley: The robot that won the DARPA Grand Challenge". In: *Journal of Field Robotics* 23.9 (2006), pp. 661–692.

[140] M. Treiber, A. Hennecke, and D. Helbing. "Congested traffic states in empirical observations and microscopic simulations". In: *Physical review E* 62.2 (2000), p. 1805.

[141] M. Treiber and A. Kesting. "The Intelligent Driver Model with stochasticity - New insights into traffic flow oscillations". In: *Transportation Research Procedia* 23 (2017). Papers Selected for the 22nd International Symposium on Transportation and Traffic Theory Chicago, Illinois, USA, 24-26 July, 2017., pp. 174–187.

[142] M. Treiber and A. Kesting. "Traffic flow dynamics: Data, models and simulation". In: 2012.

[143] M. Treiber, A. Kesting, and D. Helbing. "Delays, inaccuracies and anticipation in microscopic traffic models". In: *Physica A: Statistical Mechanics and its Applications* 360.1 (2006), pp. 71–88.

[144] A. Vahidi and A. Eskandarian. "Research advances in intelligent collision avoidance and adaptive cruise control". In: *IEEE Transactions on Intelligent Transportation Systems* 4.3 (2003), pp. 143–153.

[145] E. Vinitsky, A. Kreidieh, L. L. Flem, N. Kheterpal, K. Jang, F. Wu, R. Liaw, E. Liang, and A. M. Bayen. "Benchmarks for reinforcement learning in mixed-autonomy traffic". In: *CoRL*. 2018.

[146] E. Vinitsky, N. Lichtlé, K. Parvate, and A. M. Bayen. "Optimizing mixed autonomy traffic flow with decentralized autonomous vehicles and multi-agent RL". In: *ArXiv* abs/2011.00120 (2020).

[147] E. Vinitsky, K. Parvate, A. Kreidieh, C. Wu, and A. M. Bayen. "Lagrangian control through deep-RL: Applications to bottleneck decongestion". In: *2018 21st International Conference on Intelligent Transportation Systems (ITSC)* (2018), pp. 759–765.

[148] Z. Wadud, D. MacKenzie, and P. Leiby. "Help or hindrance? The travel, energy and carbon impacts of highly automated vehicles". In: *Transportation Research Part A: Policy and Practice* 86 (2016), pp. 1–18.

[149] L. Wang, B. K. P. Horn, and G. Strang. "Eigenvalue and eigenvector analysis of stability for a line of traffic". In: *Studies in Applied Mathematics* 138 (2017).

[150] J. G. Wardrop and J. I. Whitehead. "Correspondence. Some theoretical aspects of road traffic research". In: *ICE Proceedings: Engineering Divisions 1* (1952).

[151] T. van Woensel and N. J. Vandaele. "Modeling traffic flows with queueing models: A review". In: *Asia Pac. J. Oper. Res.* 24 (2007), pp. 435–461.

[152] D. B. Work, S. Blandin, O.-P. Tossavainen, B. Piccoli, and A. M. Bayen. "A distributed highway velocity model for traffic state reconstruction". In: 2009.

[153] C. Wu, A. M. Bayen, and A. Mehta. "Stabilizing traffic with autonomous vehicles". In: *2018 IEEE International Conference on Robotics and Automation (ICRA)*. 2018, pp. 6012–6018.

[154] C. Wu, A. Kreidieh, K. Parvate, E. Vinitsky, and A. M. Bayen. "Flow: Architecture and benchmarking for reinforcement learning in traffic control". In: *ArXiv* abs/1710.05465 (2017).

[155] C. Wu, A. Kreidieh, E. Vinitsky, and A. M. Bayen. "Emergent Behaviors in Mixed-Autonomy Traffic". In: *CoRL*. 2017.

[156] C. Wu, K. Parvate, N. Kheterpal, L. Dickstein, A. Mehta, E. Vinitsky, and A. M. Bayen. "Framework for control and deep reinforcement learning in traffic". In: *2017 IEEE 20th International Conference on Intelligent Transportation Systems (ITSC)* (2017), pp. 1–8.

[157] C. Wu, E. Vinitsky, A. Kreidieh, and A. M. Bayen. "Multi-lane reduction: A stochastic single-lane model for lane changing". In: *2017 IEEE 20th International Conference on Intelligent Transportation Systems (ITSC)*. 2017, pp. 1–8.

[158] F. Wu, G. Wang, S. Zhuang, K. Wang, A. Keimer, I. A. Stoica, and A. M. Bayen. "Composing MPC with LQR and neural networks for efficient and stable control". In: *ArXiv* abs/2112.07238 (2021).

[159] A. Xie, D. Losey, R. Tolsma, C. Finn, and D. Sadigh. "Learning latent representations to influence multi-agent interaction". In: *Proceedings of the 4th Conference on Robot Learning (CoRL)*. 2020.